CHARACTERIZATION OF LRIG1^{+} COLONIC STEM/PROGENITOR CELLS AND THEIR TRANSFORMATIVE CAPACITY

By

Emily Jean Poulin

Dissertation

Submitted to the Faculty of the

Graduate School of Vanderbilt University

in partial fulfillment of the requirements

for the degree of

DOCTOR OF PHILOSOPHY

in

Cell and Developmental Biology

May, 2015

Nashville, TN

Approved:

Christopher Wright, D.Phil.

Christopher Williams, M.D., Ph.D.

Ethan Lee, M.D., Ph.D.

William Tansey, Ph.D.

Robert Coffey, M.D.

To my parents

For their constant love and support

ACKNOWLEDGEMENTS

I must first thank Bob for the giving me the opportunity to join his lab and mature into a scientist under his tutelage. Bob has provided unfailing support during my time in his lab, where he has created an exciting environment of scientific exploration. To the amazing group of people that make up the Coffey lab, thank you for being such great friends and colleagues. You have all taught me so much and made the Coffey lab a place I look forward to every day. First, thank you to Ramona, who takes care of all us and without whom the lab would fall apart. Thank you so much to Julia who has been a great help with all of my endless mouse work. Thank you to Michelle, Yang, Annie, and Alina. You are all such fantastic ladies and I have been so lucky to have you as friends. Thank you to Jarred, Greg, Daniel, Jumpei, and Eliot, who have been great sports when subjected to probably a little too much over-sharing from the aforementioned ladies. Thank you to Jeff, Bhumi, Galina, Jennie, Will, and Jim for providing expert advice, I have learned so much from all of you. Thank you to Meghan for providing such great support, not only for me, but also for the entire lab. To the newer members, Yuping, Wei, Qin, Yuanyuan, Xiaodi, and Dennis, I wish you the best of luck in the Coffey lab and in the future. Thank you also to Kay Washington, who has taught me quite a bit about pathology and Matthew Hight, who made the imaging experiments possible.

I would not be writing this dissertation without the support of my thesis committee. Thank you to Chris Wright, Ethan Lee, Bill Tansey, William Pao, and more recently, Chris Williams for keeping me on track and for your constant support and advice through my convoluted path to a thesis project. You have always challenged me to be a better scientist. In particular, thank you to Chris for taking the extra time to talk

through problems and help me navigate. This work would not have been possible without financial support from the National Institutes of Health and Jim Patton for offering me a place on the CBMS training grant for two years.

Outside of lab, I have been so lucky to meet great people who have made my time in Nashville feel like home. Thank you for all the happy hours, game nights, holiday parties, and nights downtown. To Christine, for all the coffees, lunches, pizza nights, and everything else, I am lucky to have you as a friend. Finally, I would like to thank my family, best friend, and fiancé, without whom none of this would be possible. Thank you to my parents and my two amazing sisters. Thank you for all of your love and support, no matter far away I have been. Thank you to Nicola, whose GChat window has been a constant these past five years. Thank you always for being there no matter how many oceans are between us, or how many apps I have to download to talk to you. Most importantly, thank you to Jonathan for all of your unending support every day. You are my everything and I can't wait to continue our adventures together.

TABLE OF CONTENTS

LIST OF TABLES

LIST OF FIGURES

LIST OF ABBREVIATIONS

4-OHT	4-hydroxytamoxifen
Apc/APC	Adenomatous polyposis coli
Areg	Amphiregulin
β-gal	β-galactosidase
BAC	Bacterial artificial chromosome
Bmi1	Bmi1 polycomb ring finger oncogene
BSA	Bovine serum albumin
Car1/CAC	Carbonic anhydrase 1
CBC(s)	Crypt base columnar cell(s)
Cdkn1a	Cyclin-dependent kinase inhibitor 1a
CK1α	Casein kinase 1 isoform alpha
CRC	Colorectal cancer
DIG	Digoxygenin
Dll1	Delta-like 1
DTA	Diphtheria toxin A
DTR	Diphtheria toxin receptor
Egfr/EGFR	Epidermal growth factor receptor
Erk	Extracellular signal-regulated kinase
Fabp1	Fatty acid binding protein 1
FACS	Fluorescence-activated cell sorting
FAP	Familial adenomatous polyposis
GFP	Green fluorescent protein
GSK3β	Glycogen synthase kinase-3 beta
H&E	Hematoxylin and eosin
H2B-YFP	Histone 2B yellow fluorescent protein
HBEGF	Heparin-binding EGF-like growth factor
HEK293T	Human embryonic kidney 293T
HRP	Horseradish peroxidase
Kras/KRAS	Kirsten rat sarcoma viral oncogene homolog
LC-MS	Liquid chromatography mass-spectrometry
Lgr5	Leucine-rich-repeat-containing G-protein coupled receptor 5
LOH	Loss of heterozygosity
LRC(s)	Label-retaining cell(s)
Lrig1/LRIG1	Leucine-rich repeats and immunoglobulin-like domains protein 1
LRP 5/6	LDL receptor-related protein 5/6
M cell	Microfold cell
mTert	Mouse telomerase reverse transcriptase
Muc2	Mucin 2
OCT	Optimal cutting temperature
p53	Tumor protein 53
PBS	Phosphate-buffered saline
PCR	Polymerase chain reaction
PDGFRA	Platelet-derived growth factor receptor alpha

PET	Positron emission tomography
PFA	Paraformaldehyde
RankL	Rank Ligand
RFP	Red fluorescent protein
SH3	SRC Homology 3 Domain
TBST	Tris-buffered saline/Tween 20
TCF/LEF	T-cell factor/lymphoid enhancer-binding factor 1
TCGA	The Cancer Genome Atlas
WT	Wild type
X-gal	5-bromo-4-chloro-3-indolyl-β-D-galactopyranoside

CHAPTER I

INTRODUCTION

Structure and Function of the Colonic Epithelium

After food leaves the stomach, it enters the small intestine, where the majority of digestion and absorption occurs. The large intestine, or colon, absorbs any remaining water and electrolytes and secretes a protective layer of mucus (*2*). The colon is composed of four tissue layers: the outermost serosa, the muscularis, the submucosa, and the mucosa (*3*). The innermost layer, the colonic mucosa, is composed of a single layer simple columnar epithelium that contains specialized cell types. This epithelium is organized into invaginations known as the crypts of Lieberkühn, an arrangement that increases the functional surface area of the epithelium (Figure 1.1). Individual epithelial cells establish contacts with adjacent cells, forming a semi-permeable barrier that separates the intestinal contents from the internal environment. Contained in the lamina propria, a subepithelial region of the mucosa, are various mesenchymal cell types that interact with the epithelium, supporting epithelial growth and maintenance through secretion of multiple factors, including growth factors, cytokines, and hormones (Figure 1.1) (*4*-*6*).

The colonic epithelium experiences continuous physical insults as food and fecal matter transit through the lumen. To maintain barrier integrity, cells are shed at the crypt surface and continually replaced. This rapid turnover is fueled by resident adult intestinal stem cells that reside at the crypt base and divide to generate transit-amplifying cells about once per day (*7*). Bulk cell proliferation is performed by transit-

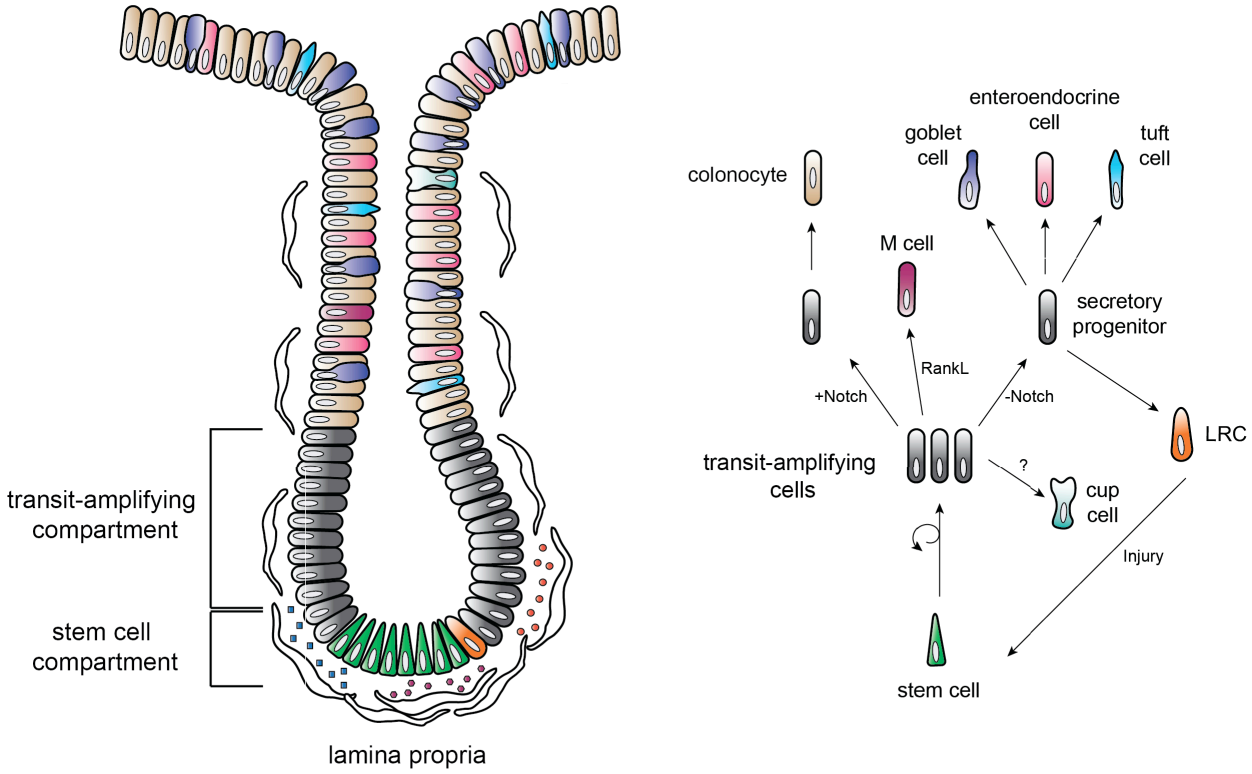

Figure 1.1. Schematic of crypt structure and the differentiated cell types of the colonic epithelium. Stem cells (green) at the base of the crypt divide and give rise to transit-amplifying cells (gray) that proliferate and differentiate into the specialized cell types of the colonic epithelium. Active Notch signaling in transit-amplifying cells pushes cells down the absorptive lineage, while absence of Notch signaling pushes cells down the secretory pathway (*8*). Microfold cell (M cell) differentiation is induced in organoid culture after treatment with Rank Ligand (RankL) (*9*). Label-retaining cells (LRC, orange) are committed secretory progenitors that retain stem cell potential and have regenerative capacity after injury (*1*). Mesenchymal cells in the lamina propria participate in crosstalk with the epithelium to help maintain epithelial integrity and homeostasis. This model largely reflects experimental results from the small intestine rather than the colon. For simplicity, stem cells are depicted as one uniform population. For more detail regarding different stem cell populations, see Figure 1.3. Adapted from (*10*).

amplifying cells, a progenitor cell population that undergoes about four to six cell divisions, once about every 12-16 hours (*11*). As transit-amplifying cells mature and move up the crypt, they differentiate and are eventually shed at the luminal surface. This crypt renewal cycle from stem cell division to shedding at the luminal surface takes approximately five to seven days (*7, 10, 12*). The differentiated cell types of the colon include absorptive colonocytes, mucus-secreting goblet cells, secretory enteroendocrine cells, and the less understood microfold cells (M cells), tuft cells, and cup cells (Figure 1.1) (*10, 13-18*).

The Intestinal Stem Cell: Identity and Debate

Stem cells are characterized based on two main characteristics: self-renewal and multipotency, the ability to generate all the differentiated cells types of a tissue (*19*). The debate over the identity of the intestinal stem cell began almost fifty years ago and continues today. Two theories have prevailed. The first, pioneered by Cheng and Leblond, proposed that crypt base columnar cells (CBCs), distinctive cells identified by electron microscopy, were the intestinal stem cells (Figure 1.3) (*20*). Following ^{3}H-thymidine injection, Cheng and Leblond observed phagosomes in CBCs containing ^{3}H-thymidine label and hypothesized that they were the result of ingestion of cells killed by ^{3}H-thymidine-induced radiation. After time, these labeled phagosomes had moved to the differentiated cell types of the crypt, suggesting that CBCs could give rise to other cell types and were therefore stem cells (*20*). The second theory, championed by Potten and colleagues, is based on nucleotide analogue label retention. DNA label retention has long been thought to be characteristic of stem cells since stem cells are more

quiescent than their daughter transit-amplifying cells; due to an increased rate of proliferation, DNA labels are more quickly diluted from transit-amplifying cells with subsequent cell divisions (*21*). This theory is also supported by Cairns' hypothesis, which posits that stem cells selectively retain the template DNA strand after every cell division and pass the newly synthesized DNA strand to their daughter cells (*7, 22-24*). According to this second theory, after long-term time periods, quiescent LRCs are present around the +4 position (4 cells from the base of the crypt) and were therefore proposed to be the intestinal stem cell (Figure 1.3) (*24*). Marker-based studies have become possible only within the past decade, and, while many details of intestinal stem cell identity and biology have been elucidated using lineage tracing and reporter techniques, many questions still remain.

Intestinal Stem Cell Markers

Leucine-rich-repeat-containing G protein-coupled receptor 5 (Lgr5), a G protein coupled-receptor and Wnt target gene, was the first *bona fide* intestinal stem cell marker to be identified using lineage tracing analysis (*25*). *Lgr5* is expressed in CBCs of the small intestine and colon, which give rise to all of the differentiated intestinal epithelial cell types (*25*). $Lgr5^+$ CBCs are a proliferative cell population, dividing about once per day (*25*). On a molecular level, Lgr5 associates with the Frizzled/LDL receptor-related protein 5/6 (LRP5/6) Wnt receptor complex and binds the Wnt agonist R-spondin proteins (*26-28*). Together, these results identified a direct mechanism by which Wnt signaling contributes to stem cell identity and maintenance.

Subsequent identification of +4 cell markers by lineage tracing analysis suggested that multiple stem cell populations with different proliferative properties exist in the intestinal epithelium. *Bmi1 polycomb ring finger oncogene* (*Bmi1*), a component of the polycomb-repressing complex 1, was reported to be expressed in cells at the +4 position in the small intestine; lineage tracing analysis confirmed that $Bmi1^+$ cells give rise to all epithelial lineages, but predominantly in the duodenum and jejunum (*29*). In contrast to the $Lgr5^+$ population, $Bmi1^+$ cells are radio-resistant and largely quiescent, but can be activated after radiation injury to contribute to epithelial repair (*30*); additionally, *in vitro* spheroid culture demonstrated that $Bmi1^+$ cells could give rise to $Lgr5^+$ cells (*30*). Of note, other studies have demonstrated that the *Bmi1* transcript is expressed in cells that express *Lgr5* (*10, 31-33*) and that $Bmi1^+$ cells are not restricted to the +4 position, but can often be observed in the transit-amplifying zone (*34*). *Bmi1* mRNA and protein has also been reported in the colon, suggesting its expression is more widespread than originally reported (*32*). These recent studies have generated debate about the true expression pattern of *Bmi1* and the identity of $Bmi1^+$ stem cells.

A second +4 cell marker, mouse telomerase reverse transcriptase (mTert), was identified based on the hypothesis that long-lived stem cells have high telomerase activity, which prevents cellular senescence induced by telomeric shortening after many cell divisions (*35*). Lineage tracing confirmed that $mTert^+$ cells are *bona fide* stem cells that give rise to and maintain entire crypts (*33*). Multipotent $mTert^+$ small intestinal and colonic stem cells are relatively quiescent, resistant to radiation injury, and express *Bmi1* mRNA. Like the $Bmi1^+$ population, $mTert^+$ cells can be activated to proliferate and regenerate the epithelium—including $Lgr5^+$ cells—after radiation damage (*33*).

Hopx, an atypical homeobox protein, marks multipotent +4 cells that also express *Bmi1* and *mTert*; the $Hopx^+$ cell population is quiescent and distinct from the $Lgr5^+$ population (*36*). Interestingly, organoid culture demonstrated that single $Hopx^+$ cells could generate organoids that contained $Lgr5^+$ cells and conversely, single Lgr5-$EGFP^+$ cells isolated from a Lgr5 reporter mouse generated organoids that contained $Hopx^+$ cells (*30*).

Leucine-rich repeats and immunoglobulin-like domains 1 (Lrig1) was identified as an intestinal stem cell marker based on its expression in the crypt base (*32, 37*). LRIG1 (Figure 1.2) is a single pass transmembrane protein that acts as a negative regulator of multiple receptor tyrosine kinases, including epidermal growth factor receptor (EGFR) and its family members (*38, 39*), MET (*40*), RET (*41*), and platelet-derived growth factor receptor alpha (PDGFRA) (*42*). LRIG1-mediated EGFR negative regulation is thought to occur upon association of the LRIG1 ectodomain with that of EGFR, resulting in recruitment of the E3 ligase, c-CBL, which ubiquitylates EGFR, initiating its internalization and degradation (*38*).

Lineage tracing analysis demonstrated that $Lrig1^+$ cells are multipotent stem cells in both the small and large intestine (*32*). Of note, Lrig1 loss results in tumor formation, suggesting that Lrig1 has tumor suppressor activity, consistent with its role in modulation of EGFR activity (*32*). However, conflicting observations have been reported regarding $Lrig1^+$ cell identity and characteristics. Wong and colleagues showed that 30% of intestinal epithelial cells express Lrig1 in a broad pattern in the crypt base (*37*). In contrast, Powell and colleagues showed that Lrig1 is expressed in 2.4% of small intestinal epithelial cells and 4.8% of all colonic epithelial cells and is present in select

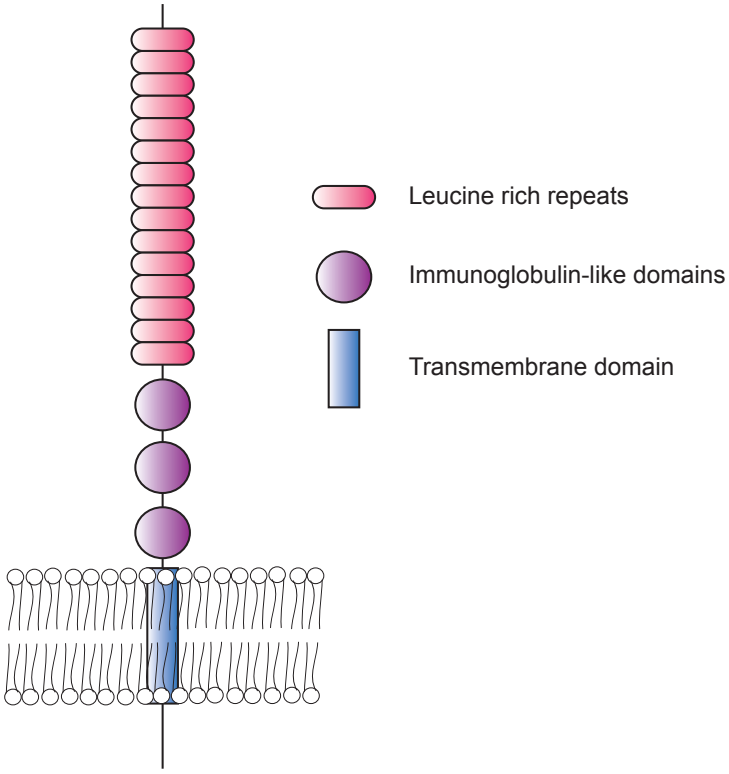

Figure 1.2. Schematic of leucine-rich repeats and immunoglobulin-like domains protein 1 (LRIG1). LRIG1 is a 1093 amino acid single pass transmembrane protein. The LRIG1 ectodomain contains fifteen leucine-rich repeats (pink) and three immunoglobulin-like domains (purple). The cytoplasmic domain of LRIG1 contains predicted c-CBL-binding and SRC Homology (SH3) domains (not pictured). Not to scale.

cells in the colonic crypt base, most often at positions 3-5 (*32*).

The relationship of Lrig1$^+$ stem cells to Lgr5$^+$ stem cells is complicated. It was first reported that *Lrig1* transcript levels were most highly expressed in Lgr5$^+$ stem cells, suggesting that Lrig1 and Lgr5 marked the same proliferative stem cell population (*37*). However, it was also shown that Lrig1 marked largely quiescent cells that rarely overlapped with Lgr5$^+$ cells (*32*). Further transcriptome analysis demonstrated that multiple stem cell-associated transcripts were similarly expressed in Lrig1$^+$ and Lgr5$^+$ populations, confirming their stem cell identity (*32, 37*). However, global transcriptome differences were observed, suggesting that these two cell populations have different biological characteristics. Of most interest, *Lgr5* was lowly expressed in Lrig1$^+$ cells, but *Lrig1* was highly expressed in Lgr5$^+$ cells, suggesting the relationship between the two populations is incompletely understood (*32*).

Ablation of either the Bmi1$^+$ or Lgr5$^+$ populations has shed light on the relationships that exist between these two stem cell populations. Diphtheria toxin-induced ablation of Bmi1$^+$ cells resulted in large-scale epithelial destruction, demonstrating the requirement of Bmi1$^+$ cells for crypt maintenance and survival (*29*). However, ablation of the Lgr5$^+$ population using similar methods had no overt effect on the epithelium, suggesting Lgr5$^+$ stem cells are not absolutely required for crypt homeostasis (*43*). These results suggest there may be a reserve stem cell population that is activated to compensate for loss of Lgr5$^+$ cells; in fact, at least in the proximal small intestine, the reserve stem cells were identified as the Bmi1$^+$ population (*43*). These studies were supported by radiation ablation of Lgr5$^+$ cells and subsequent expansion of Bmi1$^+$ cells (*30*).

The identification of multiple markers of stem cell populations with different characteristics suggests there is not one single stem cell population in the intestine, but that multiple stem cell populations maintain the epithelium in an organized manner. mTert^{+}, Bmi1^{+}, and Lrig1^{+} cells can be activated to proliferate upon damage (*30, 32, 33*), and Hopx^{+} and Lgr5^{+} stem cells can interconvert, giving rise to either cell type (*36*). In addition, upon loss of Lrig1 in a *Lrig1*$^{CreERT2/CreERT2}$ background, the percent of Lgr5-EGFP^{+} crypts increases (*32*).

While many questions remain to be answered, these studies support a model in which Lgr5^{+} CBCs are the major cycling stem cells responsible for replenishing the crypt and supporting homeostatic crypt turnover. However, upon epithelial injury and loss of the Lgr5^{+} population, quiescent “reserve” stem cells—potentially LRCs—can be activated to proliferate and regenerate the epithelium. The stemness of LRCs had been largely untested until recently. Elegant genetic techniques enabling lineage tracing from histone 2B yellow fluorescent protein-tagged (H2B-YFP)-labeled LRCs demonstrated that LRCs were progenitor cells committed to the secretory lineage and could not give rise to fully labeled crypts after three days (*1*). However, YFP-LRCs did retain stem cell potential, as they could generate organoids *ex vivo* and regenerate epithelial crypts after injury. Therefore, while LRCs are committed progenitors, they act as a reserve stem cell population that can be activated during the regenerative response after injury (*1, 44*). Supporting this idea, a second study, recently demonstrated that delta-like 1-expresssing (Dll1^{+}) secretory precursor cells around the +5 position could adopt stem cell potential after damage (*45*).

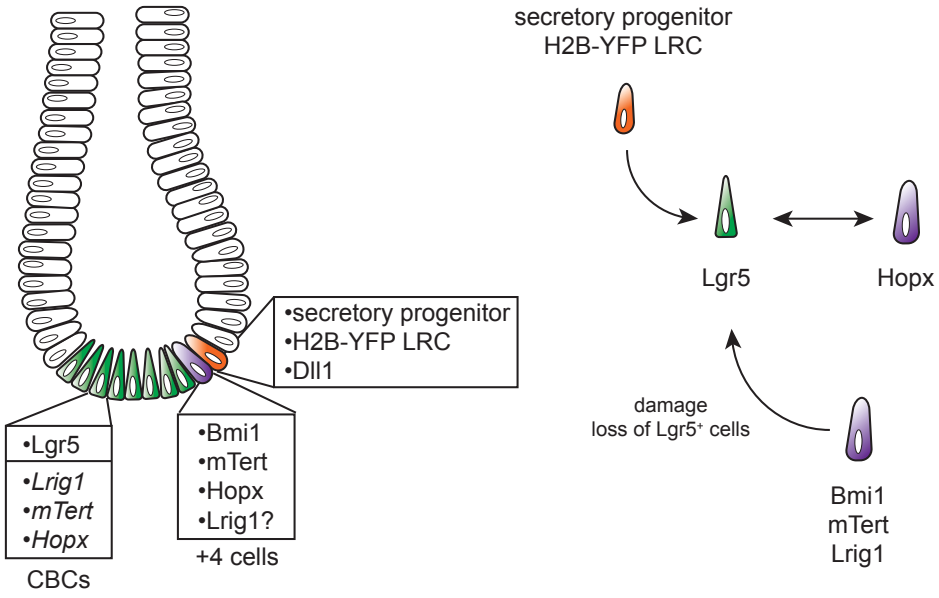

Figure 1.3. Overview of intestinal stem cell markers and interconversion of proposed stem cell populations. Lgr5 marks crypt base columnar cells (CBCs, green), which contain *Lrig1, mTert, and Hopx* transcripts. The originally proposed +4 cell (purple) markers include Bmi1, mTert, and Hopx. Recent evidence suggests that label-retaining cells (LRCs, orange) are not stem cells, but secretory precursors that possess stem cell potential (*1*). Note that studies from the small intestine have been extrapolated here to the colon.

Together, these studies highlight the broad cell plasticity present in the intestinal epithelium, suggesting that stemness may not be a fixed hierarchy dependent on lineage fate decisions as previously thought. Rather, stemness might be a characteristic acquired by the location of a cell within the crypt, as well as the presence or absence of environmental factors, such as injury, the microbiome, or the fasted/fed state (*45, 46*). Supporting a dynamic model, analysis of chromatin marks in committed secretory or absorptive progenitors demonstrated almost no difference, highlighting the potential for plasticity and suggesting that lineage may not be specified at the epigenetic level, but may be defined by the expression and activity of lineage-specific transcription factors (*47*).

Genetics of Colorectal Cancer

Colorectal cancer (CRC) is the third leading cause of cancer-related death in the United States (*48*). The progression from normal epithelium to malignancy is thought to occur in a series of stages: initiation, promotion or establishment, progression, and invasion and metastasis (Figure 1.4) (*49*). In 1990, Fearon and Vogelstein presented a genetic model for CRC, proposing that CRC arises from the accumulation of mutational events that result in inactivation of tumor suppressor genes and activation of oncogenes (*49*). They proposed that each mutational event on the spectrum from normal epithelium to malignancy leads to tumor progression; eventually, enough mutations accumulate to form a carcinoma. In a now classic depiction, often referred to as the “Vogelgram”, they presented the most common genetic alterations and the position in the CRC spectrum at which each mutation was most often observed (Figure 1.4) (*49*). Twenty-two years

later, in 2012, The Cancer Genome Atlas Network (TCGA) reported results from a comprehensive genome sequencing screen of 224 colon tumors and matched normal tissue. They found the top three mutated genes in non-hypermutated tumors were *adenomatous polyposis coli* (*APC*) (81%), *tumor protein p53* (*TP53*) (60%), and *Kirsten rat sarcoma viral oncogene homolog (KRAS*) (43%), supporting Fearon and Vogelstein's model and confirming these pathways play a major role in CRC (*50*).

The most common CRC-initiating mutation occurs in the gatekeeper tumor suppressor gene, *APC*. *APC* was identified as the long sought gene at the 5p locus responsible for a form of hereditary CRC, known as familial adenomatous polyposis, or FAP. FAP patients harbor a germline mutation in *APC* and develop hundreds to thousands of colonic adenomas, some of which progress to CRC if left untreated (*51, 52*). APC is a critical modulator of Wnt signaling, a pathway essential for crypt development and stem cell proliferation and maintenance (*13, 53-56*). In the absence of Wnt signaling, β-catenin transcriptional activity is inhibited by the β-catenin destruction complex—composed of APC, Axin, Glycogen synthase kinase-3 beta (GSK3β), and Casein kinase I isoform alpha (CK1α)—that mediates β-catenin phosphorylation, ubiquitylation, and degradation by the proteasome. Wnt signaling is activated when Wnt ligands bind to the Frizzled and LRP5/6 co-receptors, relieving APC-mediated β-catenin degradation. β-catenin accumulates and enters the nucleus where it binds T-cell factor and lymphoid enhancing factor (TCF/LEF) transcription factors, releasing them from repression by Groucho and activating Wnt target gene expression (*13, 51, 57, 58*).

Loss-of-function *APC* mutations result in a failure of β-catenin degradation, causing β-catenin accumulation in the nucleus and activation of Wnt target gene transcription in an unregulated manner, which can culminate in tumor initiation (*59-63*). *APC* loss in CRC is thought to occur in two stages. The "first hit" occurs sporadically, and most often results in a truncated APC protein (*64-66*). Heterozygous *APC* crypts are histologically normal, but exhibit an upward shift in the proliferative region toward the top of the crypt (*12*). In addition, *APC* heterozygosity induces expansion of the stem cell compartment, which may result in the perpetuation of *APC* mutant crypts, increasing the chances for loss of the second allele (*67, 68*). The "second hit" occurs by a process called loss of heterozygosity (LOH), after which a cell becomes null for functional APC protein (*69-71*).

Stem Cells as the Cells-of-Origin of Colorectal Cancer

Due to the rapid renewal of the intestinal epithelium, stem cells are thought to be the only cells that persist long enough to acquire a mutation and initiate tumorigenesis (*46, 67*). Studies suggest that multiple equipotent stem cell clones exist within a crypt in a state of neutral drift, whereby symmetrical cell division replaces stochastic cell loss from the stem cell compartment to the transit-amplifying compartment; as stem cells are lost to the transit-amplifying compartment, existing stem cell clones expand or contract to replace those that are lost (*46, 72, 73*). Once a mutation has occurred in one stem cell within a crypt, that clone may acquire an advantage that allows it to outcompete other stem cell clones in the same crypt and colonize the entire crypt with mutant cells (*67, 74, 75*). In fact, clonal lineage tracing analysis confirmed that *Apc* loss

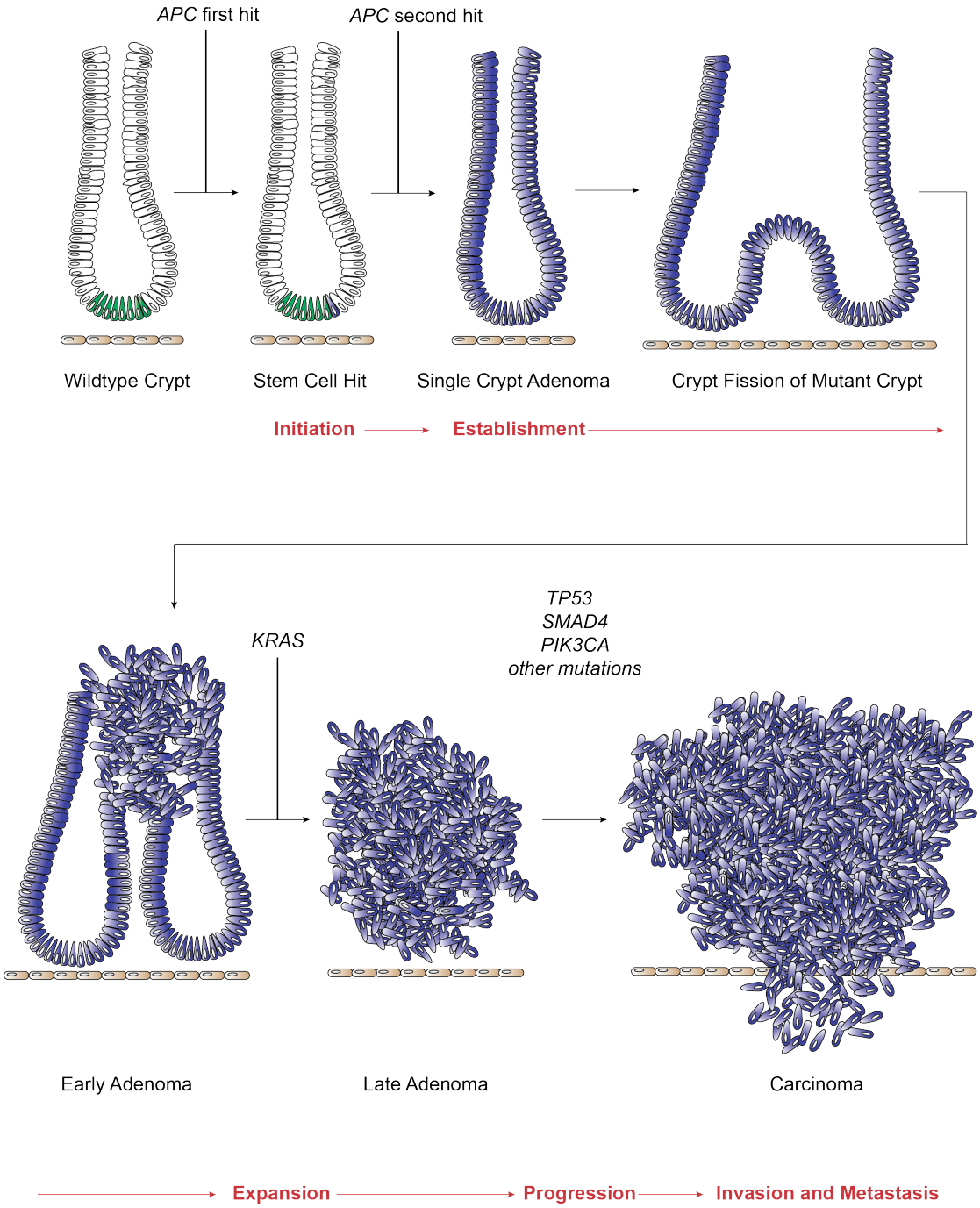

Figure 1.4. Colorectal cancer development and progression. Acquisition of a mutation in one *APC* allele and subsequent loss of the second allele is sufficient for tumor initiation. Increased rate and frequency of crypt fission eventually leads to adenoma establishment. Additional mutations result in adenoma expansion and progression, eventually leading to a carcinoma, capable of invasion and metastasis.

.

and oncogenic activation of the small GTPase Kras confer a competitive replacement advantage; in this setting, *Apc* or *Kras* mutant clones replaced wild type stem cells at a significantly greater frequency than wild type clones replaced mutant clones (*74*). A microadenoma eventually develops as mutant crypts increase the rate and frequency of crypt fission (the bifurcation of one crypt to become two), forming a field of mutant tissue (Figure 1.4) (*12, 46, 67, 75*).

Supporting the proposal that stem cells act as a tumor-initiating population, studies have demonstrated that tumor-initiating *Apc* mutations in the $Lgr5^+$ and $Lrig1^+$ stem cell populations, or activating β-catenin mutations in the $Bmi1^+$ population, result in tumorigenesis (*29, 32, 76*). However, there is also evidence to suggest that in the setting of heightened Wnt signaling and additional activation of NF-κB signaling, tumor initiation can occur in non-stem cells upon dedifferentiation and acquisition of stem cell properties (*77*). Therefore, activation of the Wnt pathway in a stem cell population is sufficient for tumor initiation and, although tumor initiation can occur in a differentiated cell population, additional mutations are necessary (*46*).

Importantly, *Apc* loss alone in the above stem cell populations results in adenomas that do not progress, suggesting that additional mutations are required to advance beyond the adenoma stage (*29, 32, 76*). Combined *Apc* loss and oncogenic activation of Kras in $Lgr5^+$ cells causes rapid morbidity and increased tumor burden within seven to ten days, complicating the use of this model for tumor studies (*78*). Combined *Apc* loss and Kras activation has been studied using other drivers; these strategies result in different degrees of tumor progression, including high-grade dysplasia (*79-81*), local invasion (*79, 80*), and metastasis (*80*). Importantly, the

oncogenic mutations in these studies were not confined to stem cells populations, but rather cells along the entire crypt axis, complicating the identity of the cell population(s) important for initiation and progression.

Rationale for Dissertation Research

The Coffey lab has historically studied EGFR and its ligands in the context of the polarized intestinal epithelium, both in homeostasis and cancer. Our work characterizing Lrig1^{+} cells in 2012 has implications not only for stem cell biology, but also for the role of Egfr signaling in the crypt epithelium. We reported the important observation that Lrig1 can act as a tumor suppressor in the proximal duodenum. In this context, loss of Lrig1 results in the development of adenomas that are likely initiated by disrupted Egfr signaling, rather than by the canonical Wnt signaling pathway (studies are underway to confirm this) (*32*). Additionally, the identification of Lrig1 as a stem cell marker came at a propitious time in the intestinal stem cell field. Now, almost three years later, evidence from the intestinal stem cell field is moving toward a new model. This model suggests that rather than existing in a fixed hierarchy, stem cells exist in a dynamic metastable state. Remarkably, this dynamic system has adapted failsafe measures—present in reserve stem cell populations and progenitor cells—to accommodate tissue injury and damage, retaining the ability to regenerate itself without significantly affecting whole organism physiology.

In the field of genetically engineered mouse models, there has been a struggle to replicate features of human CRC in the mouse. Many models of *Apc* loss have been developed using both germline mutations as well as inducible models, but the vast

majority of these models develop tumors only in the small intestine, while the colon is largely spared. Additionally, mouse models that induce *Apc* loss with Cre-loxP technology use Cre drivers that are not restricted to stem cells; rather, cells along the entire length of the crypt express Cre recombinase, stem cells included. Without the stem cell specificity, it is difficult to determine the cell population(s) responsible for neoplastic transformation—although it is assumed to be the stem cells. To date, intestinal tumors develop when *Apc* loss or mutant β-catenin have been introduced into to Lgr5$^+$ (*76*), Lrig1$^+$ (*32, 82*), and Bmi1$^+$ (*29*) cells, demonstrating that these stem cell populations can act as tumor-initiating populations. Importantly, work in the Coffey lab has demonstrated that loss of a single *Apc* allele in Lrig1$^+$ cells leads to loss of the second allele through LOH and development of distal colon tumors. This work is a significant advance in the field of colonic neoplasia mouse modeling for two reasons: 1) *APC* mutations in human CRC are thought to occur stochastically though LOH, a process exhibited in this inducible mouse model; and 2) the prevalence of distal colon tumors is largely novel for an inducible model of colorectal neoplasia as most previous studies reported high frequency of small intestinal tumors, but few colon tumors. Largely due to animal morbidity, tumor studies using intestinal stem cell-driven oncogenic mutations have failed to demonstrate that secondary mutations in stem cells (after *Apc* loss) can lead to advanced colonic neoplasia (advancing beyond the adenoma stage). Additionally, the ability of Lrig1$^+$ cells to progress to such advanced neoplasia—including invasion and metastasis—has not been investigated.

My dissertation research aims to further characterize Lrig1$^+$ colonic epithelial stem cells in homeostasis and their capacity to become transformed in the context of

multiple oncogenic mutations. The net result of the past eight years of intestinal stem cell marker identification has largely led to more confusion, especially regarding the identity of Lrig1$^+$ cells. Two studies reporting discordant results have made it difficult to fit Lrig1 into the ever-expanding list of intestinal stem cell markers. In particular, the potential overlapping expression of Lrig1 and Lgr5 has led to assumptions that these markers mark the same cell population. Chapter II was published in *Stem Cell Research* in 2014 (*83*) and appears as published, apart from additional details and discussion points. This chapter focuses on the following questions: Are Lrig1$^+$ cells different from Lgr5$^+$ cells, or are they overlapping populations? Does the Lrig1 transcriptional readout correlate with Lrig1 protein expression? I address the overlap of Lrig1 protein expression in Lgr5$^+$ cells and further define the distinction between the populations using multiple reagents and a new Lrig1 reporter mouse. From this research, we were able to conclude there are two Lrig1$^+$ populations in the colon that can be distinguished based on *Lgr5* expression and potentially the glycosylation status of Lrig1; these populations can also be physically separated using a Lrig1 reporter mouse. This work has opened new questions about the identity of Lrig1$^+$ cells, and resolves important questions that have sparked debate over the position and identity of Lrig1$^+$ cells and their distinction from Lgr5$^+$ cells.

Chapter III documents three years of ongoing work, describing my attempts to develop an advanced model of colonic neoplasia in the mouse using inducible *Lrig1*^{CreERT2} stem/progenitor cell driver mice to drive oncogenic mutations in *Apc* and *Kras*. This research addresses the following questions: Can multiple oncogenic mutations in Lrig1$^+$ cells result in advanced colonic neoplasia? How do different

oncogenic mutations in Lrig1^{+} cells affect neoplastic progression? This research has capitalized on the ability of Lrig1^{+} cells to initiate distal colon tumors using our inducible *Lrig1*^{CreERT2} mouse model. However, due to the broad expression of Lrig1 in many epithelial tissues, I encountered a number of technical obstacles, ultimately developing a model of colonic neoplasia that while not novel, can be used in the future to address questions related to heterozygous versus homozygous *Apc* loss. We found that expression of oncogenic Kras does not significantly alter tumor characteristics, but may contribute to increased invasion.

Future studies will address the significance of Lrig1 glycosylation status and if and how glycosylation affects the function of Lrig1. In particular, it will be important to determine whether Lrig1 glycosylation status affects modulation of Egfr signaling or the behavior of Lrig1^{+} stem cells. Additionally, the role of Lrig1^{+} and Lgr5^{+} populations will be interrogated in the context of epithelial damage and cancer. The strategy I have developed to activate restricted Cre recombinase in the distal colon has allowed us to study the effects of homozygous *Apc* loss in Lrig1^{+} cells, previously impossible due to animal morbidity. Therefore, future studies will address the differences between tumors that develop after loss of one *Apc* allele compared to tumors that develop after loss of both *Apc* alleles. This localized system will also allow for additional mutational events to be studied in the colon without concern for effects in off-target tissues.

CHAPTER II

CHARACTERIZATION OF LRIG1^{+} COLONIC STEM/PROGENITOR CELLS

This work was published under the title:
"Using a new Lrig1 reporter mouse to assess differences between two Lrig1 antibodies in the intestine"
Poulin et al., *Stem Cell Research* (2014) **13**, 422-430.

Introduction

Until recently, adult intestinal stem cells have been difficult to study due to the lack of specific markers and genetic techniques. Following the discovery of the first *bona fide* intestinal stem cell marker, Lgr5, by Barker and colleagues in 2007, there has been an explosion of stem cell marker identification. As the field develops, it has become clear that there may be multiple stem cell populations in the intestine, at different positions within the crypt and with different proliferative properties. Lgr5 has become the most notable marker of crypt base columnar cells (CBCs), first observed by Cheng and Leblond in 1974 (*20, 25*).

Leucine-rich repeats and immunoglobulin-like domains protein 1 (Lrig1) was identified as an intestinal stem cell marker in 2012 (*32*). At the same time, Wong et al. demonstrated that Lrig1 was important for intestinal homeostasis; upon *Lrig1* loss, the intestine becomes enlarged, an effect this group attributed to crypt hyperplasia (*37*). While both groups demonstrated that Lrig1 is expressed in cells in the intestinal epithelial stem cell zone, discrepant observations of Lrig1 protein distribution in the intestinal crypt were observed.

Wong and colleagues, focused on the small intestine, demonstrated that Lrig1 transcript and protein are expressed in the progenitor cell zone of the crypt base using *in situ* hybridization and immunofluorescent analysis. Using flow cytometry, they showed that 30% of intestinal epithelial cells express Lrig1 and these Lrig1^{+} cells express intestinal stem cell marker transcripts (*37*). In addition, they demonstrated that the Lrig1 protein overlapped with expression of green fluorescent protein (GFP) in *Lgr5*$^{EGFP\text{-}ires\text{-}creERT2}$ reporter mice and concluded that Lrig1 and Lgr5 marked the same stem cell population (*37*).

Our group, focused on the colon, demonstrated that Lrig1 marks a *bona fide* intestinal stem cell population that gives rise to all differentiated intestinal epithelial cell types by lineage tracing analysis (*32*). Additionally, we found that Lrig1 protein is expressed in select cells in the colonic crypt base, rather than in a broad pattern. Flow cytometry demonstrated only 4.8% of all colonic epithelial cells express Lrig1; RNA-Seq analysis of this Lrig1^{+} flow-sorted population also revealed enrichment of intestinal stem cell marker transcripts. Lrig1 and Lgr5-EGFP expression overlapped in only 0.5% and 0.2% of all epithelial cells in the small intestine and colon, respectively, suggesting that Lrig1 and Lgr5 marked distinct cell populations (*32*). The relationship between different stem cell populations and between stem cells and committed progenitors, as well as studies of stem cell behavior, are currently largely marker-based. Therefore, it is essential to clarify the Lrig1 expression discrepancy to facilitate Lrig1-related studies.

These two independent studies utilized different antibodies to assess Lrig1 protein expression. Wong et al. used a commercial goat polyclonal anti-Lrig1 antibody from R&D Systems™, raised against nearly the entire ectodomain of mouse Lrig1

(#AF3688; hereafter anti-Lrig1-R&D) (Figure 2.1) (*37*), while in collaboration with Covance (Denver, PA), Powell et al. generated a rabbit polyclonal peptide antibody to a sequence (KILSVDGSQLKSY) in the ectodomain of mouse Lrig1 (hereafter anti-Lrig1-VU) (Figure 2.1) (*32*). Using a new Lrig1 reporter mouse (*Lrig1-Apple*), we set out to further characterize these antibodies to clarify their use for future Lrig1-related studies. We show anti-Lrig1-R&D recognizes all Lrig1$^+$ cells, while anti-Lrig1-VU recognizes a subset of Lrig1$^+$ cells, likely expressing a non-glycosylated form of Lrig1.

Results

Anti-Lrig1-VU recognizes a subset of anti-Lrig1-R&D$^+$ cells

We first compared the reactivity of each anti-Lrig1 antibody on isolated mouse colonic crypts by immunofluorescence. Consistent with previously published results, anti-Lrig1-R&D recognized nearly every epithelial cell in the bottom third of the crypt base (Figure 2.2A, A') (*37*). In contrast, anti-Lrig1-VU stained a subset of cells in the crypt base (Figure 2.2B, B'), as previously described (*32*). Co-immunofluorescence using both anti-Lrig1 antibodies revealed that anti-Lrig1-VU immunoreactivity (Figure 2.2C'; C'', C''', red) was restricted to a subset of anti-Lrig1-R&D$^+$ cells (Figure 2.2C; C'', C''', green). Lrig1 is a type I transmembrane protein and is expected to be located on the plasma membrane (Figure 1.2, page 7) (*84*). We observed that the immunoreactive patterns of both antibodies were largely restricted to the basolateral membrane of epithelial cells within the crypt base, although cytoplasmic staining was previously observed with anti-Lrig1-VU in mouse colonic tissue sections (*32*); we did not observe

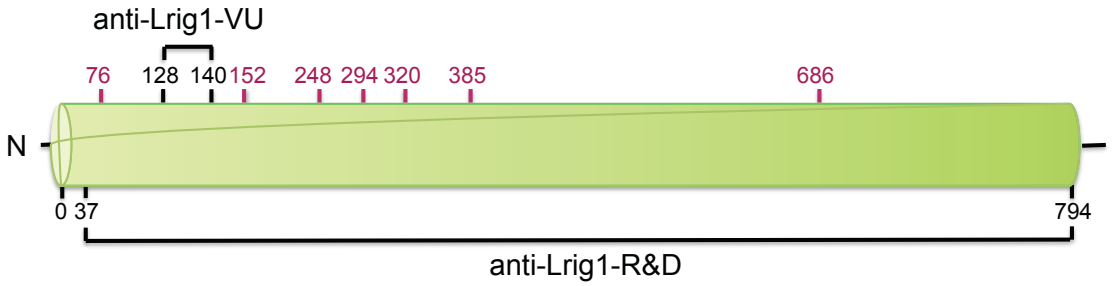

Figure 2.1. Schematic of the Lrig1 ectodomain. The respective epitopes of anti-Lrig1-VU and anti-Lrig1-R&D and predicted N-glycosylation sites (purple) are illustrated. N76 was confirmed by mass spectroscopy (Glycoprotein database). Not to scale.

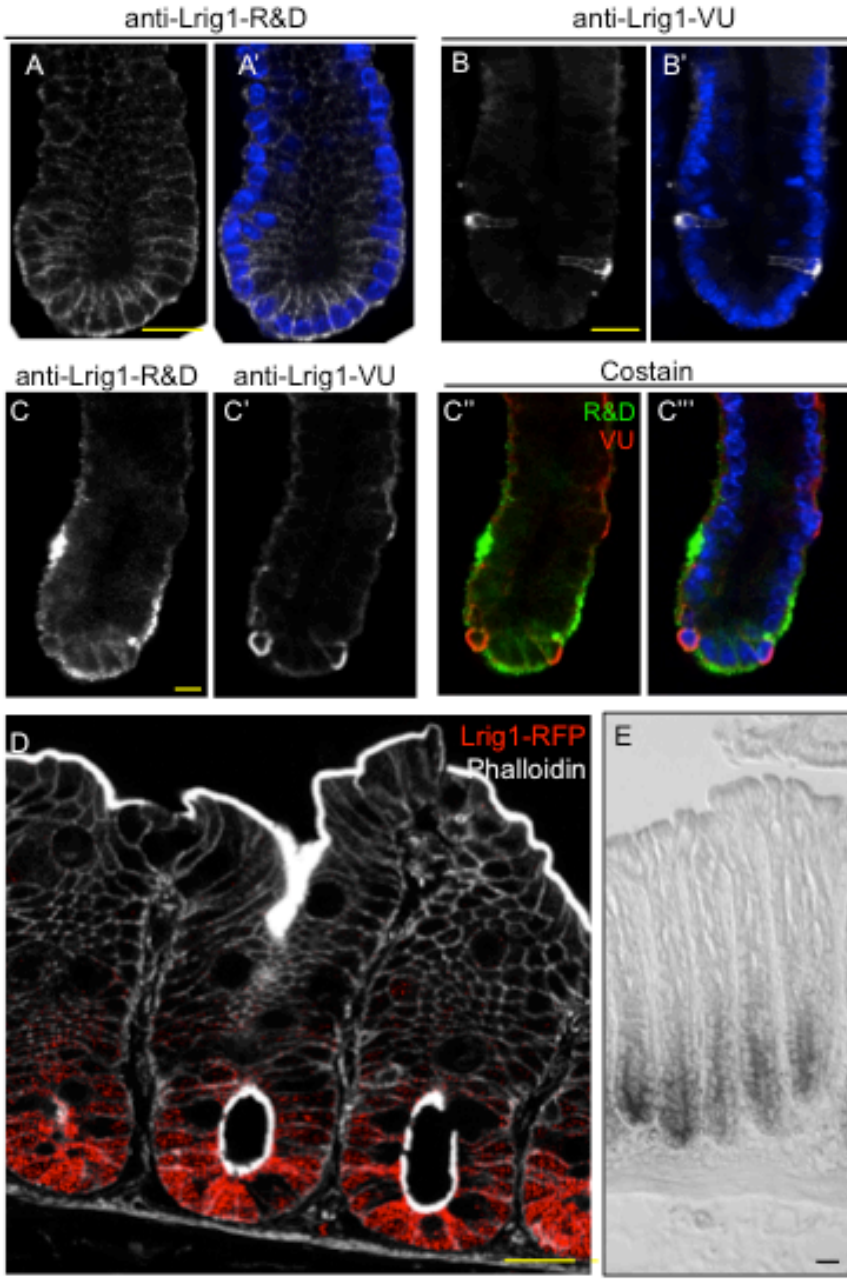

Figure 2.2. Anti-Lrig1-VU recognizes a subset of anti-Lrig1-R&D^{+} cells. A-B'. Immunofluorescent analysis of isolated mouse colonic crypts with anti-Lrig1-R&D (A; A', white) and anti-Lrig1-VU (B; B', white) counterstained with DAPI (A', B', blue). C-C'''. Single and co-immunofluorescence of isolated mouse colonic crypts with anti-Lrig1-R&D (C; C'', C''', green) and anti-Lrig1-VU (C'; C'', C''', red). D. Visualization of red fluorescent protein (RFP, red) in colonic tissue sections from *Lrig1*$^{Apple/+}$ mice, counterstained with phalloidin (white) to mark epithelial cells. E. *Lrig1 in situ* hybridization in mouse colonic tissue sections. All scale bars represent 25 μM.

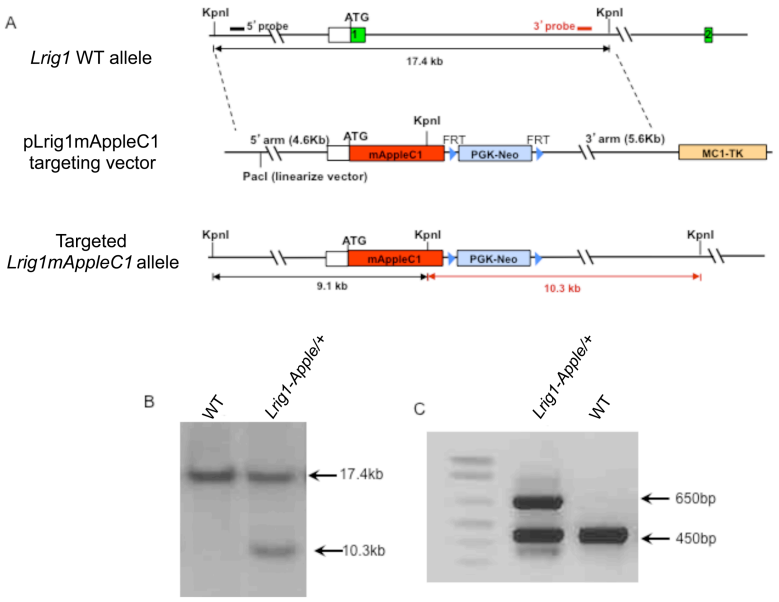

Figure 2.3. *Lrig1*$^{Apple/+}$ mice express Apple red fluorescent protein (RFP) driven from the endogenous *Lrig1* promoter. A. Schematic representation of the *Lrig1*^{Apple} allele. The coding sequence for mApple was targeted into the translational initiation site of the endogenous *Lrig1* locus. B. Southern blot analysis with the 3' probe after Kpn1 digestion of ES cell genomic DNA, demonstrating integration of the *Lrig1*^{Apple} allele into embryonic stem cells. C. Genotyping by PCR from *Lrig1*$^{Apple/+}$ and wild type (WT) mice. The *Lrig1*^{Apple} allele is 650 bp and the wild type *Lrig1* allele is 450 bp.

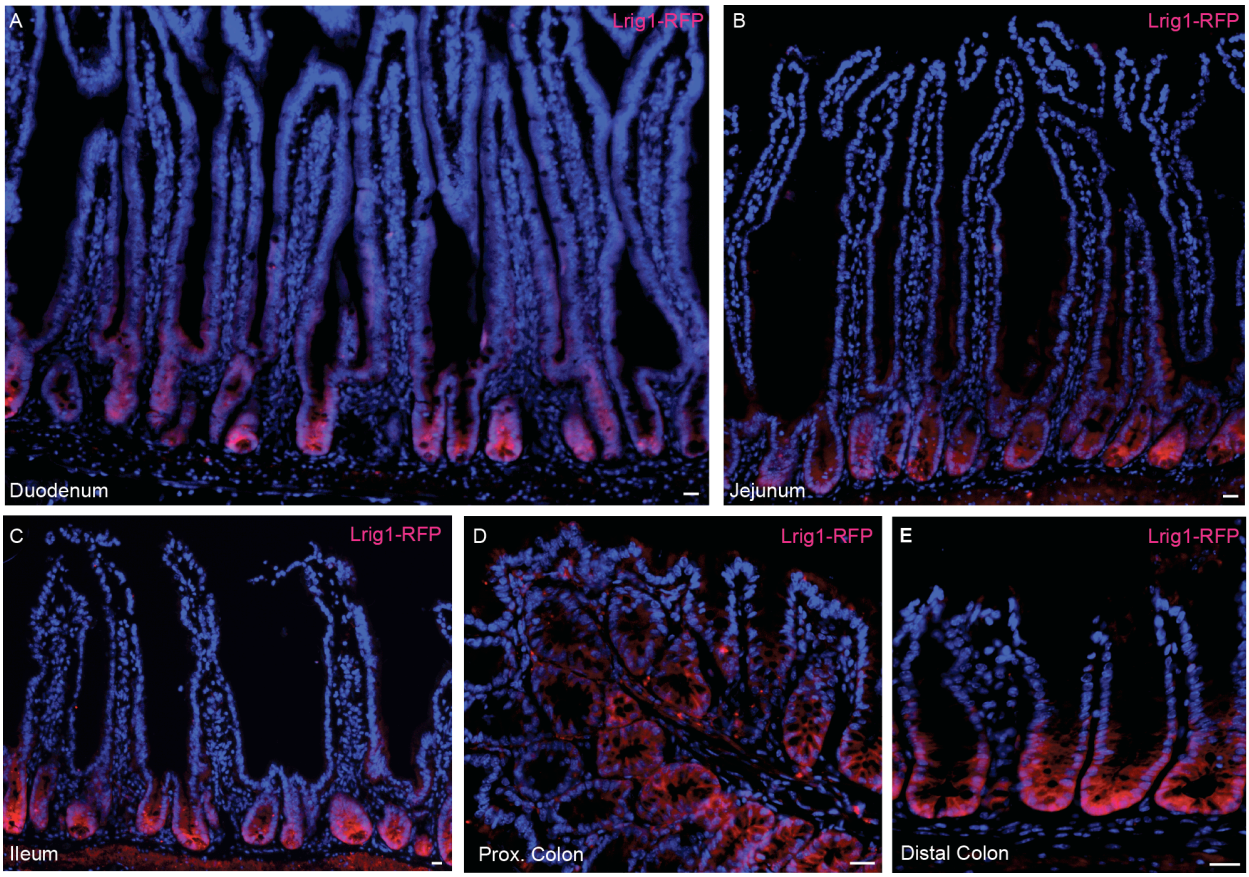

Figure 2.4. RFP fluorescence is uniformly detected in the base of small intestinal and colonic crypts. Direct RFP fluorescence detection in tissue sections from *Lrig1*$^{Apple/+}$ mice from the duodenum (A), jejunum (B), ileum (C), proximal colon (D), and distal colon (E). All sections were co-stained with DAPI. All scale bars represent 25 μM.

nuclear immunoreactivity with either antibody.

To facilitate our analysis, we generated a Lrig1 reporter mouse, *Lrig1*^{Apple}, which produces Apple fluorescent protein, a red fluorescent protein (RFP) variant, under control of the *Lrig1* promoter (Figure 2.3). Hereafter, we refer to this reporter mouse as *Lrig1*^{Apple} and Apple fluorescence as RFP. While RFP expression may not directly correlate with *Lrig1* transcript expression, it serves as a surrogate marker for *Lrig1* promoter activity. We detected RFP expression in the base of every crypt along the length of both the small and large intestine (Figure 2.2D; Figure 2.4) and observed consistent immunoreactive patterns with both Lrig1 antibodies in small intestinal and colonic tissue sections from *Lrig1*$^{Apple/+}$ mice (Figure 2.5). In particular, RFP was expressed in the colonic crypt base of *Lrig1*$^{Apple/+}$ mice in a pattern that closely resembled the anti-Lrig1-R&D immunoreactive zone (Figure 2.2D compared to A), consistent with *Lrig1 in situ* hybridization in mouse colon (Figure 2.2E). These observations suggest that the anti-Lrig1-R&D immunoreactive pattern more faithfully mirrors the *Lrig1* transcriptional readout than anti-Lrig1-VU, which recognizes a subset of cells with *Lrig1* promoter activity and anti-Lrig1-R&D immunoreactivity.

Lrig1-R&D and Lrig1-VU antibodies react specifically with Lrig1 protein

To determine the basis for the discrepancy in tissue staining patterns, we took a biochemical approach to directly compare anti-Lrig1-R&D and anti-Lrig1-VU. We previously validated anti-Lrig1-VU on *Lrig1*$^{-/-}$ colonic tissue sections and on intestinal epithelial cell lysates from *Lrig1*$^{CreERT2/CreERT2}$ mice, which lack Lrig1 protein (*32*). To further test the specificity of the two anti-Lrig1 antibodies, we performed western blot

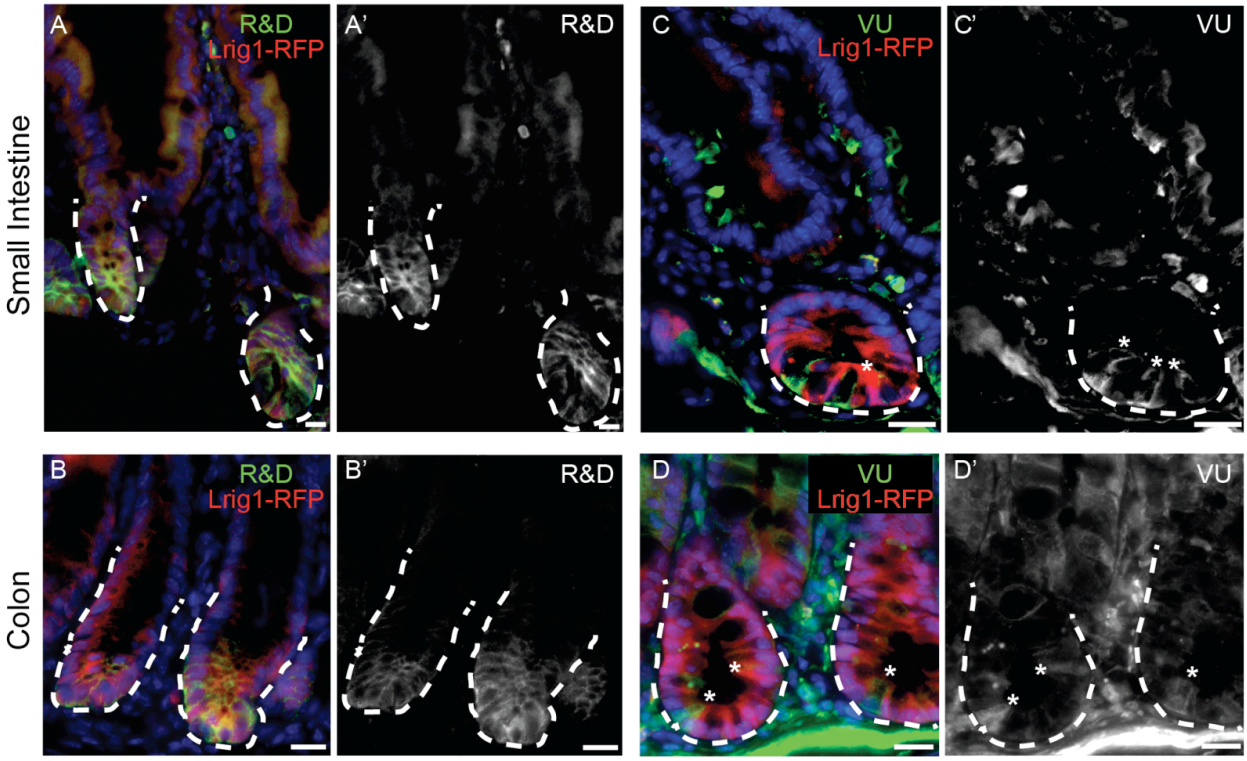

Figure 2.5. Anti-Lrig1-R&D and anti-Lrig1-VU immunoreactive patterns in small intestine and colon of *Lrig1*$^{Apple/+}$ mice. Small intestinal and colonic tissue sections from *Lrig1*$^{Apple/+}$ mice (red) stained with anti-Lrig1-R&D (green in A and B, and white in A' and B') and anti-Lrig1-VU (green in C and D, and white in C' and D'). All scale bars represent 25 μM.

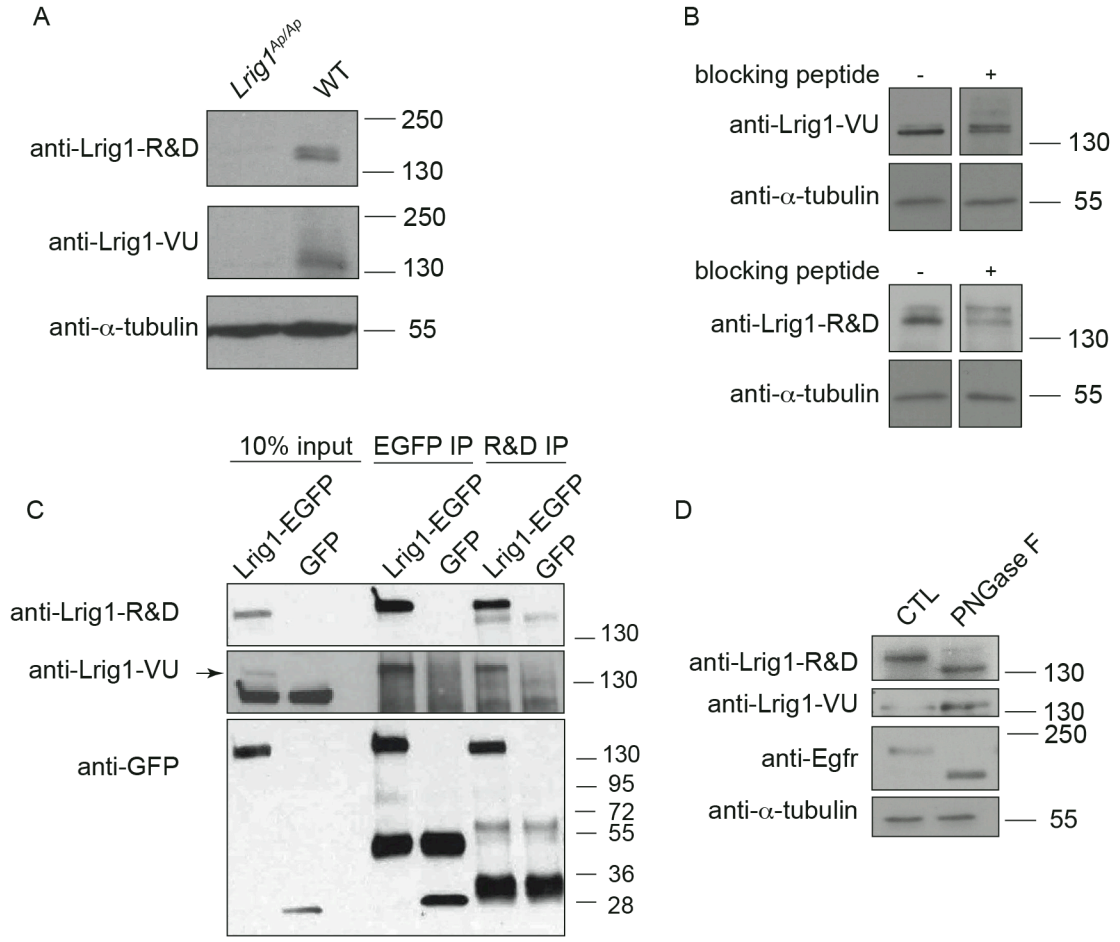

Figure 2.6. Anti-Lrig1-R&D and anti-Lrig1-VU are specific for Lrig1 protein. A. Western blot analysis of *Lrig1*$^{Apple/Apple}$ (*Lrig1*$^{Ap/Ap}$) or wild type (WT) mouse colonic epithelial cell lysates for Lrig1 using anti-Lrig1-R&D or anti-Lrig1-VU. α-tubulin serves as a loading control. B. Western blot analysis of wild type mouse colonic crypt lysates probed with anti-Lrig1-R&D and anti-Lrig1-VU with or without an anti-Lrig1-VU blocking peptide. C. GFP (lanes 3-4) or anti-Lrig1-R&D (lanes 5-6) immunoprecipitation from human HEK293T cell lysates, followed by western blot analysis for Lrig1 using anti-Lrig1-R&D, anti-Lrig1-VU, or anti-GFP. Lrig1-EGFP is predicted to be 146 kDa. Arrow indicates the Lrig1-specific band. D. Western blot analysis of wild type mouse colonic crypt lysate after treatment with the N-glycosidase, PNGaseF, using anti-Lrig1-R&D and anti-Lrig1-VU. Egfr serves as a positive control to demonstrate effective PNGaseF activity. CTL, control, untreated sample.

analysis using colonic epithelial cell lysates from *Lrig1*$^{Apple/Apple}$ (*Lrig1*$^{Ap/Ap}$) mice. The *Lrig1*^{Apple} allele was designed such that the *mAppleC1* coding sequence replaces that of the endogenous *Lrig1* gene at the translational initiation site; *Lrig1*$^{Apple/Apple}$ mice are therefore null for Lrig1 (Figure 2.3). Neither Lrig1 antibody detected Lrig1 protein in *Lrig1*$^{Apple/Apple}$ tissue lysates compared to lysates from wild type mice (Figure 2.6A). Addition of an anti-Lrig1-VU blocking peptide to anti-Lrig1-VU and anti-Lrig1-R&D partially blocked Lrig1 detection by western blot analysis (Figure 2.6B), supporting the specificity of anti-Lrig1-VU and confirming the anti-Lrig1-VU epitope lies within that of anti-Lrig1-R&D.

To further examine specificity, we generated a construct encoding EGFP-tagged mouse Lrig1 construct (*Lrig1-EGFP*), transiently expressed it in human embryonic kidney 293T (HEK293T) cells, and performed reciprocal immunoprecipitation and western blot analysis (Figure 2.6C). Both Lrig1 antibodies detected Lrig1-EGFP following GFP immunoprecipitation, indicating specificity for Lrig1 protein. In addition, anti-Lrig1-VU detected Lrig1-EGFP following immunoprecipitation with anti-Lrig1-R&D. We observed numerous non-specific bands that may reflect non-specific binding of anti-Lrig1-VU and GFP cleavage or degradation products. These results suggest that anti-Lrig1-R&D and anti-Lrig1-VU recognize the same protein *in vitro*.

The main difference between these two antibodies is their respective epitopes. Anti-Lrig1-R&D was raised against nearly the entire Lrig1 ectodomain (Ala37-Thr794). In contrast, anti-Lrig1-VU was raised against a short peptide sequence in the Lrig1 ectodomain (KILSVDGSQLKSY), corresponding to Lys128-Tyr140 within the third leucine-rich repeat (Figure 2.1) (*84*). The anti-Lrig1-R&D antigen is much larger, which

may allow greater epitope accessibility and be more permissive of post-translational modifications, such as glycosylation. In 2012, Kaji et al. published a global liquid chromatography mass-spectrometry (LC-MS) glycoprotein analysis using lysates from multiple mouse tissues (*85*). Using the GlycoProtein Database (GlycoProtDB, see Methods) constructed by this group, we found seven predicted N-glycosylation sites within the Lrig1 protein (Figure 2.1) (*85*). Without taking the three-dimensional folded structure into account, there is one predicted N-glycosylation site near the linear anti-Lrig1-VU antigenic peptide sequence: Asp152 (GlycoProtDB). To test whether glycosylation blocked the ability of anti-Lrig1-VU to recognize Lrig1 protein, we treated wild type mouse colonic crypt lysates with the N-glycosidase, PNGaseF, and observed that the form of Lrig1 recognized by anti-Lrig1-R&D underwent a shift to a faster migrating form, consistent with deglycosylation (Figure 2.6D). The band recognized by anti-Lrig1-VU did not change migration patterns, indicating that form is not glycosylated; we occasionally observed increased intensity of the anti-Lrig1-VU-specific band, suggesting deglycosylation generated a larger pool of the Lrig1 form recognized by anti-Lrig1-VU (Figure 2.6D). These data suggest that both anti-Lrig1 antibodies are specific for the mouse Lrig1 protein, but Lrig1 glycosylation may affect the ability of anti-Lrig1-VU to recognize Lrig1.

FACS reveals differences between anti-Lrig1-R&D^{+} and anti-Lrig1-VU^{+} cell populations

To characterize the cell populations recognized by these two Lrig1 antibodies, we performed fluorescence-activated cell sorting (FACS) analysis on colonic epithelial cells from *Lrig1$^{Apple/+}$* mice. Cells were isolated on the basis of RFP expression into RFP-hi, -

mid, and -neg cells (Figure 2.7A). We performed qRT-PCR to validate FACS-isolated cells expressed proportional *Lrig1* transcript levels (Figure 2.7B). RFP-neg cells did not express *Lrig1*, supporting the use of RFP as a *Lrig1* readout in this *in vivo* system. To determine whether there were differences between the RFP-hi and -mid populations other than *Lrig1*, we performed qRT-PCR for additional intestinal transcripts of interest. There were no appreciable differences in expression of *Villin1, carbonic anhydrase 1* (*Car1*)*,* and *Mucin 2* (*Muc2*) (Figure 2.8A-C); *Villin1* and *Car1* are expressed in both differentiated and undifferentiated cells from crypt base to lumen, while *Muc2* is expressed by goblet cells (*86-88*). Muc2 protein expression was distributed evenly throughout colonic crypts (Figure 2.8D). *c-Kit,* a proposed marker of a subset of colonic goblet cells that support $Lgr5^+$ cells (*89*), was not detectable by qRT-PCR (Figure 2.8E), which likely reflects the small number of RFP^+ cells that express c-Kit protein (Figure 2.8F). Importantly, we observed the RFP-hi population contained *Lgr5* expression, while RFP-mid and -neg populations did not (Figure 2.7C). This supports previous data where we showed there is a population of Lrig1-expressing cells that are distinct from the Lgr5 stem cell population (*32*).

To determine which RFP subpopulation was preferentially recognized by each antibody, we individually stained live RFP-hi, -mid, and -neg cells with each anti-Lrig1 antibody, and immediately re-analyzed them by flow cytometry. Anti-Lrig1-R&D (conjugated to Alexa-488) recognized 98% of RFP-hi cells, while anti-Lrig1-VU (conjugated to Alexa-647) recognized only 12% (Figure 2.7D). Anti-Lrig1-VU recognized mostly RFP-mid cells (44%) and displayed three apparent populations of reactivity,

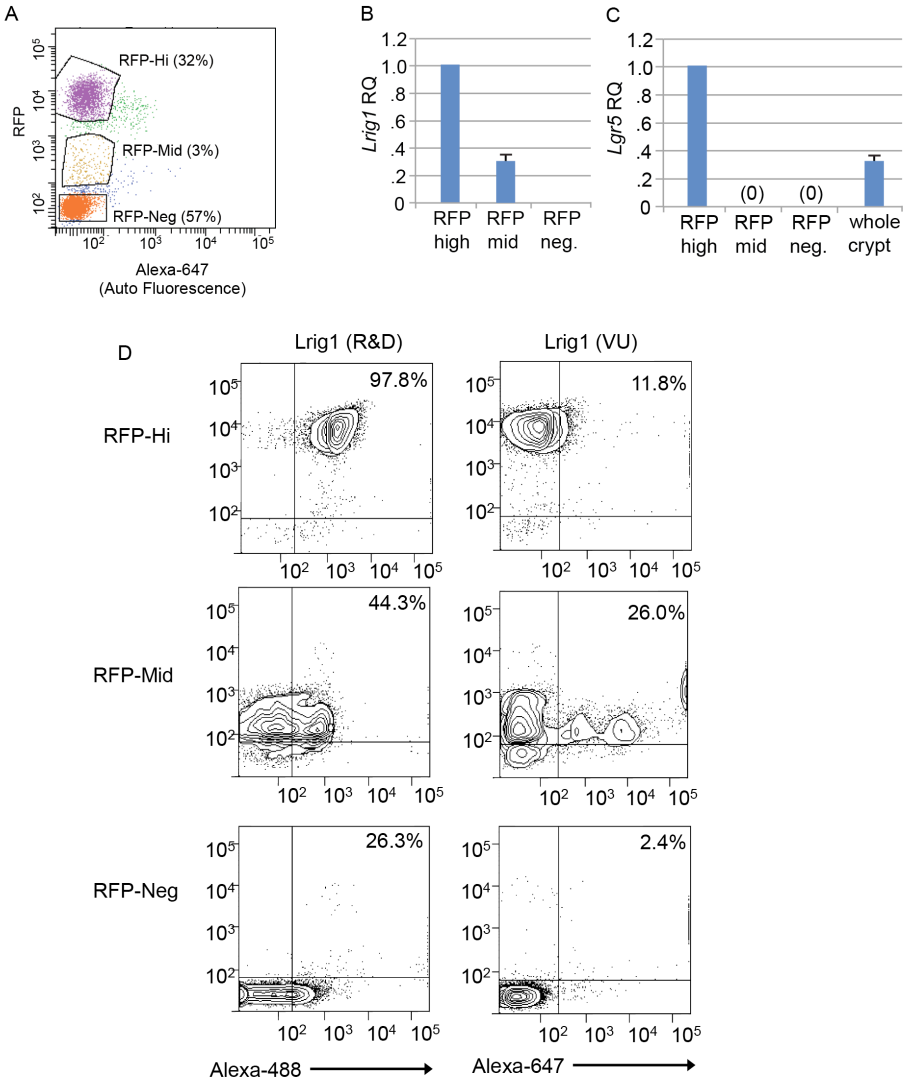

Figure 2.7. FACS sorting reveals differences between anti-Lrig1-R&D^{+} and anti-Lrig1-VU^{+} cell populations. A. Fluorescence-activated cell sorting (FACS) analysis of isolated colonic epithelial cells from *Lrig1*$^{Apple/+}$ mice into RFP-hi, -mid, and -neg populations. B, C. Relative *Lrig1* (B) and *Lgr5* (C) expression from FACS-isolated RFP-hi, -mid, and -neg colonic epithelial cells from *Lrig1*$^{Apple/+}$ mice (expression levels from whole colon crypts are shown for *Lgr5* as a control). RQ, relative quantity. D. FACS analysis of RFP-hi, -mid, and -neg colonic epithelial cells from *Lrig1*$^{Apple/+}$ mice co-sorted with anti-Lrig1-R&D (conjugated to Alexa-488) or anti-Lrig1-VU (conjugated to Alexa-647). Percentages indicate the number of cells present above 10^2 cells in each isolated population.

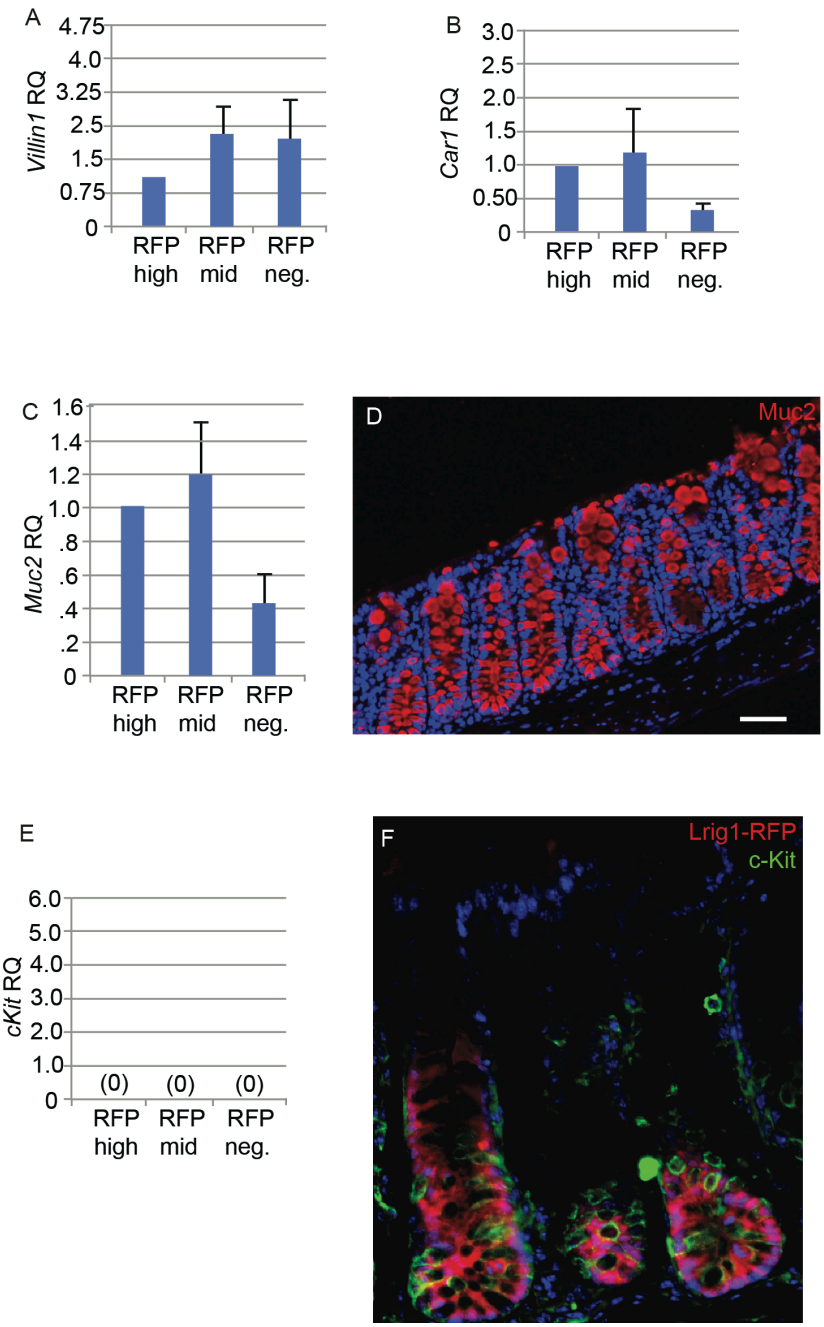

Figure 2.8. qRT-PCR and immunofluorescent analysis of RFP-hi, -mid, and -neg populations from *Lrig1*$^{Apple/+}$ mice. Relative expression of *Villin1* (A), *carbonic anhydrase 1* (*Car1*) (B) *and mucin 2* (*Muc2*) (C). D. Immunofluorescent staining for Muc2 (red) on wild type colon. E. *c-Kit* was undetectable by qRT-PCR. F. c-Kit immunofluorescence (green) on *Lrig1-Apple/+* colon tissue (red). All measurements are shown as relative quantity (RQ) compared to the RFP-hi expression set to 1. All scale bars represent 50 μM.

similar to what was observed when we applied this antibody to total colonic epithelium (*32*). Interestingly, anti-Lrig1-R&D recognized 26% of RFP-neg cells, which may complicate its use for cell sorting.

Discussion

Lrig1 marks an intestinal stem cell population, but due to antibody differences, the position of Lrig1 in the intestinal epithelium is unclear. To begin to decipher how the use of these reagents led to different conclusions about Lrig1$^+$ cells in the intestine, we set out to characterize the differences between two Lrig1 antibodies: one available commercially, anti-Lrig1-R&D, and one generated independently, anti-Lrig1-VU. In addition, we generated a new tool to study Lrig1: a Lrig1 reporter mouse, *Lrig1*^{Apple} that reflects *Lrig1* transcriptional activity. From our studies here, we conclude: (1) both Lrig1 antibodies are specific to Lrig1; (2) anti-Lrig1-R&D immunoreactivity closely mirrors *Lrig1* transcriptional activity, as determined by high RFP reporter expression and *Lrig1 in situ* hybridization; and (3) there are two subpopulations of Lrig1$^+$ cells in the intestinal epithelium that may differ based on the glycosylation status of Lrig1, RFP reporter expression, and *Lgr5* expression. Anti-Lrig1-VU recognizes a subset of Lrig1$^+$ cells, likely cells expressing a non-glycosylated form of Lrig1, while anti-Lrig1-R&D recognizes both glycosylated and non-glycosylated forms of Lrig1. However, it is important to note that we have not conclusively determined that the glycosylation status of Lrig1 explains the discrepancy in the immunoreactive pattern of each antibody in tissue sections.

The most obvious explanation for the observed discrepancy between these two antibodies is their respective antigenic differences: anti-Lrig1-R&D is raised against

nearly the entire Lrig1 ectodomain (Ala37-Thr794), while anti-Lrig1-VU is raised against twelve amino acids (Lys128-Tyr140) in the third leucine-rich repeat of the ectodomain (Figure 2.1) (*84*). When an anti-Lrig1-VU-specific blocking peptide was added, anti-Lrig1-R&D immunoreactivity was partially blocked (Figure 2.6B), suggesting that while the anti-Lrig1-VU epitope lies within that of anti-Lrig1-R&D, anti-Lrig1-R&D recognizes additional regions within the Lrig1 ectodomain. While there is little information known about Lrig1 structure, the anti-Lrig1-VU peptide lies within the leucine-rich repeat domains of the ectodomain, which alone are not required for Egfr association (*90*).

As the anti-Lrig1-VU epitope lies within that of anti-Lrig1-R&D, it follows that anti-Lrig1-VU recognizes a subset of anti-Lrig1-R&D$^+$ cells. Interestingly, we have demonstrated this subset is likely marked by a form of Lrig1 that is not glycosylated. As anti-Lrig1-VU recognizes the RFP-mid population, we expect this population would express mostly non-glycosylated Lrig1, while the RFP-hi population would express mostly glycosylated Lrig1. Glycosylation is involved in multiple cell functions, including protein-protein interactions, cell-cell adhesion, protein trafficking, cell surface receptor activation, and endocytosis (*91*). Glycosylation marks are dynamic and often change as the differentiation status of a cell changes, as in the immune system (*92*), and abnormal glycosylation states are often associated with cancer (*93*). It will be important to determine whether the differential glycosylation status of Lrig1 between the total anti-Lrig1-R&D$^+$ population and the anti-Lrig1-R&D/anti-Lrig1-VU$^+$ subpopulation has consequences relating to Lrig1 function and cell behavior.

To begin to investigate how the total Lrig1$^+$ population differs from the anti-Lrig1-VU subset, we compared gene expression of various intestinal genes between RFP-hi, -

mid, and -neg cell populations in colonic epithelial cells from *Lrig1*$^{Apple/+}$ mice. Of interest, we found *Lgr5* was expressed at the highest level in RFP-hi cells, which are mostly recognized by anti-Lrig1-R&D. In contrast, there was no *Lgr5* expression in RFP-mid (largely recognized by anti-Lrig1-VU) or RFP-neg cells. Since cells marked by the Lgr5-EGFP reporter are highly proliferative, this observation indicates that the proliferative status of RFP-hi and RFP-mid populations may differ. We previously showed that 25% of anti-Lrig1-VU^{+} cells express the proliferative marker Ki-67 at any given time, while 75% of Lgr5-EGFP^{+} cells express Ki-67 at any give time (*32*). We also demonstrated that anti-Lrig1-VU^{+} cells express little *Lgr5* transcript, but Lgr5-EGFP^{+} cells highly express *Lrig1* (*32*). Here, we demonstrate that most Lrig1^{+} cells do express *Lgr5*, but there is a distinct subset (RFP-mid) that does not, and anti-Lrig1-VU mostly recognizes this subset.

This study describes a useful new tool for the study of Lrig1: the *Lrig1*^{Apple} reporter mouse. Other intestinal stem cell reporter mice, such as Lgr5 (*25, 35*) and mTert (*35*) express GFP. The *Lrig1*^{Apple} RFP reporter mouse is therefore perfectly compatible with such GFP reporters to compare multiple stem cell populations in the same tissue. As Lrig1 is broadly expressed in many tissues (*94*), the *Lrig1*^{Apple} mouse will be a useful tool to examine the role of Lrig1 outside the intestine. It is important to note, however, in this model, RFP serves as a readout of *Lrig1* transcriptional activity only and may not accurately reflect the true, regulated *Lrig1* transcriptional unit or protein status in real time.

Although profiling of the entire Lrig1^{+} population is still lacking (but feasible using anti-Lrig1-R&D), RNA-Seq analysis demonstrated that the anti-Lrig1-VU^{+} cell profile is

characteristic of a stem cell population (*32*). Immunofluorescent analysis using anti-Lrig1-VU demonstrates that the position of this subpopulation in the colonic crypt varies; the anti-Lrig1-VU$^+$ cell position is not restricted to the crypt base columnar cell zone or the +4 position, but varies, most often occupying positions 2-5 [quantified in (*32*)].

In summary, we believe this study will be of interest to the intestinal stem cell field. There has been a reluctance to embrace Lrig1 as an intestinal stem cell marker because of the discrepancies between the two Lrig1-related studies published in 2012 (*32, 37*). Here, we hope to have clarified differences between two Lrig1 antibodies and the respective Lrig1$^+$ populations they recognize. We suggest the following usage for study of mouse Lrig1: to study all Lrig1$^+$ and *Lrig1*$^+$ cells in the intestinal crypt, we recommend using anti-Lrig1-R&D; when studying a Lrig1$^+$/*Lgr5*$^-$ subpopulation, we recommend using anti-Lrig1-VU. In addition, real time comparison of *Lrig1*$^+$ cells with other stem cell populations expressing GFP reporters is now possible with the use of *Lrig1*^{Apple} reporter mice in conjunction with anti-Lrig1-VU.

Materials and Methods

Mice

The *Lrig1-mAppleC1* construct was made by BAC recombineering using the *129 Lrig1* bacterial artificial chromosome (BAC) clone from the Sanger Institute (bMQ291-E18). The Apple red fluorescent protein variant excites at 568 nm and emits at 592 nm. The 5' and 3' oligonucleotide probes were generated by PCR; the primers used for their generation are listed in Table 2.1. The Transgenic Mouse/ES Cell Shared Resource at Vanderbilt University performed ES cell electroporation and blastocyst injections. ES

cell clones were screened by Southern blotting to identify *Lrig1-mAppleC1* integration. Chimeras were generated and individuals with germline transmission were identified by PCR genotyping of tail DNA (oligonucleotide primers listed in Table 2.1). Germline-transmitted *Lrig1-mAppleC1* chimeras were intercrossed with *FlpE* mice (B6.SJL strain) to eliminate the FRT-flanked PGK-neo cassette. Genotyping PCR identified wild type and *Lrig1*$^{Apple/+}$ mice. Loss of the PGK-neo cassette was detected by PCR (oligonucleotide primers listed in Table 2.1). All animal protocols were approved and performed in accordance with the Vanderbilt University Medical Center Animal Care and Use Program. Mice were fed standard rodent chow and water *ad libitum* and housed under controlled light cycle conditions.

Cloning of Lrig1-EGFP and transfection

Full-length mouse *Lrig1* cDNA (#MG50511-M, Sino Biological Inc.) was cloned into the pEGFP-N1 plasmid (#6085-1, Clonetech), resulting in the Lrig1-EGFP C-terminal fusion protein. Lrig1-pEGFP-N1 (Lrig1-EGFP) and pEGFP-N1 (EGFP) were transiently transfected into human HEK293T cells using Metafectene (Biontex, Germany) according to the manufacturer's instructions.

Isolation of colonic epithelium for western blotting, cell lysis, and immunoprecipitation

Intestinal tissue was freshly dissected and crypts were isolated as previously described (*32, 95*). Isolated crypt epithelium was lysed as previously described (*32*). Protein concentrations were determined using a microBCA assay kit (Pierce, Rockford, IL). Thirty milligrams of lysates were resolved on a 7.5% SDS-PAGE gel and western blotting was performed according to a standard western blotting protocol.

Autoradiography visualization was performed with ECL reagents (Perkin Elmer, Waltham, MA). The following primary antibodies were used for western blotting: anti-Lrig1-R&D 1:300 (#AF3688, R&D Systems, Minneapolis, MN); anti-Lrig1-VU 1:300 (made in collaboration with Covance, Denver PA (*32*)); anti-GFP 1:1000 (#A11122, Invitrogen, Grand Island, NY); and anti-α-tubulin 1:10,000 (#CP06, Calbiochem, San Diego, CA). Species-specific horseradish peroxidase (HRP)-conjugated secondary antibodies were obtained from Jackson ImmunoResearch (West Grove, PA). Transfected HEK293T cells were lysed with RIPA buffer (50mM Tris pH7.2; 150mM NaCl; 1% NP-40; 0.5% deoxycholic acid; 0.1% SDS) containing protease inhibitors (#P2714, Sigma, St. Louis, MO). Lysates were centrifuged to remove the insoluble pelleted fraction and the supernatant was used for immunoprecipitation. Five hundred micrograms of cell lysates were immunoprecipitated with anti-Lrig1-R&D, anti-Lrig1-VU, or anti-GFP, and recovered using Dynabeads® Protein A (#10001D, Invitrogen) or Dynabeads® Protein G (#10009D, Invitrogen). Immunoprecipitates were resolved with SDS-PAGE and western blotting as above.

Peptide blocking

Wild type mouse colonic crypt lysates were resolved by SDS-PAGE. Twenty-fold molar excess of anti-Lrig1-VU blocking peptide was added to anti-Lrig1-VU and anti-Lrig1-R&D and incubated at 4°C for four hours. The antibody-blocking peptide solutions were diluted in 5% bovine serum albumin and tris-buffered saline/Tween-20 (BSA-TBST) as above and western blotting was performed.

Deglycosylation of colonic crypt lysates

Colonic crypt lysates were isolated and prepared as above. For PNGaseF (#P0704S, New England Biolabs, Ipswich, MA) treatment, colonic crypt protein lysates were treated according to the manufacturer's instructions. Glycoprotein Denaturing Buffer (10X) was added to lysates to 1X final concentration and the reaction denatured at 100°C for ten minutes. G7 Reaction Buffer (10X) and 10% NP-40 were added to the reaction to 1X and 1% final concentrations, respectively. Fifty microliters of PNGaseF were added to make up a total final reaction volume of 1 mL and the reaction was incubated at 37°C for one hour.

In situ hybridization (ISH)

Unfixed fresh mouse tissues were embedded in Tissue-Tek® optimal cutting temperature (OCT) compound in a cold ethanol-dry ice bath and stored at -80ºC. Cryosections were cut at 15 mm thickness. *IS*H was performed as previously described (*96*). The *Lrig1* partial cDNA used for probe synthesis was obtained by RT-PCR with total RNA from isolated adult mouse colonic crypts. Primers used for RT-PCR are provided in Table 2.1. The synthesis of digoxigenin (DIG)-labeled probes was performed according to manufacturer's protocols (Roche).

Colonic crypt isolation and staining

Colonic epithelial crypts from wild type and uninduced *Lrig1*$^{CreERT2/+}$ mice were isolated and stained as previously described (*97*). The following primary antibodies were used for staining: anti-Lrig1-R&D 1:100 (#AF3688, R&D Systems, Minneapolis,

MN) and anti-Lrig1-VU 1:100. Anti-phalloidin was a generous gift from James R. Goldenring, M.D., Ph.D. Crypts were counterstained with the nuclear marker DAPI.

Tissue preparation and staining

Tissue preparation and staining were performed as previously described (*98*). Freshly dissected intestinal tissues were fixed in 4% paraformaldehyde (PFA) for one hour at room temperature, washed and submerged in 30% sucrose overnight at 4°C. The next day, fixed tissue was embedded for cryosectioning in Tissue-Tek® OCT compound and sectioned (5 mM sections) for staining. Immunostaining on frozen cryosections was performed as previously described (*99*). Direct fluorescence in the Cy3 channel was used to visualize RFP in tissue sections from *Lrig1*$^{Apple/+}$ mice. The following primary antibodies were used for immunofluorescence: anti-Lrig1-R&D 1:100 (#AF3688, R&D Systems, Minneapolis, MN); anti-Lrig1-VU 1:200 (generation described in (*32*); anti-Muc2 conjugated to Cy5 1.5:100 (#sc-15334, Santa Cruz, Dallas, TX); and anti-CD117 1:250 (c-Kit; #CBL1360, Millipore, Billerica, MA). All sections were counterstained with DAPI. Slides were visualized with an Olympus FV-1000 and Zeiss Imager M2.

FACS

Tissue for FACS was prepared as previously described (*32*). Briefly, freshly dissected mouse intestine was prepared and isolated crypts from *Lrig1*$^{Apple/+}$ mice were collected by slow centrifugation (400 rpm, five minutes). Crypts were resuspended in 3% pancreatin solution for ninety minutes (*95*), pipetted to single cells, and

resuspended in Hams F12 media with 1% FCS. DAPI (1:10,000; Sigma, St. Louis, MO) was used as a viability marker. RFP-hi, RFP-mid, and RFP-neg populations were isolated with a Becton Dickson FACSAria II using a 100 mm nozzle and placed on ice. Each cell fraction was subsequently stained with either anti-Lrig1-VU conjugated to Alexa-647 fluorophore (1:250) or anti-Lrig1-R&D conjugated to Alexa-488 fluorophore (1:250; #FAB3688G, R&D Systems) for thirty minutes on ice. Cells were then washed and subsequently analyzed on a Becton Dickson FACSAria II, using DAPI (1:10,000) as a viability marker. Cell doublets were eliminated on the basis of pulse width.

qRT-PCR analysis

Total RNA was isolated from FACS-isolated colonic epithelial cells using a RNeasy Micro Kit (#14004, Qiagen, Germantown, MD) and cDNA was made by reverse transcription using SuperScriptII (Invitrogen, Grand Island, NY). Triplicate qPCR was performed using the StepOnePlus Real-Time PCR system (Applied Biosystems, Grand Island, NY). qRT-PCR reaction components were as follows: 0.1 mM primers; 4 mM MgCl2; and EXPRESS SYBR GreenER Supermix with premixed ROX (A10315, Invitrogen, Grand Island, NY) in a 20 mL reaction. The reaction conditions were as follows: 50°C for two minutes; 95°C for two minutes; 95°C for fifteen seconds; 58°C for forty-five seconds (45 cycles); followed by a melting curve. Data were analyzed using the $\Delta\Delta$CT method. The primer sequences for genes assayed are shown in Table 2.1. All qRT-PCR assays were performed three times in triplicate.

Identification of Lrig1 glycosylation sites

We utilized the Glycoprotein database (found at http://jcggdb.jp/rcmg/gpdb/index) to identify predicted and confirmed Lrig1 N-glycosylation sites (*85*). This group confirmed N-glycosylation sites using LC-MS from mouse tissue lysates (*100, 101*). One confirmed Lrig1 N-glycosylation site was identified from murine brain tissue at N76; predicted Lrig1 N-glycosylation sites included: N152, N248, N294, N320, N385, and N686.

Southern Blot Screening			
Southern5'Probe5'	AGTTGCTGGCAGTGAGGAAT		
Southern5'Probe3'	AGGAATGCCACAAAGGGTTA		
Southern3'Probe5'	CCCCTGCCTTGTTCTTTGTA		
Southern3'Probe3'	ACACCTGCATTCTTCCAAGC		
Genotyping			
Lrig1 wild type 5'	TCTGGCTGCTCTTGCTGCTACT		
Lrig1 Apple 5'	ACGAGCTGTACAAGTAACCGGACT		
Lrig1 wild type 3'	GACTTCACGAGGCACACTCGAT		
PGK-Neo Cassette Detection			
Neo 5'	CTGTGCTCGACGTTGTCACTG		
and Neo 3'	GATCCCCTCAGAAGAACTCGT		
qRT-PCR			
Lrig1 5'	TAGAGGAGTGGCATCTGGAG		
Lrig1 3'	CCATGCGCTAAGGATTAAAA		
Lgr5 5'	GGAAGCGCTACAGAATTTGA		
Lgr5 3'	AGGCGTAGTCTGCTATGTGG		
cKit 5'	TCATCGAGTGTGAGGGAAA		
cKit 3'	GGTGACTTGTTTCAGGCACA		
Muc2 5'	GGTCCAGGGTCTGGATCACA		
Muc2 3'	GCTCAGCTCACTGCCATCTG		
Villin 5'	GATCTCCCAGGTGGTGGCTGC		
Villin 3'	CGGGAGTGGTGATGTTGAGAGAGC		
Car1 5'	AGAAAATGGCAAGTGCAGAC		
Car1 3'	AATTTCTTTGGCAGTTGCAG		
***Lrig1 IS*H**			
Lrig1 probe5'	GCTCTAGAGGGGGTCCCTCTATCCAA	antisense: XhoI/T7	750bp
Lrig1 probe3'	GGACTAGTATGCCCTCCTTTCCAACC	sense: SpeI/T3	

Table 2.1. Primer and probe sequences.

CHAPTER III

CHARACTERIZATION OF THE TRANSFORMATIVE CAPACITY OF LRIG1$^+$ CELLS

Introduction

Colorectal cancer (CRC) is thought to arise from the accumulation of mutational events (Figure 1.4, page 14) (*102*). The first event, a driver mutation, initiates transformation and most often occurs in the Wnt signaling modulator, *Adenomatous polyposis coli* (*APC*), a tumor suppressor "gatekeeper" gene. Upon loss of one *APC* allele, the second copy is lost through loss of heterozygosity (LOH) and regulation of Wnt signaling, through β-catenin transcriptional activity, is disrupted. *APC* mutations occur in about 80% of sporadic human CRCs (*50*) and are one of the most common ways to induce tumorigenesis in mouse models of intestinal neoplasia. The second event, often in an oncogene, causes tumor expansion, increasing the probability of acquiring additional mutations (*102*). About 30-40% of human CRCs contain an activating mutation in the small GTPase, KRAS, a downstream signaling modulator of many growth factor signaling pathways that is thought to contribute to tumor progression (*50, 103*).

Due to their longevity, adult intestinal stem cells are thought to be a tumor-initiating population. Supporting this idea, homozygous *Apc* loss in the crypt base columnar Lgr5$^+$ stem cell population and heterozygous *Apc* loss in the Lrig1$^+$ stem/progenitor population result in intestinal and colonic adenomas (*32, 76, 82*). Interestingly, tumorigenesis initiated by *Apc* loss in Lgr5$^+$ stem cells requires loss of

both *Apc* alleles, while loss of a single *Apc* allele in Lrig1$^+$ cells is sufficient for tumorigenesis, suggesting that these cell populations may differ in their inherent transformative capacity.

The above studies confirm that stem cells have tumor initiation potential; however, the ability of stem cell-driven *Apc* and *Kras* mutations to cause advanced colorectal neoplasia has been difficult to study in the mouse. Homozygous *Apc* loss combined with simultaneous expression of oncogenic Kras in the Lgr5$^+$ intestinal stem cell population causes morbidity within seven to ten days, precluding a study of tumorigenesis (*78*). A newer mouse model of colorectal neoplasia involves oncogenic Kras expression in *Apc*$^{fl/fl}$ mice using adenoviral delivery of Cre recombinase; mice develop colonic adenomas and carcinomas that invade and metastasize to the liver (*80*). In this model, adenoviral-cre mostly infects cells in the upper crypt, while cells in the stem cell zone are infected sporadically (*80*), complicating identification of the cell population(s) important for tumor initiation and progression.

Here, we set out to evaluate the transformative potential of combined *Apc* and *Kras* mutations in the Lrig1$^+$ population to determine whether multiple oncogenic events in Lrig1$^+$ stem/progenitor cells could lead to advanced colonic neoplasia. To avoid off-target effects of systemic expression of oncogenic Kras, we delivered 4-hydroxytamoxifen (4-OHT) directly to the distal colonic epithelium by enema to induce oncogenic mutations in *Apc* and *Kras*. We found that expression of mutant Kras activation did not significantly affect tumor histology in the setting of heterozygous or homozygous *Apc* loss, although may have contributed to increased invasion.

Results

Systemic oncogenic Kras expression in Lrig1^{+} cells causes oral tumors

We previously demonstrated that tumor-initiating events in Lrig1^{+} cells lead to tumorigenesis in an inducible mouse model of *Apc* loss: *Lrig1$^{CreERT2/+}$;Apc$^{fl/+}$* (*32, 82*). To investigate the role of Lrig1^{+} cells in tumor progression, we layered on a second oncogenic event, an activating mutation in the small GTPase Kras. The most common CRC-associated mutations in Kras are activating mutations that interfere with its GTPase activity. Such mutations lock the protein in a constitutively active state, stimulating growth-promoting and survival pathways (*104*). The widely used *Kras$^{LSL-G12D}$* allele permits tamoxifen-inducible expression of the G12D *Kras* mutant from the endogenous *Kras* locus; therefore, in this model, the inducible expression of oncogenic Kras occurs without overexpression (*105*). We first generated *Lrig1$^{CreERT2/+}$;Apc$^{fl/+}$* and *Lrig1$^{CreERT2/+}$;Apc$^{fl/+}$;Kras$^{LSL-G12D/+}$* mice to determine whether oncogenic Kras expression in the context of heterozygous *Apc* loss could lead to tumor progression. We found that systemic expression of mutant Kras using intraperitoneal tamoxifen injection resulted in rapid development of papillomas in the oral cavity (Figure 3.1), a phenotype reported elsewhere (*106*). *Lrig1$^{CreERT2/+}$;Kras$^{LSL-G12D/+}$* mice also developed oral papillomas within a similar time frame; *Lrig1$^{CreERT2/+}$;Apc$^{fl/+}$* mice did not develop oral tumors (data not shown). Tumors developed in the oral cavity within four to six weeks after tamoxifen injection (0.5 mg per mouse), a time frame too short to begin to observe changes within the intestine using this induction strategy (data not shown).

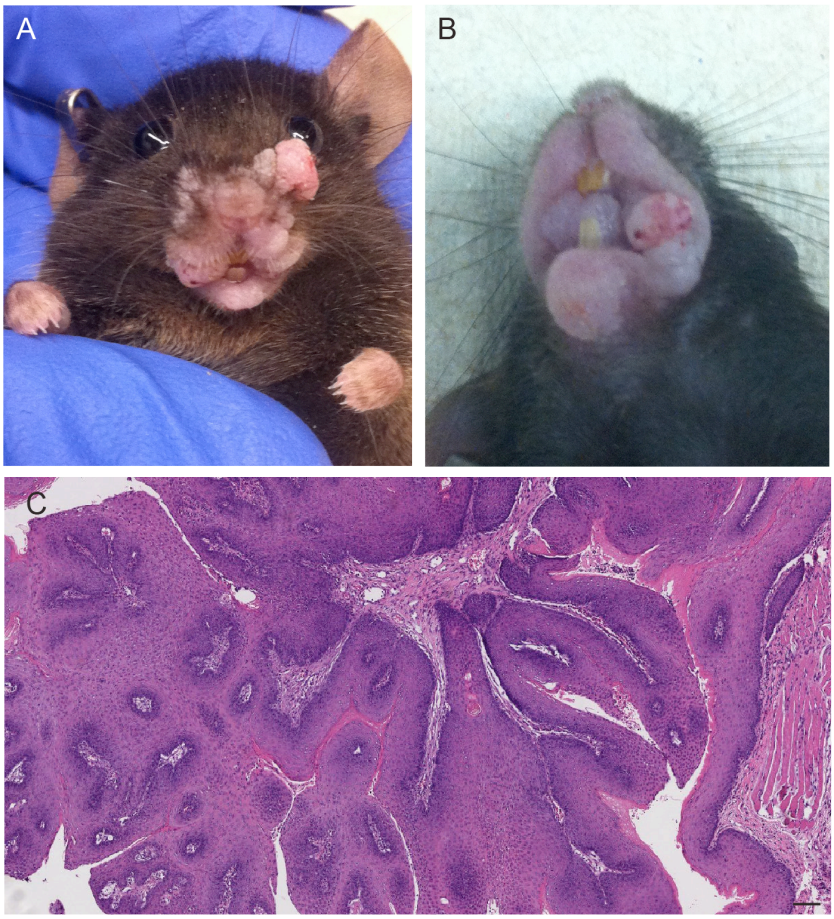

Figure 3.1. Systemic tamoxifen administration to *Lrig1*$^{CreERT2/+}$;*Apc*$^{fl/+}$;*Kras*$^{LSL-G12D/+}$ mice results in oral tumors. A, B. Representative examples of papillomas found in *Lrig1*$^{CreERT2/+}$;*Apc*$^{fl/+}$;*Kras*$^{LSL-G12D/+}$ mice following intraperitoneal injection of 0.5 mg tamoxifen per mouse. C. Cross sectional view of hematoxylin and eosin (H&E) stain of an oral tumor showing squamous papilloma histology. Scale bar represents 100 μm.

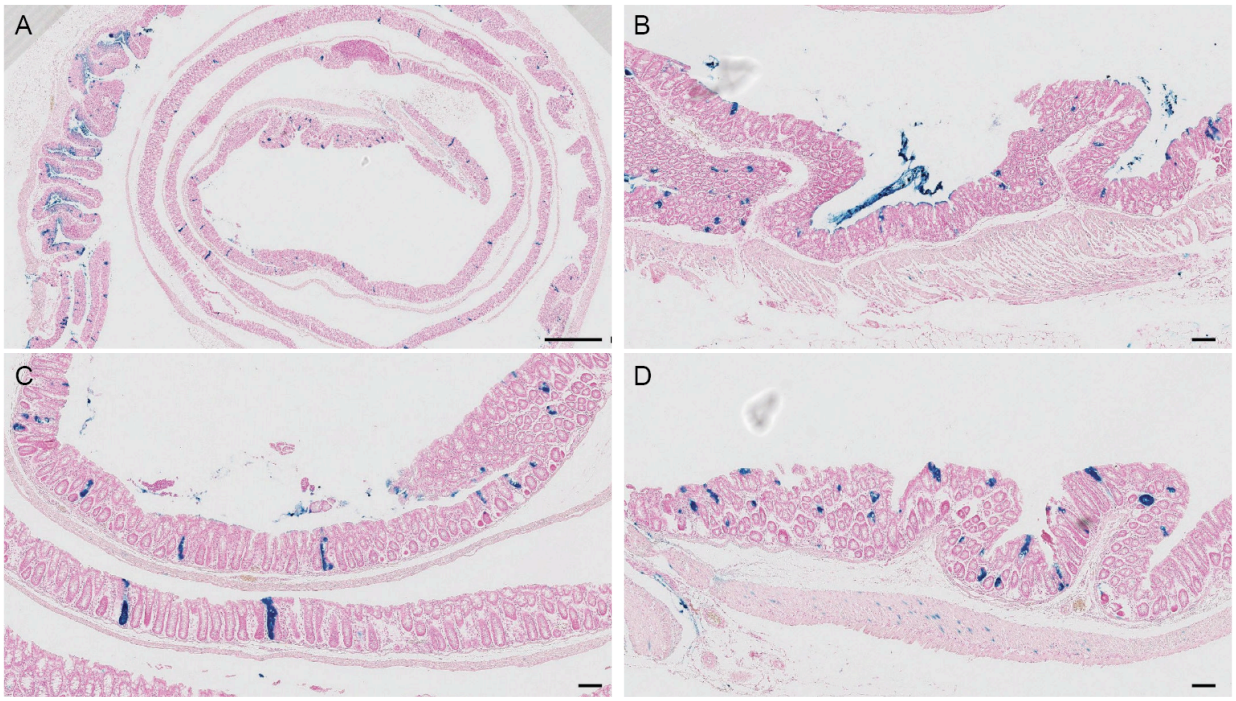

Figure 3.2. Lineage tracing after 4-hydroxytamoxifen (4-OHT) enema. *Lrig1*$^{CreERT2/+}$;*R26R*$^{lacZ/+}$ mice were sacrificed ten days after 4-OHT enema administration and staining for β-galactosidase (β-gal, blue) activity was performed. A. Cross sectional view of the entire colon at low power. High power views of areas from the proximal colon (B), medial colon (C), and distal colon (D). Scale bars represent 1 mm (A) and 100 μm (B-D).

4-OHT enema administration activates Cre recombinase in the colon

Tamoxifen must first be metabolized in the liver into its active form, 4-hydroxytamoxifen (4-OHT) before being distributed to distant tissues to activate Cre recombinase (*107*). To circumvent the systemic effects of mutant Kras expression, we delivered 4-OHT directly to the distal colon via enema. To verify that 4-OHT enema was an efficient method of activating Cre recombinase activation in the colonic epithelium, we performed lineage tracing analysis using *Lrig1*$^{CreERT2/+;}$*R26R*$^{lacZ/+}$ mice. Following Cre recombinase activation in Lrig1$^+$ cells, the *lacZ* gene is expressed from the ubiquitous *Rosa26* promoter and its gene product, β-galactosidase (β-gal), is made. β-gal activity is detected using 5-bromo-4-chloro-3-indolyl-β-D-galactopyranoside (X-gal), which produces a blue product in Lrig1$^+$ cells when hydrolyzed. Lrig1$^+$ stem cells and their progeny can then be visualized. Indeed, we observed fully labeled colonic crypts ten days after 4-OHT enema administration, confirming that Cre recombinase was activated; of note, we observed lineage tracing along the length of the colon, although the highest frequency of recombination occurred in the distal colon (Figure 3.2).

Colonic neoplasia in Lrig1$^{CreERT2/+}$*;Apc*$^{fl/+}$ and *Lrig1*$^{CreERT2/+}$*;Apc*$^{fl/+}$*;Kras*$^{LSL-G12D/+}$ *mice*

We then proceeded to administer 4-OHT enemas to *Lrig1*$^{CreERT2/+}$*;Apc*$^{fl/+}$ and *Lrig1*$^{CreERT2/+}$*;Apc*$^{fl/+}$*;Kras*$^{LSL-G12D/+}$ mice. We first observed that *Lrig1*$^{CreERT2/+}$*;Apc*$^{fl/+}$*;Kras*$^{LSL-G12D/+}$ mice developed marked crypt hyperplasia in the colon after 4-OHT enema compared to *Lrig1*$^{CreERT2/+}$*;Apc*$^{fl/+}$ mice (Figure 3.3A, B). Quantification of hyperplasia throughout the colon demonstrated that mutant Kras

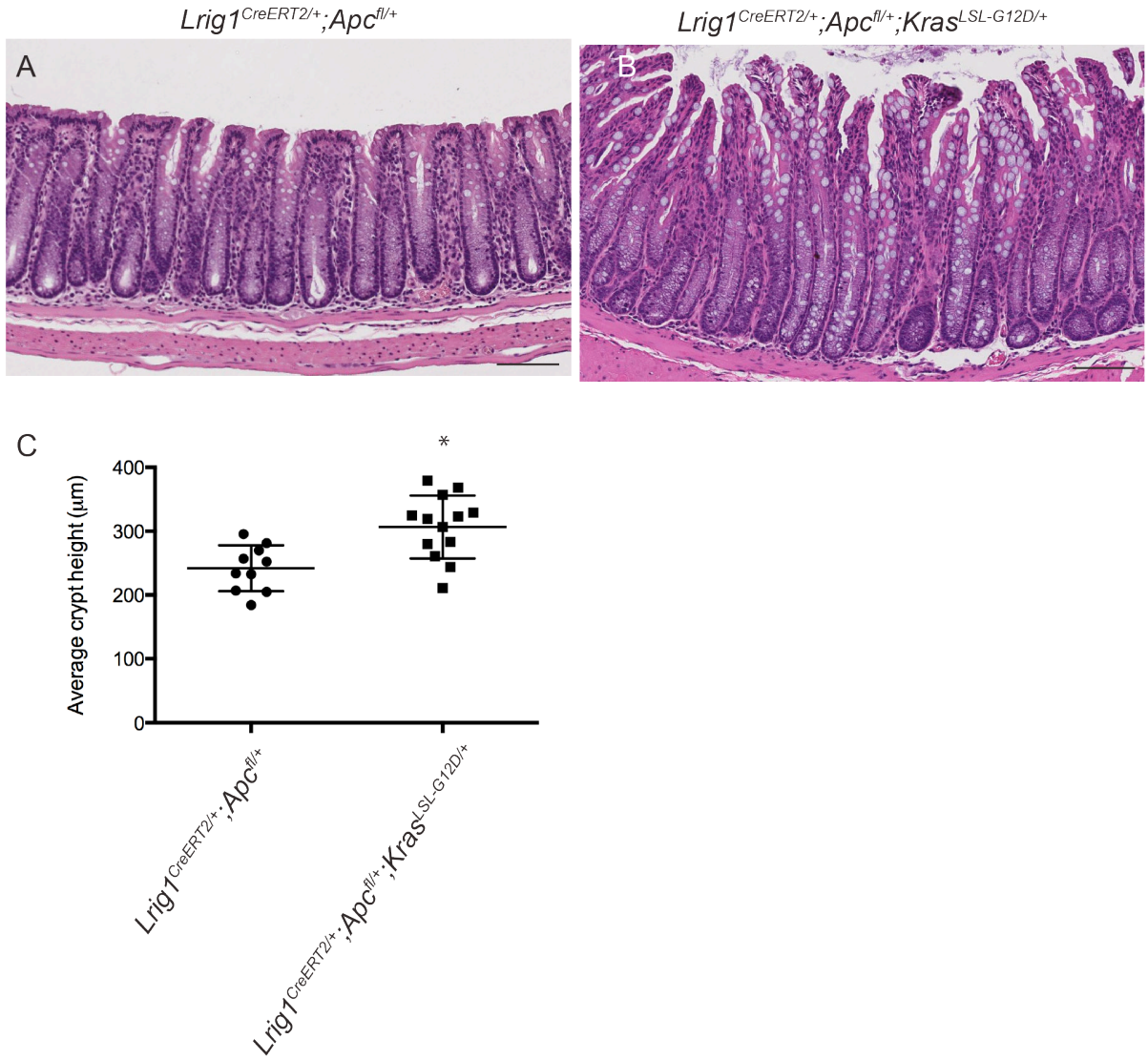

Figure 3.3. Mutant Kras causes crypt hyperplasia. A. H&E stain of colonic tissue from a *Lrig1*$^{CreERT2/+}$;*Apc*$^{fl/+}$ mouse 51 days after 4-OHT enema. B. H&E stain from an aged-matched *Lrig1*$^{CreERT2/+}$;*Apc*$^{fl/+}$;*Kras*$^{LSL-G12D/+}$ mouse. C. Dot plot quantifying average crypt height per individual mouse colon. Significance of $p<0.05$ is indicated by *. $p = 0.0015$. Scale bars represent 100 µm.

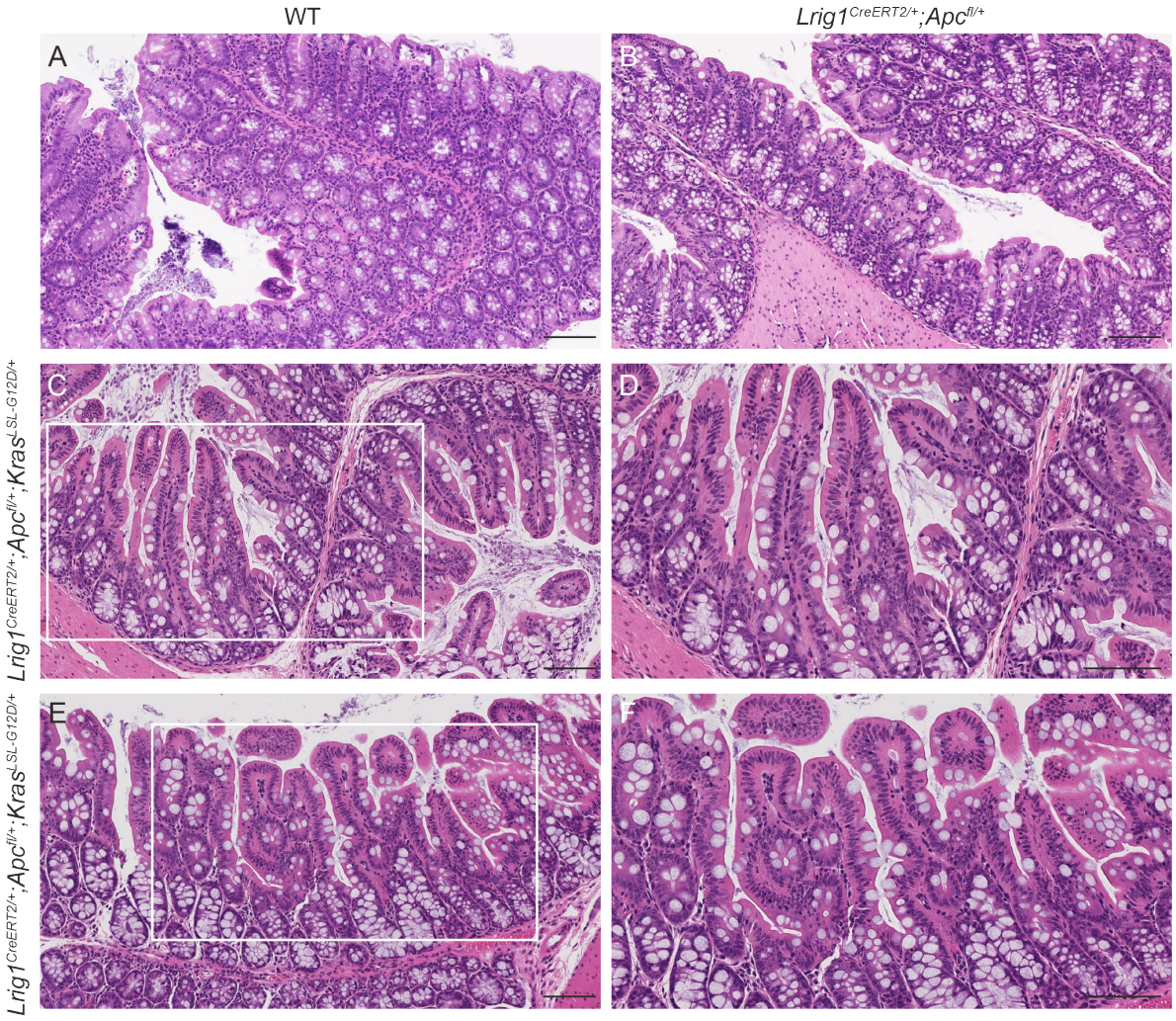

Figure 3.4. Mutant Kras causes morphological changes in the proximal colonic epithelium. H&E stain of proximal colon tissue sections from a wild type (WT) mouse (A), an *Lrig1*$^{CreERT2/+}$;*Apc*$^{fl/+}$ mouse 76 days after 4-OHT enema administration (B), and *Lrig1*$^{CreERT2/+}$;*Apc*$^{fl/+}$;*Kras*$^{LSL-G12D/+}$ mice 27 days (C, D) and 51 days (E, F) after 4-OHT enema administration. Boxed regions in (C) and (E) are magnified in (D) and (F), respectively. Scale bars represent 100 μm.

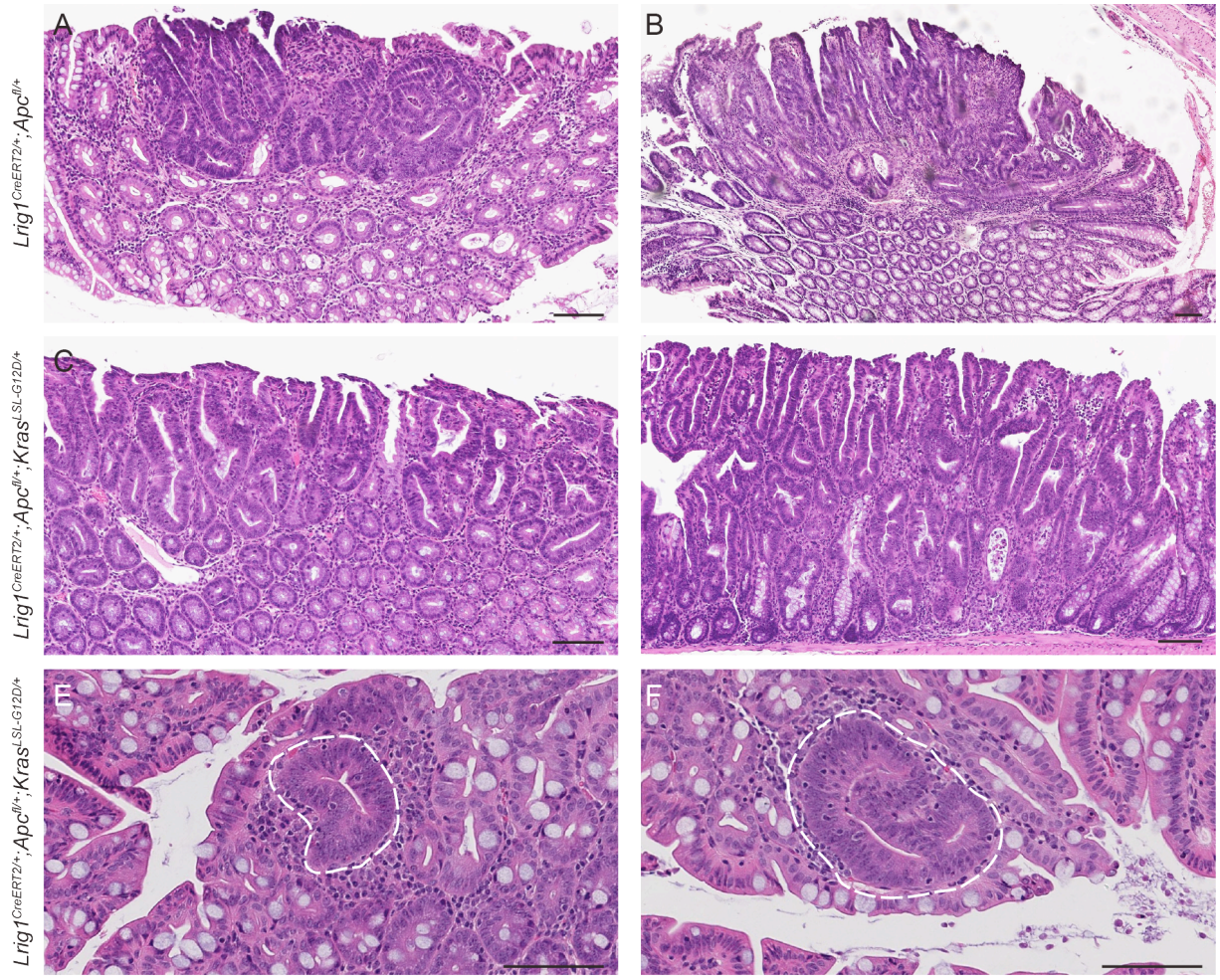

Figure 3.5. Adenoma development in *Lrig1*$^{CreERT2/+}$;*Apc*$^{fl/+}$ and *Lrig1*$^{CreERT2/+}$;*Apc*$^{fl/+}$;*Kras*$^{LSL-G12D/+}$ mice. H&E-stained colonic tissue sections showing adenomas from *Lrig1*$^{CreERT2/+}$;*Apc*$^{fl/+}$ (A, B) or *Lrig1*$^{CreERT2/+}$;*Apc*$^{fl/+}$;*Kras*$^{LSL-G12D/+}$ (C, D) mice 84 days (A), 76 days (B), or 21 days (C, D) after 4-OHT enema. E, F. Proximal colon single crypt adenomas (denoted by dotted white line) from *Lrig1*$^{CreERT2/+}$;*Apc*$^{fl/+}$;*Kras*$^{LSL-G12D/+}$ mice 35 days after 4-OHT enema administration.

expression significantly increased crypt height (Figure 3.3C). This phenotype has been previously reported upon oncogenic Kras expression in the intestine using multiple drivers (*79, 104, 108-110*). In addition, we observed morphological changes in the proximal colon of *Lrig1*$^{CreERT2/+}$;*Apc*$^{fl/+}$;*Kras*$^{LSL-G12D/+}$ mice compared to wild type or *Lrig1*$^{CreERT2/+}$;*Apc*$^{fl/+}$ mice. Proximal colonic crypts in wild type and *Lrig1*$^{CreERT2/+}$;*Apc*$^{fl/+}$ mice had a flat surface and were of uniform size (Figure 3.4A, B), while proximal colonic crypts in *Lrig1*$^{CreERT2/+}$;*Apc*$^{fl/+}$;*Kras*$^{LSL-G12D/+}$ mice displayed long villus-like structures with central fibrovascular cores; this phenotype was observed in 13/15 mice (Figure 3.4C-F). There appeared to be increased numbers of goblet cells (Figure 3.4C-F, compared to A, B) (not quantified) in the proximal colons of *Lrig1*$^{CreERT2/+}$;*Apc*$^{fl/+}$;*Kras*$^{LSL-G12D/+}$ mice. This phenotype is consistent with a previous study demonstrating that Kras activation alters differentiation within the colonic epithelium, leading to increased goblet cell differentiation (*109*).

We observed mostly small histologically low-grade colonic adenomas or microadenomas in *Lrig1*$^{CreERT2/+}$;*Apc*$^{fl/+}$ and *Lrig1*$^{CreERT2/+}$;*Apc*$^{fl/+}$;*Kras*$^{LSL-G12D/+}$ mice (Figure 3.5A-D); there were no histological differences in adenomas between the two genotypes. Interestingly, we did observe single crypt adenomas in the proximal colon of *Lrig1*$^{CreERT2/+}$;*Apc*$^{fl/+}$;*Kras*$^{LSL-G12D/+}$ mice (Figure 3.5E-F). High-grade dysplasia was not observed in either *Lrig1*$^{CreERT2/+}$;*Apc*$^{fl/+}$ or *Lrig1*$^{CreERT2/+}$;*Apc*$^{fl/+}$;*Kras*$^{LSL-G12D/+}$ mice up to 120 days after 4-OHT administration. In addition, oral tumors still developed in *Lrig1*$^{CreERT2/+}$;*Apc*$^{fl/+}$;*Kras*$^{LSL-G12D/+}$ mice given 4-OHT enema, although at a delayed and decreased frequency than in *Lrig1*$^{CreERT2/+}$;*Apc*$^{fl/+}$;*Kras*$^{LSL-G12D/+}$ mice given systemic

tamoxifen (data not shown). These observations complicate the use of this model for intestinal tumor studies.

Kras activation is not thought to be sufficient for tumor initiation (*104*). In fact, high Kras activity in the colonic epithelium in the absence of tumor-initiating events can result in oncogene-induced senescence, whereby growth suppressive pathways are activated to prevent transformation; such senescence markers can include $p16^{Ink4a}$ or $p19^{Arf}$ (*108*). Since we did not observe significant differences in tumorigenesis upon expression of oncogenic Kras, we hypothesized that oncogene-induced senescence may occur in mice expressing mutant Kras. We observed p19 immunoreactivity was significantly increased in crypts that were histologically normal in *Lrig1*$^{CreERT2/+}$*;Apc*$^{fl/+}$*;Kras*$^{LSL\text{-}G12D/+}$ mice compared to *Lrig1*$^{CreERT2/+}$*;Apc*$^{fl/+}$ mice (Figure 3.6). Although not confirmed, normal-appearing crypts likely contained wild type Apc protein, and therefore, were not transformed. p19 immunoreactivity in histologically normal crypts suggests that cell cycle inhibitory pathways might be upregulated through an oncogene-induced senescence pathway to combat Kras activity in the absence of *Apc* loss. Confirmation of oncogene-induced senescence is ongoing.

Colonic neoplasia in Lrig1$^{CreERT2/+}$*;Apc*$^{fl/fl}$ *and Lrig1*$^{CreERT2/+}$*;Apc*$^{fl/fl}$*;Kras*$^{LSL\text{-}G12D/+}$ *mice*

Lrig1$^{CreERT2/+}$*;Apc*$^{fl/+}$ and *Lrig1*$^{CreERT2/+}$*;Apc*$^{fl/+}$*;Kras*$^{LSL\text{-}G12D/+}$ mice were not ideal models of advanced colonic neoplasia. This could be due to inefficient Cre recombinase activity or low 4-OHT concentration. Additionally, expression of oncogenic Kras did not significantly affect tumor progression. To initiate tumorigenesis in a more robust way, we generated *Lrig1*$^{CreERT2/+}$*;Apc*$^{fl/fl}$ and *Lrig1*$^{CreERT2/+}$*;Apc*$^{fl/fl}$*;Kras*$^{LSL\text{-}G12D/+}$ mice. In this

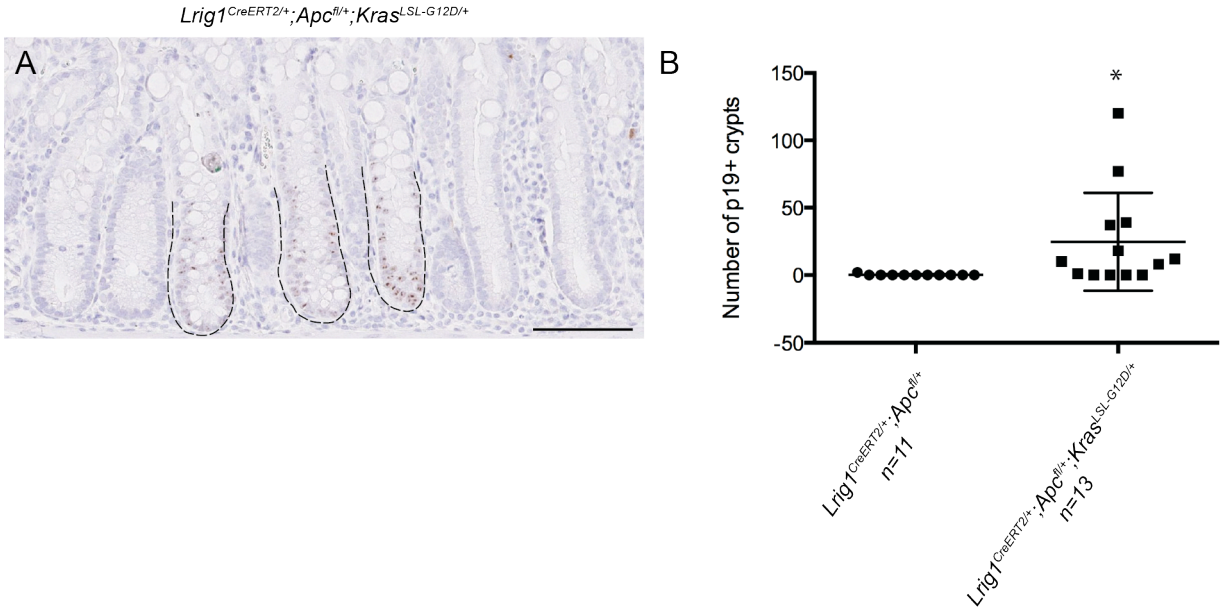

Figure 3.6. Oncogenic Kras increases p19 expression in normal-appearing crypts. (A) p19 immunohistochemistry (brown) of colonic tissue from a *Lrig1*$^{CreERT2/+}$;*Apc*$^{fl/+}$;*Kras*$^{LSL\text{-}G12D/+}$ mouse 41 days after 4-OHT enema administration, displaying normal-appearing crypts (dotted line) with p19^{+} nuclei. (B) Dot plot quantifying the number of normal-appearing p19^{+} crypts per colon per mouse. Significance of $p<0.05$ is indicated by *. p = 0.0360. Scale bars represent 100 μm.

model, both *Apc* alleles are simultaneously lost, resulting in rapid tumor initiation. Of note, systemic tamoxifen administration to *Lrig1*$^{CreERT2/+}$;*Apc*$^{fl/fl}$ mice results in death within five days due to loss of differentiated intestinal epithelial cells (data not shown). However, since 4-OHT enema only affects the distal region of the colon, mice are viable for up to two months.

As expected, tumorigenesis occurred rapidly in both genotypes after 4-OHT administration (Figure 3.7). Tumor formation was highly variable mouse-to-mouse (Figure 3.7A-F), possibly due to variable 4-OHT delivery and/or recombination efficiency. Tumors occurred in the distal colon, as expected, and we occasionally observed tumors in the small intestine (data not shown), likely due to systemic uptake of 4-OHT. About 40% of *Lrig1*$^{CreERT2/+}$;*Apc*$^{fl/fl}$ mice and almost 80% of *Lrig1*$^{CreERT2/+}$;*Apc*$^{fl/fl}$;*Kras*$^{LSL\text{-}G12D/+}$ mice developed rectal prolapse, which arose as early as 18 days after 4-OHT administration (Figure 3.7G).

Mice from both genotypes developed polypoid tumors that arose in the distal colon, away from the rectal prolapsed areas (Figure 3.7C, E, F). These tumors could progress to histologically high-grade adenomas (Figure 3.8). Invasion was never observed in these polypoid adenomas. The epithelium of the rectal prolapse in both *Lrig1*$^{CreERT2/+}$;*Apc*$^{fl/fl}$ mice and *Lrig1*$^{CreERT2/+}$;*Apc*$^{fl/fl}$;*Kras*$^{LSL\text{-}G12D/+}$ mice was composed of adenomatous tissue (Figure 3.9). These adenomas had a flat appearance and were mostly histologically low-grade. However, we did observe occasional invasion in these tumors (Figure 3.9B, C, E, F, black arrows). Of note, invasion in mice expressing oncogenic Kras was more infiltrative and associated with a greater desmoplastic response (Figure 3.9D-F).

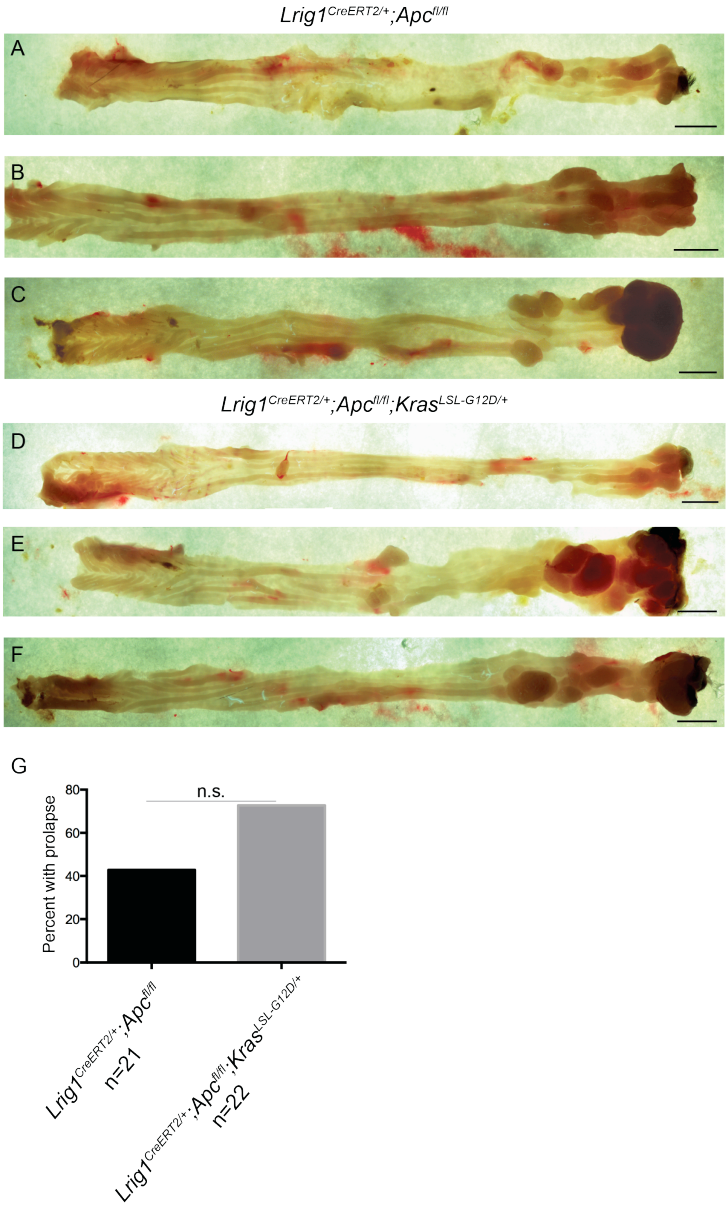

Figure 3.7. Tumor burden in *Lrig1*$^{CreERT2/+}$;*Apc*$^{fl/fl}$ and *Lrig1*$^{CreERT2/+}$;*Apc*$^{fl/fl}$;*Kras*$^{LSL-G12D/+}$ mice. Representative wholemount images of colons from *Lrig1*$^{CreERT2/+}$;*Apc*$^{fl/fl}$ mice four weeks (A), seven weeks (B), and ten weeks after 4-OHT enema (C); or *Lrig1*$^{CreERT2/+}$;*Apc*$^{fl/fl}$;*Kras*$^{LSL-G12D/+}$ mice four weeks (D), or eight weeks (E, F) after 4-OHT enema. G. Bar graph quantifying the percentage of each genotype that developed rectal prolapse. n.s., not significant. Scale bars represent 5 mm.

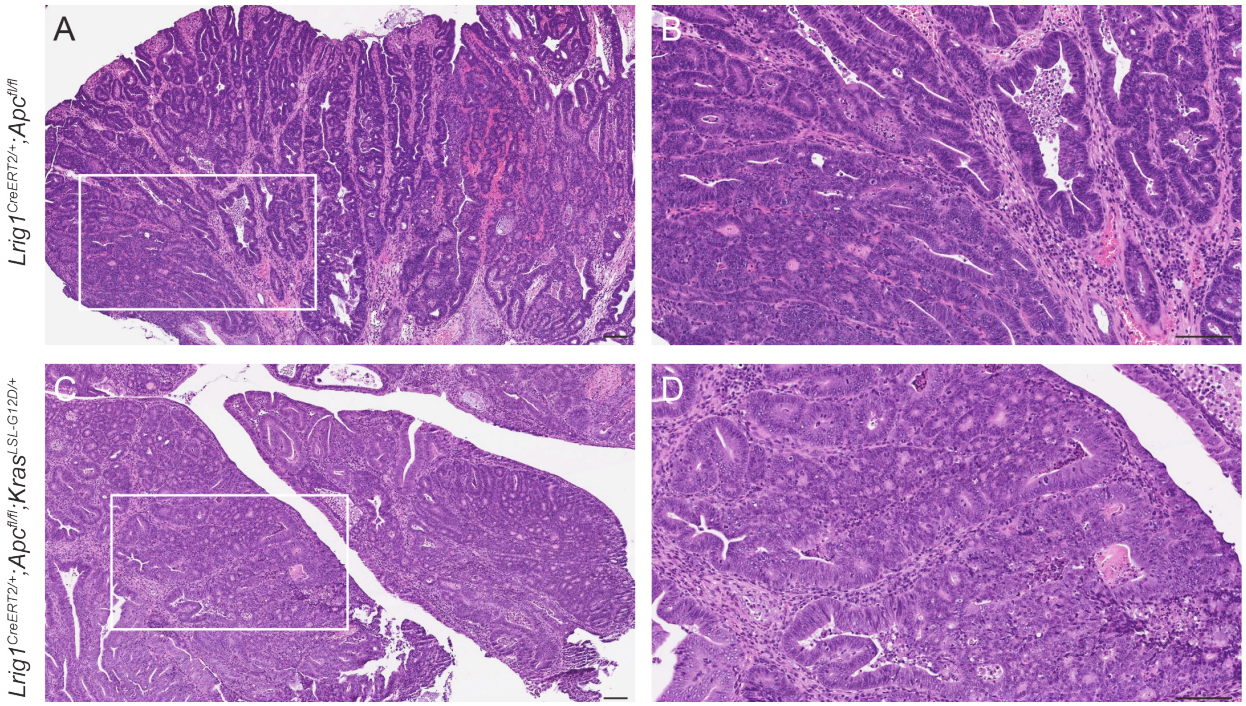

Figure 3.8. Histologically high-grade colonic adenomas from *Lrig1*$^{CreERT2/+;}$*Apc*$^{fl/fl}$ and *Lrig1*$^{CreERT2/+;}$*Apc*$^{fl/fl}$*;Kras*$^{LSL-G12D/+}$ mice. H&E staining of polypoid tumors from *Lrig1*$^{CreERT2/+;}$*Apc*$^{fl/fl}$ (A, B) and *Lrig1*$^{CreERT2/+;}$*Apc*$^{fl/fl}$*;Kras*$^{LSL-G12D/+}$ (C, D) mice 70 days (A, B) and 45 days (C, D) after 4-OHT administration. Boxed regions in (A) and (C) are magnified in (B) and (D), respectively. Scale bars represent 100 μm.

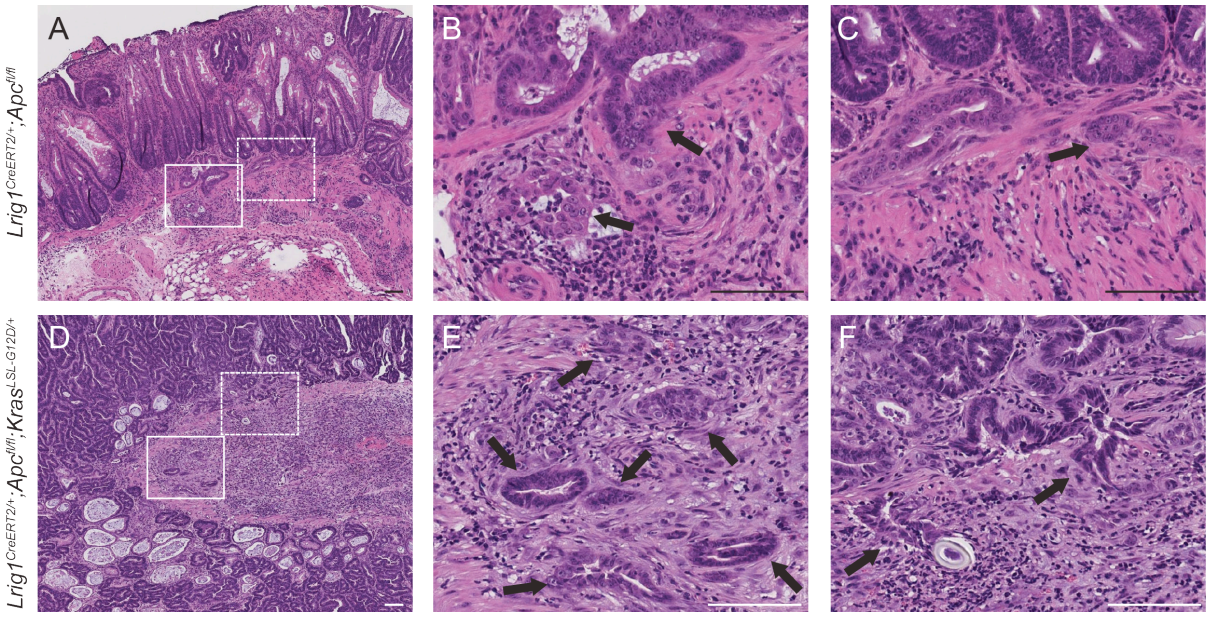

Figure 3.9. *Apc* loss causes invasion in areas of rectal prolapse independent of oncogenic Kras expression. H&E staining of tumor tissue from within the rectal prolapse of *Lrig1*$^{CreERT2/+;}$*Apc*$^{fl/fl}$ (A-C) and *Lrig1*$^{CreERT2/+;}$*Apc*$^{fl/fl}$;*Kras*$^{LSL-G12D/+}$ (D-F) mice 70 days (A-C) and 30 days (D-F) after 4-OHT administration. Solid line boxed regions in (A) and (D) are magnified in (B) and (E), respectively. Dashed boxed regions in (A) and (D) are magnified in (C) and (F), respectively. Black arrows denote instances of invasion. Scale bars represent 100 μm.

These observations suggest that complete loss of *Apc* in Lrig1^{+} cells can result in invasion, independent of Kras mutations, but might cause more infiltrative invasion. Unfortunately, we cannot study mice past 60-80 days due to the severity of rectal prolapse. Additionally, the rectal prolapse is an inflammatory environment, which may contribute to invasion in both genotypes.

To evaluate Apc loss of function and subsequent dysregulation of Wnt signaling in tumors, we performed immunofluorescence for β-catenin. β-catenin is normally expressed on the cell membrane, but is mislocalized when Apc function is perturbed. We observed β-catenin localization in the cytoplasm and nucleus of tumor cells from both *Lrig1*$^{CreERT2/+}$*;Apc*$^{fl/fl}$ mice and *Lrig1*$^{CreERT2/+}$*;Apc*$^{fl/fl}$*;Kras*$^{LSL\text{-}G12D/+}$ mice (Figure 3.10), suggesting that in this model, *Apc* loss activates canonical Wnt signaling. Of note, β-catenin immunoreactivity was often heterogeneous, with some transformed glands displaying both membranous and cytoplasmic/nuclear β-catenin localization (Figure 3.10D). Studies are ongoing to confirm whether β-catenin localization is correlated with *Apc* status.

Kras activation results in downstream phosphorylation and activation of extracellular signal-regulated kinase (Erk1/2). To determine whether p-Erk1/2 could serve as a potential readout of oncogenic Kras in tumors, we performed immunohistochemistry for p-Erk1/2 in tumors from *Lrig1*$^{CreERT2/+}$*;Apc*$^{fl/fl}$ (Figure 3.11A-D) and *Lrig1*$^{CreERT2/+}$*;Apc*$^{fl/fl}$*;Kras*$^{LSL\text{-}G12D/+}$ (Figure 3.11E-H) mice. Surprisingly, we observed Erk1/2 activation in tumors from both genotypes and found that its localization was highly heterogeneous. Some tumors expressed nuclear or cytoplasmic p-Erk1/2, and both localizations could be found within the same tumor (Figure 3.11A, B, E, F).

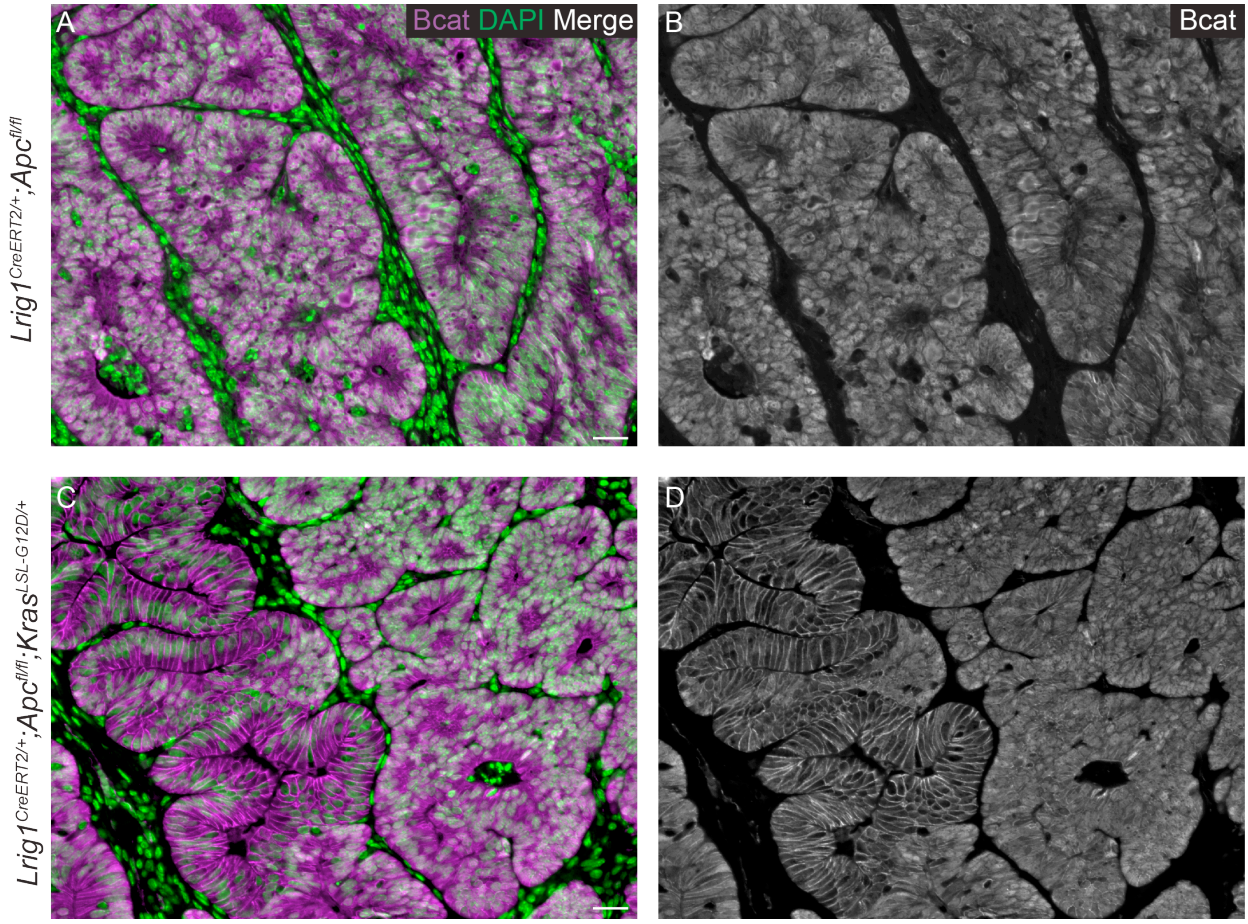

Figure 3.10. *Apc* loss results in activation of canonical Wnt signaling. β-catenin immunofluorescence (A, C, purple; B, D) of tumors from *Lrig1*$^{CreERT2/+}$;*Apc*$^{fl/fl}$ or *Lrig1*$^{CreERT2/+}$;*Apc*$^{fl/fl}$;*Kras*$^{LSL-G12D/+}$ mice 62 or 45 days after 4-OHT administration, respectively. Nuclei were stained with DAPI (A, C, green). Scale bars represent 25 μm.

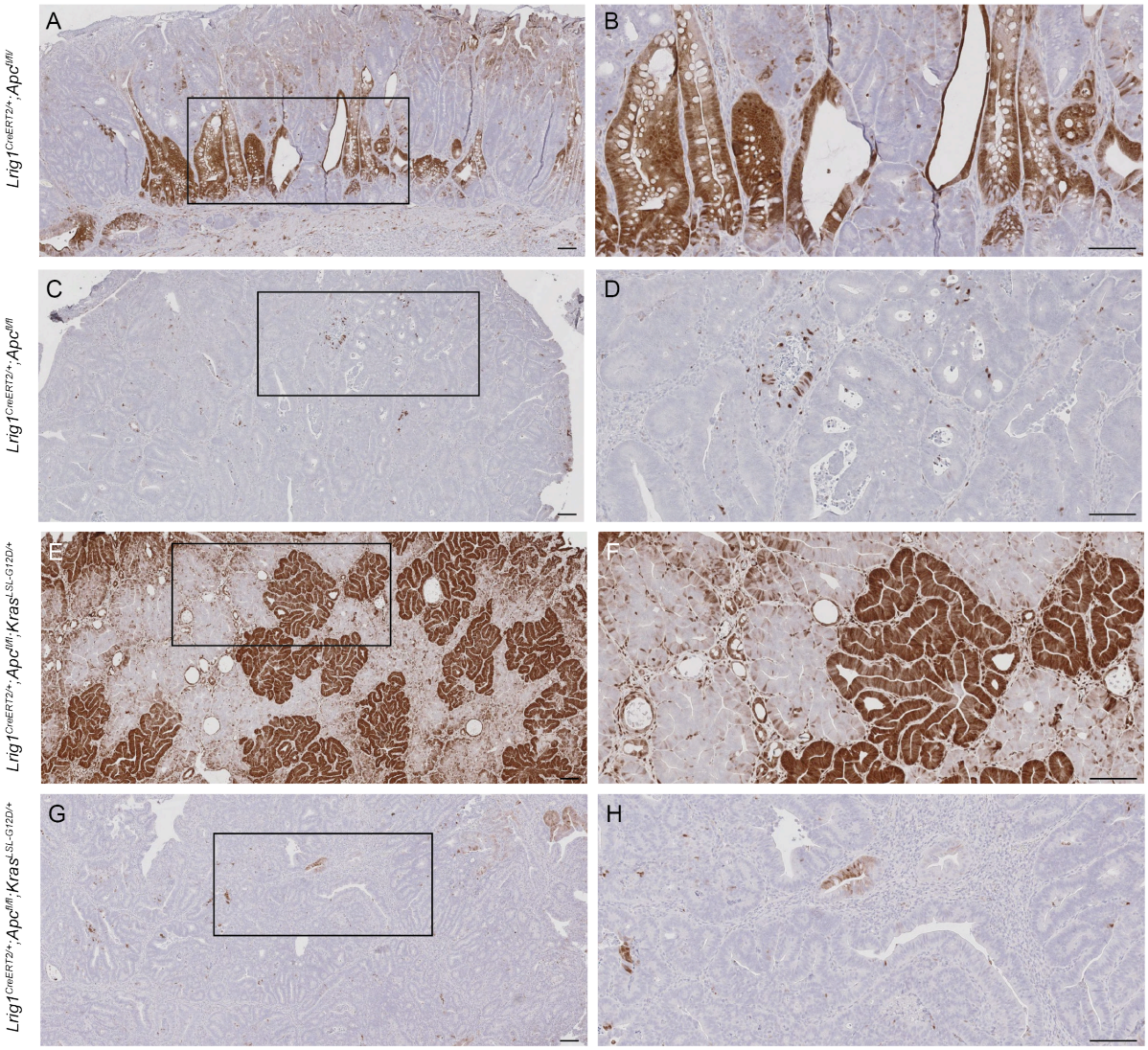

Figure 3.11. p-Erk1/2 is expressed heterogeneously in tumors from *Lrig1*$^{CreERT2/+}$;*Apc*$^{fl/fl}$ and *Lrig1*$^{CreERT2/+}$;*Apc*$^{fl/fl}$;*Kras*$^{LSL-G12D/+}$ mice. Immunohistochemistry for p-Erk1/2 (brown) in tumors from *Lrig1*$^{CreERT2/+}$;*Apc*$^{fl/fl}$ mice 71 days (A, B) and 36 days (C, D) after 4-OHT enema administration. Immunohistochemistry for p-Erk1/2 (brown) in tumors from *Lrig1*$^{CreERT2/+}$;*Apc*$^{fl/fl}$;*Kras*$^{LSL-G12D/+}$ mice 36 days (E, F) and 45 days (G, H) after 4-OHT enema administration. Boxed regions in A, C, E, and G are magnified in B, D, F, and H respectively. Scale bars represent 100 μm.

In addition, some tumors were almost completely negative for p-Erk1/2 expression (Figure 3.11C, D, G, H). Together, these data suggest that p-Erk1/2 may not be an accurate readout of oncogenic Kras. The variability in p-Erk1/2 expression is an example of tumor heterogeneity; the significance of this heterogeneity is unknown, but will be addressed in future experiments (see Chapter IV).

Although expression of oncogenic Kras increased tumor burden, it did not significantly alter the histology of tumors resulting from simultaneous *Apc* loss. To confirm that the $Kras^{LSL\text{-}G12D}$ allele was efficiently recombined after 4-OHT enema, we isolated DNA from colonic epithelial tissue from $Lrig1^{CreERT2/+};Apc^{fl/fl}$ and $Lrig1^{CreERT2/+};Apc^{fl/fl};Kras^{LSL\text{-}G12D/+}$ mice and performed polymerase chain reaction (PCR) using primers that differentiate between the wild type *Kras* allele (WT), the unrecombined $Kras^{LSL\text{-}G12D}$ allele (LSL), and recombined $Kras^{LSL\text{-}G12D}$ allele (rec) (Figure 3.12). We found that while the LSL allele was still present, recombination had occurred in epithelial cells from the proximal colon (P), distal colon (D), and from tumors (Tum) (Figure 3.12).

Mutant Kras expression increases glutamine uptake in the colonic epithelium of $Lrig1^{CreERT2/+};Apc^{fl/fl};Kras^{LSL\text{-}G12D/+}$ *mice*

One of the more recent appreciated hallmarks of cancer is the ability of cancer cells to alter cellular metabolism (*111*). Cells in the interior of a solid tumor can undergo a switch from oxidative phosphorylation to aerobic glycolysis in low oxygen conditions; however, this switch requires more fuel to sustain the same level of cellular energy. To compensate, cells must increase glucose utilization (*111*). Clinical imaging techniques

have capitalized on this characteristic: ^{18}F-FDG positron emission tomography (PET) is a non-invasive metabolic imaging technique that measures glucose uptake by tissues and is used to identify the location of potential tumors in patients (*112*). Glutamine is another metabolic nutrient important for cellular metabolism, providing both carbon and nitrogen sources, which fuel both cellular energetics and proliferation (*112*). Studies from pancreatic cancer models in mice (in which Kras mutations are the main drivers) have suggested that one of the ways oncogenic Kras maintains malignancy is through altered cellular metabolism to favor aerobic glycolysis (*113*). Additionally, observations in pancreatic cancer cell lines demonstrated that oncogenic KRAS alters glutamine metabolism to help maintain cell growth (*114*).

To determine whether oncogenic Kras affected glutamine uptake in tumors from *Lrig1*$^{CreERT2/+}$*;Apc*$^{fl/fl}$*;Kras*$^{LSL\text{-}G12D/+}$ mice, we performed *in vivo* non-invasive imaging using a radiolabeled glutamine probe, [^{18}F]4-F-GLN. *Lrig1*$^{CreERT2/+}$*;Apc*$^{fl/fl}$ and *Lrig1*$^{CreERT2/+}$*;Apc*$^{fl/fl}$*;Kras*$^{LSL\text{-}G12D/+}$ mice were imaged before 4-OHT enema and two and four weeks after 4-OHT enema. Preliminary data demonstrated that glutamine uptake increased in the colons of *Lrig1*$^{CreERT2/+}$*;Apc*$^{fl/fl}$*;Kras*$^{LSL\text{-}G12D/+}$, but not in *Lrig1*$^{CreERT2/+}$*;Apc*$^{fl/fl}$ mice (Figure 3.13A, B). The positive signal (Figure 3.13B, white bracket) appeared to be diffuse throughout the colon. In addition, quantification of glutamine uptake illustrated that uptake was increased both at two and four weeks after 4-OHT administration (Figure 3.13C). These experiments are currently being expanded and molecularly validated.

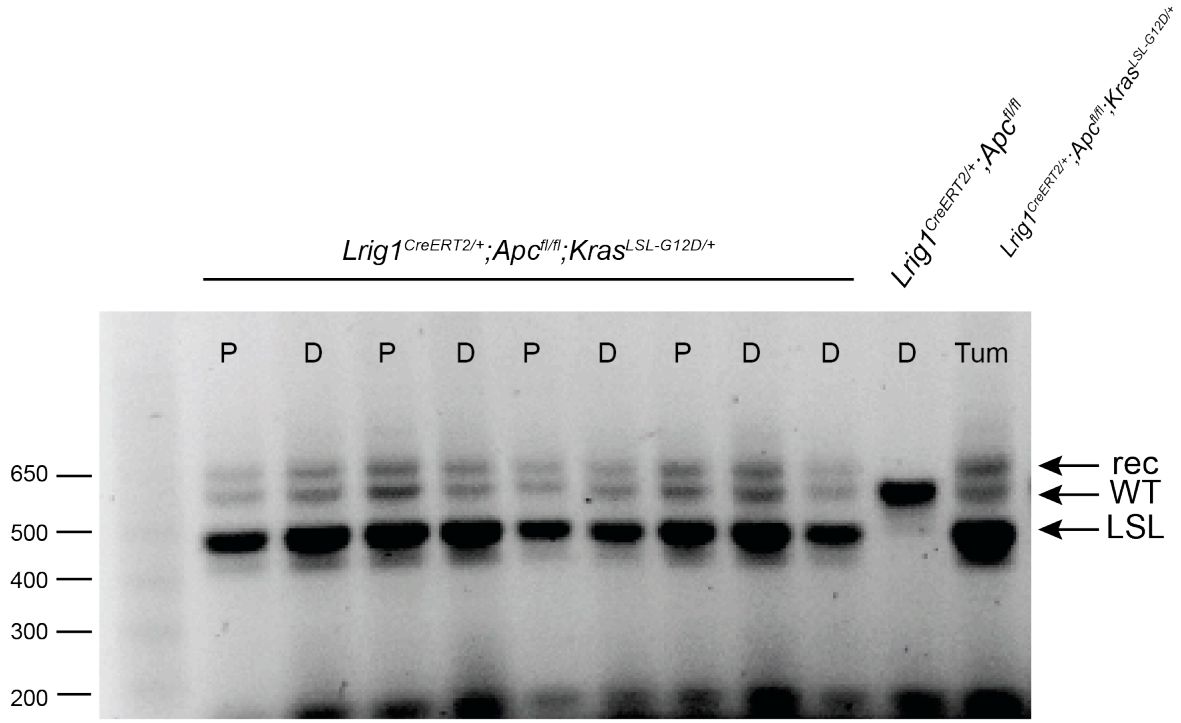

Figure 3.12. Evidence of *Kras*$^{LSL\text{-}G12D}$ allele recombination. Results from *Kras* PCR from epithelial DNA from the proximal colon (P), distal colon (D), or colon tumors (Tum) from *Lrig1*$^{CreERT2/+}$;*Apc*$^{fl/fl}$ or *Lrig1*$^{CreERT2/+}$;*Apc*$^{fl/fl}$;*Kras*$^{LSL\text{-}G12D/+}$ mice. Primers differentiate between the wild type (WT) *Kras* allele and the unrecombined (LSL), and recombined (rec) *Kras*$^{LSL\text{-}G12D}$ alleles. WT= 622 bp rec= 650 bp LSL= 500 bp. Primer sequences listed in Table 3.1.

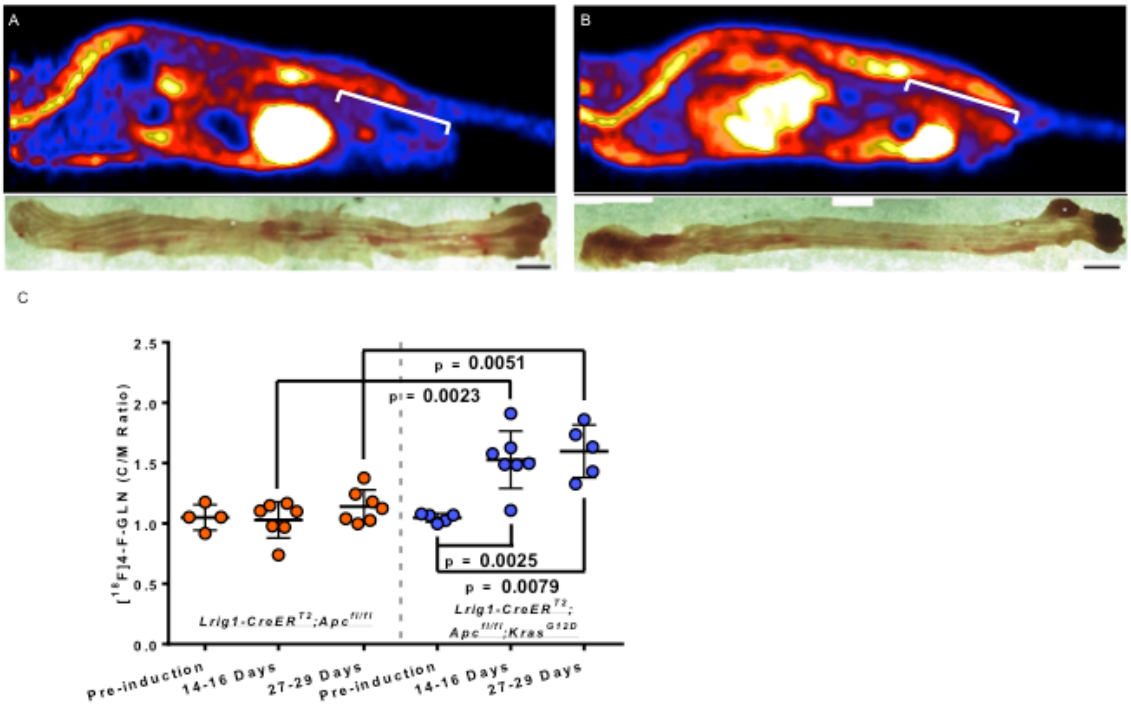

Figure 3.13. Preliminary *in vivo* glutamine imaging of *Lrig1*$^{CreERT2/+}$;*Apc*$^{fl/fl}$ and *Lrig1*$^{CreERT2/+}$;*Apc*$^{fl/fl}$;*Kras*$^{LSL-G12D/+}$ mice. A, B. Sagittal images of [^{18}F]4-F-GLN uptake in *Lrig1*$^{CreERT2/+}$;*Apc*$^{fl/fl}$ (A) and *Lrig1*$^{CreERT2/+}$;*Apc*$^{fl/fl}$;*Kras*$^{LSL-G12D/+}$ (B) mice four weeks after 4-OHT enema administration. Corresponding colon wholemounts are illustrated below. White bracket indicates uptake in the colon. C. Dot plot quantifying [^{18}F]4-F-GLN uptake as a ratio of colon-specific uptake, compared to muscle (negative). Imaging was performed before 4-OHT enema (pre-induction), two weeks, and four weeks after 4-OHT enema. Each dot represents an individual mouse.

Discussion

This is the first report to characterize the transformative capacity of Lrig1$^+$ cells in the colon after *Apc* loss and oncogenic Kras expression. We found that oncogenic Kras did not significantly alter tumor characteristics after simultaneous *Apc* loss, although may have contributed to increased invasion. It is important to note that mice did not typically live longer than 60-80 days due to development of severe rectal prolapse; therefore, it is unknown if oncogenic Kras could lead to tumor progression—perhaps greater invasive potential and metastasis—at later time points.

The cooperation between *Apc* loss and mutant Kras in the colon has been studied in different contexts using multiple driver cell populations [reviewed in (*104*)], including fatty acid binding protein 1-positive (Fabp1$^+$; high-grade dysplasia) (*79*), Carbonic anhydrase-positive (CAC$^+$; no invasion and histology not graded) (*81*), adenoviral-cre-infected (described in Introduction) (*80*), and Lgr5$^+$ cells (*78*). Of note, the aforementioned studies utilized a conditional *Apc* allele and the *Kras*$^{LSL\text{-}G12D}$ knock-in latent allele; this strategy (repeated here in this study) helps guarantee cell specificity and avoid overexpression of oncogenic Kras. With the exception of Lgr5, the drivers used in these models are specific for intestinal and colonic epithelium, but are not restricted to stem cells (*76, 79, 104*). Therefore, it is likely that *Apc* tumor-initiating mutations in stem cells initiate transforming events, but mutations in cells throughout the crypt could contribute to tumor growth and progression.

Prior to this study, the only stem cell population from which these mutations have been directed is the Lgr5$^+$ population; however, these mice become moribund in seven to ten days and tumors cannot be analyzed (*78*). Interestingly, for Lgr5$^+$ cells to drive

tumorigenesis, both copies of *Apc* must be lost simultaneously, while tumorigenesis driven by *Apc* mutation in the Lrig1^{+} population requires loss of only a single copy of *Apc (76, 82)*. When *Lrig1*$^{CreERT2/+}$;*Apc*$^{fl/fl}$ mice are administered tamoxifen via intraperitoneal injection, they die within five to seven days (data not shown), while *Lgr5*$^{EGFP\text{-}IRES\text{-}creERT2}$;*Apc*$^{fl/fl}$ mice live up to about 36 days (*76*). These differences may suggest a difference in the transforming capacity between the two populations, but could also reflect the efficiency of Cre recombination—in fact, lineage tracing from Lgr5^{+} cells is not very efficient in the colon compared with lineage tracing from Lrig1^{+} cells (*32*).

Of interest, a recent study suggested that non-stem cell populations can dedifferentiate and initiate tumorigenesis under certain conditions (*77*). In particular, this group demonstrated that β-catenin activating mutations, combined with elevated NF-κB signaling driven from Lgr5^{-}/Bmi1^{-} cells, resulted in small adenomatous foci within the differentiated compartment of small intestinal villi, suggesting that, at the very least, Lgr5^{-}/Bmi1^{-} cells can be tumor cells-of-origin (*77*). However, since other stem cell populations were not considered, it is hard to conclude that they did not contribute to initiation.

Here, we describe the different results of simultaneously driving *Apc* and *Kras* mutations in Lrig1^{+} cells in the colon. Kras activation *in vitro* and in the colonic epithelium without an initiating event (i.e. *Apc* or *Ink4a/Arf* loss) can cause cellular senescence, a process termed oncogene-induced senescence (*108, 115*). In this setting, intact tumor suppressive pathways, such as the p19^{Arf}-p53 pathway can become upregulated, resulting in replicative senescence and preventing tumor initiation

(*115*). We observed that the cell cycle inhibitor p19 was detected in histologically normal crypts in *Lrig1*$^{CreERT2/+}$;*Apc*$^{fl/+}$;*Kras*$^{LSL-G12D/+}$ mice, suggesting that these crypts had not undergone *Apc* loss and had become senescent. These data support previous studies in which Kras induces a senescence phenotype in the absence of an initiating mutation (*108*).

We found that the proximal colon is particularly sensitive to mutant Kras. In particular, we observed a villus-like morphology in the proximal colonic epithelium of *Lrig1*$^{CreERT2/+}$;*Apc*$^{fl/+}$;*Kras*$^{LSL-G12D/+}$ mice that was never observed in *Lrig1*$^{CreERT2/+}$;*Apc*$^{fl/+}$ mice. In addition, we observed single crypt adenomas in the proximal colon of *Lrig1*$^{CreERT2/+}$;*Apc*$^{fl/+}$;*Kras*$^{LSL-G12D/+}$ mice, suggesting mutant Kras might predispose the proximal colon epithelium to transformation. Interestingly, in the setting of *Ink4a/Arf* loss, Kras activation can be an initiating event (in the absence of Wnt pathway mutations), resulting in invasive proximal serrated adenomas (*108*). For unknown reasons, *Apc* loss in Lrig1^{+} cells spares the proximal colon from tumorigenesis, although Lrig1 is expressed throughout the length of the colon (*32, 82*). In addition, lineage tracing after 4-OHT enema revealed that recombination occurred in the proximal colon, yet mice lacking one or both copies of *Apc* had no proximal colon phenotype.

Downstream Kras signaling leads to Erk1/2 phosphorylation, which is often used as a readout of hyperactive Kras activity *in vitro*. However, we observed that p-Erk1/2 was expressed in tumors from both genotypes and was highly heterogeneous where it was expressed (Figure 3.11). In particular, nuclear p-Erk1/2 localization has been correlated with the histological grade of human colon tumors and in this study, p-Erk1/2 expression occurred independent of *KRAS* mutational status (*116*). Similarly, we

observed cytoplasmic and nuclear p-Erk1/2 immunoreactivity in tumors from mice independent of *Kras* status. Experiments are underway to determine whether areas of nuclear p-Erk1/2 correlate with higher histological grade or, in the setting of mutant Kras, whether nuclear p-Erk1/2 localization correlates with recombination of the *Kras* allele. Given its expression in *Lrig1*$^{CreERT2/+}$;*Apc*$^{fl/fl}$ mice, and consistent with a previous report of Kras activation in the mouse colon (*79*), we conclude that, at least in this model, p-Erk1/2 expression does not seem to be a reliable marker of Kras activation in the mouse colon.

While the phenotypes of *Lrig1*$^{CreERT2/+}$;*Apc*$^{fl/fl}$ and *Lrig1*$^{CreERT2/+}$;*Apc*$^{fl/fl}$;*Kras*$^{LSL-G12D/+}$ mice are not novel, these models can be useful in the future to study high-grade distal colon tumorigenesis and invasion, especially invasion after simultaneous *Apc* loss. In particular, in future experiments, we will evaluate the *Kras* status in areas of invasion that were more infiltrative to determine whether mutant Kras contributes to a more aggressive invasive phenotype. We have also demonstrated the usefulness of 4-OHT enema to activate Cre recombinase in a localized manner to avoid systemic effects of mutant Kras. Future experiments will follow up on the heterogeneity of p-Erk1/2 expression in tumors; this model may be relevant for studying tumor heterogeneity. Finally, we have described preliminary *in vivo* imaging observations that suggest mutant Kras may affect glutamine uptake in the colon. Future experiments will evaluate whether this observation could be clinically relevant for diagnostic imaging in human CRC.

Materials and Methods

Mice

Lrig1<tm1.1(cre/ERT)Rjc> (*Lrig1*^{CreERT2}) mice were generated as described in (*32*). B6.129S4-*Kras*^{tm4Tyj}/J mice were a generous gift from Anna Means (Vanderbilt University Medical Center). *Apc*^{flox} mice (*117*) were a generous gift from Kevin Haigis (Beth Israel Deaconess Medical Center). *R26R*^{lacZ} mice were obtained from Jackson Laboratories (Bar Harbor, ME). Mice were intercrossed to generate *Lrig1*$^{CreERT2/+}$*;R26R*$^{lacZ/+}$, *Lrig1*$^{CreERT2/+}$*;Apc*$^{fl/+}$, *Lrig1*$^{CreERT2/+}$*;Apc*$^{fl/fl}$, *Lrig1*$^{CreERT2/+}$*;Apc*$^{fl/+}$*;Kras*$^{LSL-G12D/+}$, and *Lrig1*$^{CreERT2/+}$*;Apc*$^{fl/fl}$*;Kras*$^{LSL-G12D/+}$ mice. All animal protocols were approved and performed in accordance with the Vanderbilt University Medical Center Animal Care and Use Program. Mice were fed standard rodent chow and water *ad libitum* and housed under controlled light cycle conditions.

Intraperitoneal tamoxifen injection and 4-OHT enema

Six to eight-week-old mice were administered intraperitoneal injection with 0.5 mg tamoxifen (#T5638, Sigma, St. Louis, MO) dissolved in corn oil as in (*32*). 4-hydroxytamoxifen (4-OHT) (#T76, Sigma, St. Louis, MO) was resuspended in 100% ethanol at a 1 mg/mL stock solution concentration. Six to eight-week-old mice were anesthetized with isoflurane (#2099589, Henry Schein, Nashville, TN) and given a phosphate-buffered saline (PBS) enema to clear the colon of fecal matter using a gavage feeding needle (#18061-22, Fine Science Tools). Fifty microliters of the 4-OHT solution was delivered by enema at a final concentration of 0.05 mg per animal.

Tissue preparation

Freshly dissected intestinal tissues were fixed in 10% formalin overnight at room temperature. The following day, tissues were washed three times with PBS and submerged in 70% ethanol for embedding in paraffin.

Immunofluorescence, immunohistochemistry, and lineage tracing

Paraffin tissue sections were deparaffinized in Histo-Clear (#HS-200, National Diagnostics, Charlotte, NC) and rehydrated in an ethanol series (100%, 100%, 100%, 95%, 95%, 70%). Antigen retrieval was carried out for thirty minutes in a pressure cooker in citrate buffer, pH6 (#S236984-2, DAKO, Carpinteria, CA). Sections were blocked for one hour at room temperature (#X0909, DAKO, Carpinteria, CA). Primary antibodies were incubated overnight at 4°C in antibody diluent (#S3022, DAKO, Carpinteria, CA). Primary antibodies were as follows: β-catenin 1:750 (#610154, BD Transduction Laboratories, San Jose, CA), Ki-67 1:50 (#M7249, DAKO, Carpinteria, CA), p-Erk1/2 1:200 (#9101S, Cell Signaling Technologies, Danvers, MA), and p19 1:200 (#ab80, Abcam, Cambridge, MA). For immunofluorescence, all sections were counterstained with DAPI 1:10,000. Fluorescent secondary antibodies (1:500) (Life Technologies, Carlsbad, CA) were used for detection. Fluorescent images were captured using a Zeiss Axio Imager.M2. For immunohistochemistry brightfield developing, p19 and p-Erk1/2 primary antibodies were detected using the DAKO EnVision+ System with horseradish peroxidase-labeled polymer according to the manufacturer's instructions (#K401111-2, DAKO, Carpinteria, CA). Sections were counterstained with hematoxylin. Brightfield imaging was performed using a Leica

SCN400 slide scanner. Images were captured using the Leica Digital Image Hub. Adobe Photoshop and Illustrator were used for image overlay and preparation. Lineage tracing staining for β-galactosidase (β-gal) activity was performed as in (*32*).

Quantification of crypt height and tumor burden

H&E-stained colon tissue sections were imaged using a Leica SCN400 slide scanner. For crypt height measurements, every crypt in cross sectional view (entire crypt visible from bottom to top) in one tissue section of the entire colon per mouse was measured using Leica's Digital Image Hub software. For tumor area, colonic tissue wholemounts were imaged on a Zeiss Stereo Discovery V.8 dissecting scope immediately following dissection. Tumors area from wholemount images was measured using ImageJ software.

DNA isolation from colonic tissue and Kras PCR

Crypt epithelium was isolated from freshly dissected *Lrig1*$^{CreERT2/+}$;*Apc*$^{fl/fl}$ and *Lrig1*$^{CreERT2/+}$;*Apc*$^{fl/fl}$;*Kras*$^{LSL\text{-}G12D/+}$ colons or colonic tumors at various times after 4-OHT administration as previously described (*32, 95*). DNA was isolated from colon epithelial preparations using a DNeasy Blood and Tissue Kit (#69504, Qiagen, Germantown, MD). Primers for PCR are listed in Table 3.1. Cycling conditions were as follows: 95°C for two minutes; 95°C for thirty seconds; 61°C for thirty seconds; 72°C for forty-five seconds (35 cycles); 72°C for ten minutes; 4°C hold.

[^{18}F]4-F-Gln synthesis

[^{18}F]4-F-Gln and tosylate precursor were produced using methods analogous to those previously reported (*118*). Cyclotron-produced [^{18}F]fluoride ion in [^{18}O]water was trapped on a Waters QMA-carbonate form Sep-Pak and eluted using a solution of 18-crown-6 (10.2 mg) and potassium bicarbonate (1.8 mg) in 1.4 mL of an acetonitrile and water solution (9.3:1.7). The mixture was dried down at 99°C under a stream of helium at reduced pressure and subjected to azeotropic drying *via* iterative addition of anhydrous acetonitrile. Subsequently, tosylate precursor (6.0 mg+/-0.5 mg in 0.5 mL of anhydrous acetonitrile), provided by collaborators in the group of Charles Manning (VUMC), was added directly to [^{18}F]fluoride and the reaction mixture heated to 80°C for twenty minutes. Following cooling to 30°C, 10 mL of a 5% acetonitrile solution was added to the mixture and passed through a preconditioned Waters HLB Plus cartridge followed by 2 mL of pure water. Activity was eluted using 2 mL of acetonitrile and the solvent removed under a gentle stream of nitrogen gas at 40°C. To the dried product was added a solution of trifluoroacetic acid (0.595 mL) and anisole (0.005 mL), which was heated to 60°C for ten minutes. The solvent was once again removed under a gentle stream of nitrogen gas and the dried product taken up in sterile water. The final solution was filtered through a 0.45-micron filter directly into the sterile vial and the pH adjusted to a range of 5–8 units. Overall product yields ranged from 185–5569 MBq (5.0–150.5 mCi) (n=10). Radiochemical purity and optical purity were determined by chiral HPLC (Chirex 3216 Penicillamine 150 x 4.6 mm 5uM (P/N: 00F-3126-E0) column [Phenomenex], 1.0 mM $CuSO_4$, 1.0 mL/min, ultraviolet 254-nm and γ-detector).

Radiochemical purity and optical purity were greater than 90% and 95% (n=10), respectively, as determined by analytical HPLC.

PET Imaging and Analysis

Animal handling methods in preparation for and during all PET imaging studies were derived from protocol standards established for [^{18}F]FDG (*119-121*). Prior to imaging, animals were fasted between six to eight hours and allowed to acclimate to facility environment for at least one hour in a warmed chamber at 31.5°C. Animals were administered 10.4-11.8 MBq of PET imaging agent via intravenous injection and imaged using a dedicated Concorde Microsystems Focus 220 microPET scanner (Siemens Preclinical Solutions). Animals were maintained under 2% isoflurane anesthesia in 100% oxygen at 2 L/min and kept warm for the duration of the PET scan. [^{18}F]4-F-Gln PET imaging was collected as either twenty minute static acquisitions following a forty minute uptake period or sixty minute dynamic acquisitions initiated upon PET agent injection. Images were acquired longitudinally starting before induction with 4-OHT and proceeding to two and four weeks after.

PET data were reconstructed using a three-dimensional (3D) ordered subset expectation maximization/maximum a posteriori (OSEM3D/MAP) algorithm. Dynamic data was binned into twelve five-second (0-1 minutes) and fifty-nine sixty-second (2-60 minutes) frames. The resulting three-dimensional reconstructions had an x-y voxel size of 0.474 mm and inter-slice distance of 0.796 mm. ASIPro software (Siemens Preclinical Solutions) was used to manually draw three-dimensional regions of interest (ROI) surrounding the entire tumor volume. PET agent uptake was quantified as the

percentage of the injected dose per gram of tissue (%ID/g). For dynamic scans, only data points collected within the time frame analyzed for analogous static scans were considered.

Statistics

Two-tailed Student's *t*-test was used for comparisons of parametric data. $p<0.05$ was considered significant. A contingency table was used to compare percent of mice that developed rectal prolapse.

Genotyping	
Kras-F1	GTCTTTCCCCAGCACAGTGC
Kras-R1	CTCTTGCCTACGCCACCAGCTC
Kras-SD5'	AGCTAGCCACCATGGCTTGAGTAAGTCTGCA
Lrig1 wt 5'	TCTGGCTGCTCTTGCTGCTACT
Lrig1 wt 3'	GACTTCACGAGGCACACTCGAT
Lrig1-CreERT2 5'	TCATCGCATTCCTTGCAAAAGT
Lrig1-CreERT2 3'	GACTTCACGAGGCACACTCGAT
Apc 2lox14 5'	GGCTCAGCGTTTTCCTAATG
Apc 2lox14 3'	GATGGGTCTGTAGTCTGGG
R1295 (R26R downstream)	GCG AAG AGT TTG TCC TCA ACC
R523 (wt downstream)	GGA GCG GGA GAA ATG GAT ATG
R25F2 (upstream)	AAA GTC GCT CTG AGT TGT TAT

Table 3.1. Primer sequences.

CHAPTER IV

DISCUSSION AND FUTURE DIRECTIONS

Summary

My dissertation research has explored questions related to Lrig1$^+$ cells in the colonic epithelium in the context of homeostasis and cancer. We have determined that there are two subpopulations of Lrig1$^+$ cells in the mouse colon that can be differentiated by expression of *Lgr5,* Lrig1-Apple RFP reporter levels, and likely the glycosylation status of Lrig1. Given the importance of stem cells in colon cancer initiation, we also explored whether *Apc* loss and Kras activation in Lrig1$^+$ colonic stem/progenitor cells could contribute to advanced colonic neoplasia. We found that homozygous *Apc* loss in Lrig1$^+$ cells can lead to histologically advanced colonic neoplasia and invasion, independent of mutant Kras expression. Additionally, we showed preliminary evidence that oncogenic Kras may increase glutamine uptake in the colon. This chapter will discuss the implications of my thesis work and consider future experiments that will address some of the questions raised.

The identity and characteristics of intestinal stem cells have been debated for the past 50 years. While both the +4 cell and CBC models have remained the most prevalent theories, the picture has become more complicated as more evidence is uncovered. Lgr5 has proven to be a reliable marker of CBCs, an established *bona fide* stem cell population. The +4 population has been more difficult to confirm and recent evidence has suggested that +4 cell markers are expressed in *Lgr5*$^+$ CBCs (*34*). Additionally, histone 2B yellow fluorescent protein-expressing label-retaining cells (H2B-

YFP LRCs) were recently shown to be secretory progenitor cells that could serve a stem cell function after injury, suggesting that LRCs have stem cell potential depending on tissue context (*1*). We identified Lrig1 as a stem cell marker in 2012, but uncertainty remains about where Lrig1$^+$ cells fall on the stem cell spectrum and whether they overlap with Lgr5$^+$ cells. Importantly, the studies reported in Chapter II demonstrate that while most Lrig1$^+$ cells express *Lgr5*, there is a small subset that does not and it is this population that is of most interest and the focus of future work. The overreaching question the Coffey lab will ask in future studies is: do Lrig1$^+$ and Lgr5$^+$ populations have distinct properties during homeostasis and in disease states like cancer?

Dissecting the Stem Cell Potential of Two Lrig1$^+$ Populations

A more immediate question is to further parse the characteristics of the two Lrig1$^+$ populations. Importantly, do both Lrig1$^+$ populations have stem cell potential? To address this question, single Lrig1-RFP-hi and Lrig1-RFP-mid cells could be isolated from *Lrig1*$^{Apple/+}$ mice and cultured to assess whether both populations generate organoids in culture. Based on work from other groups, I expect RFP-hi (Lrig1$^+$/*Lgr5*$^+$) cells will efficiently generate organoids in culture (*122*); the stem cell potential of the RFP-mid (Lrig1$^+$/*Lgr5*$^-$) population remains to be determined. If both subsets are able to generate organoids, they could both be considered stem cell populations.

If RFP-mid single cells fail to give rise to organoids in culture, they could not be classified as true stem cells. We know little about what this cell population could be. It is a rare population, only ~3% of all colonic epithelial cells. We have some preliminary clues about the transcriptome of the anti-Lrig1-VU$^+$ population [described in (*32*)]. For

instance, we know that the expression of *mTert* and *Bmi1* are similar between Lrig1-VU$^+$ and Lgr5$^+$ cells; additionally, Lrig1-VU$^+$ cells express significantly greater levels of the following: the Egfr ligand, *Amphiregulin* (*Areg*); the cell cycle inhibitor, c*yclin-dependent kinase inhibitor 1a* (*Cdkn1a*); and the cell surface antigen involved in hematopoietic stem cell function, *Sca-1 (32, 123)*. Further interrogation of the differentially regulated genes from this data set might aid in determining the identity of this population. However, since anti-Lrig1-VU still recognizes 12% of RFP-hi cells, which express *Lgr5*, global transcriptome or proteomic analyses of RFP-hi and RFP-mid cells would need to be performed using the *Lrig1^{Apple}* reporter mouse.

Reconciling Lrig1 Lineage Tracing Results

If both Lrig1$^+$ populations have stem cell potential, the next questions to be answered are: do both the Lrig1$^+$/*Lgr5*$^+$ and Lrig1$^+$/*Lgr5*$^-$ populations give rise to fully labeled crypts in lineage tracing experiments? And if not, which population gave rise to fully labeled crypts in our original lineage tracing analysis? Chapter II confirmed that most Lrig1$^+$ cells are *Lgr5*$^+$ and lineage tracing from Lgr5$^+$ cells has been definitively shown elsewhere (*25*); therefore, future experiments should address whether the Lrig1$^+$/*Lgr5*$^-$ population can give rise to fully labeled crypts. To begin to answer this question, it would be possible to ablate the Lrig1$^+$/Lgr5$^+$ population using directed diphtheria toxin-induced ablation (*Lgr5$^{DTR\text{-}EGFP}$*), combined with lineage tracing from Lrig1$^+$ cells: *Lgr5$^{DTR\text{-}EGFP}$;Lrig1$^{CreERT2/+}$;R26R^{lacZ}*. This *Lgr5* allele has been recently acquired by our lab and has more uniform EGFP reporter expression in the colonic epithelium compared to the original patchy Lgr5-EGFP reporter mouse (*Lgr5$^{EGFP\text{-}ires\text{-}}$*

creERT2) (*25*). In this experiment, the Lrig1$^+$/Lgr5$^+$ population would be ablated, leaving the Lrig1$^+$/Lgr5$^-$ population intact; the presence of fully labeled crypts after tamoxifen administration would suggest that Lrig1$^+$/Lgr5$^-$ cells are capable of giving rise to crypts.

The main caveat of this experiment is that diphtheria toxin-induced cell death may cause injury to the epithelium, which would potentially mimic our original studies that showed quiescent Lrig1 lineage-traced cells could be activated after radiation damage (*32*); therefore, careful analysis will need to be done with this caveat in mind. In addition, a second caveat to this experiment is that the diphtheria toxin receptor (DTR) is human heparin-binding EGF-like growth factor (HBEGF) (*124*). Therefore, we should keep in mind that overexpression of HBEGF in the base of the crypt could have effects on its own. If no fully labeled crypts are observed, it would be reasonable to conclude that the original lineage tracing results were due to tracing from cells that were also *Lgr5*$^+$, suggesting the stem cell potential of Lrig1$^+$ cells is present in the Lrig1$^+$/Lgr5$^+$ population only.

In our original study, we noted that after long-term lineage tracing analysis, 8% of labeled crypts contained a single labeled cell that had not given rise to a fully labeled crypt, suggesting a subset of Lrig1$^+$ cells are quiescent (*32*). Based on the high proliferative status of Lgr5$^+$ cells [~75% are Ki-67$^+$ at any given time (*32*)] and the relatively quiescent status of anti-Lrig1-VU$^+$ cells [~25% are Ki-67$^+$ at any given time (*32*)] and single labeled β-gal$^+$ cells [14% are Ki-67$^+$ at any given time (*32*)], it is possible that Lrig1$^+$/*Lgr5*$^+$ cells generate fully labeled crypts and the anti-Lrig1-VU$^+$ cells comprise the single β-gal-labeled cells observed at long-term time points. A simple experiment to begin to answer this question would be to co-stain long-term lineage-traced tissue with

anti-Lrig1-VU and an antibody against β-gal to evaluate whether the long-lived single labeled cells are also the anti-Lrig1-VU$^+$ population.

Of note, in our original lineage tracing analysis, we observed that while 40% of colonic crypts were labeled one day after tamoxifen injection, this percentage decreased to 10% 90 days after tamoxifen injection. One explanation for this observation is that some Lrig1$^+$ cells that are marked one day after tamoxifen are transit-amplifying cells or progenitors that eventually differentiate and are lost from the crypt. Since this potential situation has not been rigorously tested, Lrig1$^+$ cells are referred to as stem/progenitor cells throughout this thesis. If this hypothesis is correct, a more detailed analysis of lineage tracing in *Lrig1*$^{CreERT2/+}$*;R26R*^{lacZ} mice at early time points (every day for the first seven days) would reveal stripes of labeled cells that begin, not in the crypt base, but further up the crypt in the transit-amplifying zone and are lost over time.

Lrig1 Glycosylation and Immunoreactive Patterns of Anti-Lrig1-VU and -R&D

We found that the subset of Lrig1$^+$/*Lgr5*$^-$ cells might be differentiated by the glycosylation status of Lrig1. This subset can be largely identified using anti-Lrig1-VU, which recognizes a non-glycosylated form of Lrig1. While Lrig1 is glycosylated and N-glycosylation sites in the Lrig1 ectodomain have been identified, only one has been confirmed by mass spectrometry (GlycoProt DB) (*90*) and whether glycosylation plays a role in Lrig1 function is unknown. Anti-Lrig1-R&D reproducibly decorates the basolateral membrane of epithelial cells in the crypt base. However, the localization of anti-Lrig1-VU immunoreactivity varies; basolateral localization and diffuse cytoplasmic localization are

observed. Since anti-Lrig1-VU largely recognizes the non-glycosylated Lrig1 protein, it is possible this also explains the localization patterns of each antibody. During exocytic processing, glycosylation occurs within the endoplasmic reticulum or Golgi (*125*). Therefore, a fraction of non-glycosylated Lrig1 should be located intracellularly, where anti-Lrig1-VU immunoreactivity is often observed (Figure 2.2, page 24) (*32, 83*). However, anti-Lrig1-VU can be used effectively for FACS, suggesting that non-glycosylated Lrig1 is expressed on the cell surface. Additionally, deglycosylation experiments demonstrated that anti-Lrig1-R&D could also recognize non-glycosylated Lrig1, suggesting it should also recognize Lrig1 within the cell if the above hypothesis is correct; it is currently unknown why the anti-Lrig1-R&D immunoreactive pattern is not cytoplasmic as well.

While performing the deglycosylation experiments, I first attempted to deglycosylate and stain isolated crypts to determine whether anti-Lrig1-VU immunoreactivity (as in Figure 2.2, page 24) could be extended in a broader pattern. The hypothesis behind this experiment was that deglycosylation would expand the pool of non-glycosylated Lrig1 available for anti-Lrig1-VU to bind. However, I encountered technical challenges during the deglycosylation procedure, which requires multiple denaturing conditions, resulting in destruction of the crypts. A modified non-denaturing protocol could be tested to repeat this experiment.

Lrig1 Glycosylation and Stem Cell Identity

How might the glycosylation status of Lrig1 be related to stem cell identity? Non-glycosylated Lrig1 may be an immature form of the protein, which matures as cell

identity changes. If this hypothesis is correct, it may suggest that anti-Lrig1-VU$^+$ cells are a precursor population of the broader anti-Lrig1-R&D$^+$ population, defined by Lrig1 glycosylation and *Lgr5* expression. Future transcriptome analysis using the *Lrig1^{Apple}* RFP reporter mouse, which separates Lrig1$^+$/*Lgr5*$^-$ (RFP-mid) from Lrig1$^+$/*Lgr5*$^+$ (RFP-hi) cells will be performed to identify differences between the two populations and attempt to decipher their relationship (described above). In addition, the glycosylation status of Lrig1 will be confirmed in each respective RFP population. I expect that RFP-mid cells express mostly non-glycosylated Lrig1, while RFP-hi cells express mostly glycosylated Lrig1.

The potential of the Lrig1$^+$/*Lgr5*$^-$ population to be a precursor population to the larger Lrig1$^+$/*Lgr5*$^+$ population—and a precursor for other cell populations as well—could be tested in multiple ways, but relies on the assumption that Lrig1$^+$/*Lgr5*$^-$ cells are true stem cells; therefore, this should be confirmed first as discussed above. If Lrig1$^+$/*Lgr5*$^-$ cells isolated as RFP-mid single cells generate organoids, RFP-mid/GFP-neg single cells isolated from *Lrig1$^{Apple/+}$;Lgr5$^{DTR-EGFP}$* mice could be grown in culture. If the Lrig1$^+$/*Lgr5*$^-$ population is a precursor to the larger Lrig1$^+$/*Lgr5*$^+$ population, single RFP-mid cells should generate Lgr5-EGFP$^+$ cells in organoids.

A caveat to these experiments is that cells from *Lrig1$^{Apple/+}$;Lgr5$^{EGFP-ires-creERT2}$* mice have not been rigorously tested using FACS experiments to demonstrate that it is feasible to isolate RFP-mid cells that are GFP-neg. The Lgr5$^+$ stem cell population is largely considered to be the EGFP-hi population; GFP-low cells can be isolated from this reporter mouse, but rarely formed organoids (*122*). Therefore, this dual reporter mouse should be used with caution only after confirming that red, green, or double-

positive populations can be reproducibly isolated and that the RFP-mid population does not express EGFP.

Additionally, this question could be addressed in a broader way *in vivo* using targeted diphtheria toxin ablation of Lgr5^{+} cells to evaluate whether the Lrig1^{+}/*Lgr5*$^{-}$ population can regenerate Lrig1^{+}/*Lgr5*$^{+}$ cells. After diphtheria toxin administration, *Lgr5*$^{DTR\text{-}EGFP/+}$;*Lrig1*$^{Apple/+}$ mice would lose GFP expression and any remaining RFP expression would comprise the Lrig1^{+}/*Lgr5*$^{-}$ population. Initial expansion of RFP^{+} cells, followed by appearance of RFP^{+}/GFP^{+} cells would suggest that Lrig1^{+}/*Lgr5*$^{-}$ cells could give rise to the Lrig1^{+}/*Lgr5*$^{+}$ population. In addition, this result would suggest that Lrig1^{+} cells are similar to Bmi1^{+} cells in the small intestine in that they serve as a reserve stem cell population (*43*). Similar caveats (described above) should be taken into account with use of the dual reporter mouse.

Effects of LRIG1 Glycosylation on EGFR regulation

Does LRIG1 glycosylation affect its function? Modulation of EGFR activity through degradation is the most well studied function of LRIG1 (*90, 126*). However, one of the biggest gaps in the LRIG1 field is that this interaction has only been described by co-immunoprecipitation and not by more direct means (*90, 126*). While the interaction domains of either protein have not been identified, co-immunoprecipitation was ablated after deletion of both the leucine-rich repeats and immunoglobulin domains of LRIG1, but not individual deletion of either domain (*90*). Additionally, LRIG1 is still able to negatively regulate the EGFR mutant, EGFRvIII, a mutant form of EGFR lacking some of the ectodomain (*127*). In the absence of structural data, these studies only suggest

that the two proteins associate, but the data do not provide a clear picture of how a possible direct interaction may occur. Although the details of LRIG1 and EGFR interaction are not completely defined, the impact of LRIG1 glycosylation—or lack of—on EGFR regulation could be evaluated using LRIG1 glycosylation mutants.

Functional Role of Lrig1 in Stem Cells

What is the function of Lrig1 in stem cells? While Lrig1 is important for intestinal homeostasis, the functional role of the protein in stem cells remains to be rigorously investigated. We hypothesized that at least in the anti-Lrig1-VU^{+} population, Lrig1 functions to keep Egfr activity low, which may account for the low proliferative rate of that population (25% Ki-67^{+}) (*32*). In addition to proliferation, Egfr activity may also impact cell differentiation; therefore, proper Lrig1 function and modulation of Egfr activity may be important for maintaining stem cell identity. Current models of Lrig1 loss are germline models, in which Lrig1 is absent from birth. Our lab has recently acquired a *Lrig1^{flox}* allele that will allow us study Lrig1 loss *in vivo* in an inducible fashion. *Lgr5$^{EGFP\text{-}ires\text{-}creERT2}$;Lrig1$^{fl/fl}$* mice will be used to evaluate whether Lrig1 loss affects the Lgr5^{+}/Lrig1^{+} stem cell population. In a broader fashion, *Villin$^{CreERT2/+}$;Lrig1$^{fl/fl}$* mice will be used to evaluate the function of Lrig1 within the context of the entire crypt.

Evaluating the Requirement of Lrig1^{+} Cells in Homeostasis

Are Lrig1^{+} cells required for intestinal homeostasis? In 2011, Tian et al. elegantly demonstrated that Lgr5^{+} cells were dispensable for intestinal homeostasis: upon targeted diphtheria toxin-induced ablation of Lgr5^{+} cells (*Lgr5$^{DTR\text{-}EGFP}$*), the intestinal

epithelium was normal; this group showed that Bmi1^{+} cells were responsible for epithelial maintenance in this model, at least in the small intestine (*43*). Following this experiment, it is reasonable to conclude that Lgr5^{+}/Lrig1^{+} cells are dispensable for epithelial homeostasis. However, if we confirm (above) that Lgr5^{+}/Lrig1^{-} cells have stem cell potential, it will be possible to ablate the total Lrig1^{+} population using *Villin*$^{CreERT2/+}$*;Lrig1*$^{DTA/+}$ mice expressing a Cre-inducible diphtheria toxin A (DTA) in Lrig1^{+} cells. These experiments are currently underway and may lend some insight as to the homeostatic role of the Lgr5^{+}/Lrig1^{-} population compared to the Lgr5^{+}/Lrig1^{+} population.

Dissecting Lgr5^{+} and Lrig1^{+} Populations in Stress, Damage and Cancer

Do the Lgr5^{+} and Lrig1^{+} populations have different roles in different tissue contexts? Above and in Chapter II, I have discussed the differences between Lgr5^{+} and Lrig1^{+} cells and how the lab will proceed to study these populations under homeostatic conditions. Ongoing and future experiments in the lab will explore these two populations in the context of epithelial stress, damage, and cancer using the *Lrig1*$^{Apple/+}$*;Lgr5*$^{DTR\text{-}EGFP}$ mice (use of the *Lgr5* allele is based on more uniform expression of the GFP reporter; studies described here will not utilize the DTR function of the allele).

Fasting has a significant impact on the proliferative capacity of the intestinal epithelium, causing a significant decrease in cell proliferation; following refeeding, proliferation rates spike before returning to homeostasis (*128*). Fasting/refeeding experiments are ongoing in the lab to address the contributions of Lgr5^{+} and Lrig1^{+} populations in recovery. Similar approaches will be taken to evaluate these populations

in damage and cancer using dextran sodium sulfate (DSS) damage and azoxymethane (AOM) treatment models, respectively. DSS is an established method of causing injury and inflammation in the mouse colon, most often used to model inflammatory bowel disease and inflammation-associated CRC in rodents (*129, 130*).

AOM is a carcinogen that can cause mutations in β-catenin and is used to model sporadic colonic neoplasia in the mouse (*131*). Unpublished observations in our lab demonstrate that tumors from *Apc*$^{Min/+}$ mice (a sporadic genetic model of intestinal neoplasia) display heterogeneous expression of *Lrig1* and *Lgr5* transcripts by *in situ* hybridization; some tumor areas express both transcripts together, while other tumor areas express only one or the other (data not shown). These preliminary results suggest that in the different tissue contexts described above, these two populations might have distinct roles. We will also evaluate RFP-hi and -mid populations and the immunoreactive patterns of anti-Lrig1-VU and anti-Lrig1-R&D to determine whether the different Lrig1^{+} subsets are differentially expressed in this tumor model.

Using *Lrig1*$^{CreERT2/+}$ Mice to Model Colonic Neoplasia

How do the tumor models presented in Chapter III fit into the field of colonic neoplasia mouse modeling? We found that oncogenic Kras expression in the setting of *Apc* loss in Lrig1^{+} cells had a similar phenotype to most models of Kras activation in the colon. We observed that invasion could occur in *Lrig1*$^{CreERT2/+}$*;Apc*$^{fl/fl}$ mice, independent of *Kras* mutations. Therefore, this model could be used in the future to study the phenotypic effects of stochastic *Apc* loss compared to simultaneous *Apc* loss. Additionally, preliminary *in vivo* non-invasive imaging data suggests that mutant Kras

expression increases glutamine uptake in the colon. We are currently breeding mice to repeat these experiments to include *Lrig1*$^{CreERT/+}$;*Kras*$^{LSL\text{-}G12D/+}$ mice to evaluate whether mutant Kras expression in the absence of *Apc* loss yields a similar result.

We observed that tumors from *Lrig1*$^{CreERT2/+}$;*Apc*$^{fl/fl}$ and *Lrig1*$^{CreERT2/+}$;*Apc*$^{fl/fl}$;*Kras*$^{LSL\text{-}G12D/+}$ mice displayed tumor heterogeneity, particularly relating to p-Erk1/2 expression. We are now using this model to interrogate whether tumor histology and expression of various markers are correlated with genetic mutations using multiplex immunofluorescence-based imaging techniques in collaboration with GE Healthcare. It is possible that efficient recombination of every floxed allele does not occur in every cell; rather, some alleles may be more efficiently recombined than others. In fact, Liu et al. demonstrated that recombination efficiency of different floxed alleles might be influenced by the distance between LoxP sites (*132*). To test whether local recombination events affect tumor phenotype, we will perform immunofluorescence on a single tissue section for β-catenin, vimentin, p-Erk1/2, and pan-cytokeratin. Each image will be compiled into one composite image, which will be correlated to H&E analysis of the same section. We will then extract DNA and RNA from areas of interest and perform PCR to determine the status of the engineered *Apc* and *Kras* alleles. For example, do areas of high-grade dysplasia have nuclear β-catenin and homozygous *Apc* loss? Do areas of p-Erk1/2 or epithelial vimentin staining correlate with tumor histology? Are there differences in *Apc* or *Kras* status between areas of cytoplasmic p-Erk1/2 compared to nuclear p-Erk1/2 expression? Additional gene expression analysis will be possible using the extracted RNA. These studies are currently underway.

Our early work demonstrated that *Lrig1*$^{CreERT2/+}$;*Apc*$^{fl/+}$ mice were a genetically relevant mouse model of human CRC, particularly due to stochastic loss of the second *Apc* allele. We had hoped that we could capitalize on this characteristic as we layered the expression of oncogenic Kras into the model. However, we found that oncogenic Kras did not have a significant effect on tumor phenotype. These mice develop a large tumor burden that causes severe rectal prolapse about two months after 4-OHT enema administration. Therefore, it is unknown whether oncogenic Kras can have additional tumor-promoting effects at later time points. Additionally, we cannot exclude the possibility that the G12D mutation is not the most relevant mutation in colonic neoplasia; unfortunately, the *Kras*$^{LSL-G12D/+}$ allele is the only inducible allele available that expresses the mutant gene from the endogenous promoter. Of note, I previously developed a model of stochastic *Apc* loss and oncogenic Kras expression using *Apc*$^{Min/+}$;*Lrig1*$^{CreERT2/+}$;*Kras*$^{LSL-G12D/+}$ mice. *Apc*$^{Min/+}$ mice carry a germline *Apc* mutation and develop sporadic intestinal tumors (*133*). At two months of age, I administered 4-OHT enema to activate Kras; however, I saw no effect of oncogenic Kras on *Apc*$^{Min/+}$ tumors up to 120 days.

Therefore, if these studies were to continue, a stochastic model should be developed using a recently developed *Kras*$^{FSF-G12D/+}$, a flippase-inducible allele. *Lrig1*$^{CreERT2/+}$;*Apc*$^{fl/+}$;*Kras*$^{FSF-G12D/+}$ mice would first receive tamoxifen to induce loss of one *Apc* allele. Distal colon tumors could be monitored and once developed, an adenovirus expressing flippase could be administered as in (*80*). Alternatively, we have made a caged tamoxifen compound as in (*134*). This compound is injected intraperitoneally, but is not activated until it is exposed to a particular wavelength of

light. We are working to obtain a light source to connect to our colonoscope so that we can control caged tamoxifen activation.

Importantly, both *Apc*$^{Min/+}$;*Lrig1*$^{CreERT2/+}$;*Kras*$^{LSL-G12D/+}$ and *Lrig1*$^{CreERT2/+}$;*Apc*$^{fl/+}$;*Kras*$^{FSF-G12D/+}$ models lose the specificity of Lrig1-driven mutations in *Apc* or *Kras*, respectively. The tumor cell-of-origin in *Apc*$^{Min/+}$ mice is not known, while adenoviral flippase infection would have to be analyzed using lineage tracing to determine in which cells the *Kras* allele is recombined. Additionally, use of the *Kras*$^{FSF-G12D/+}$ allele will not allow us to evaluate the role of the G12D mutation compared to other mutations.

Going forward, the Coffey lab is uniquely positioned to significantly advance the understanding of Lrig1 stem/progenitor cells in homeostasis and cancer. The lab has a number of genetic models for Lrig1 manipulation and Lrig1 cell-driven genetic perturbations including *Lrig1*^{CreERT2,} *Lrig1*$^{Apple/+}$, and *Lrig1*^{flox}. In addition, we possess well-characterized reagents to study Lrig1, in particular, anti-Lrig1-VU. A limitation to the complete study of Lrig1 in the intestine is a lack of an antibody for Egfr immunohistochemistry to assess Egfr status in different tissue contexts. To overcome this limitation, we are also generating an *Egfr*^{Emerald} mouse allele; Emerald, a bright green reporter has been fused to the C-terminus of endogenous mouse EGFR using CRISPR-Cas9 technology. Finally, we are poised to use *Lrig1*$^{CreERT2/+}$;*Apc*$^{fl/+}$ mice to study early events in in tumorigenesis and *Lrig1*$^{CreERT2/+}$;*Apc*$^{fl/fl}$ mice to study tumor heterogeneity using multiplex immunofluorescence.

APPENDIX A

LRIG1 TRAFFICKING IN POLARIZED INTESTINAL EPITHELIAL CELLS

Summary

A single layer of polarized epithelial cells lines the tubes of the intestinal tract, providing a barrier between the external environment and the internal milieu. Importantly, polarized epithelial cells have separate apical and basolateral membranes, with distinct protein and lipid components. In a whole tissue context, intestinal epithelial cell polarization is essential; the cellular components that mediate the different functions of the luminal (apical) and basolateral surfaces must be properly localized to establish and maintain tissue homeostasis. Protein mislocalization can lead to disease and loss of apico-basolateral polarity is a hallmark of cancer (*135*). The epidermal growth factor receptor (EGFR) is an important mediator of cell growth and proliferation; in non-transformed cells, EGFR signaling is precisely calibrated by negative regulatory mechanisms that are often disrupted in cancer (*111, 136, 137*). In addition, Egfr has been shown to play a role in tumor establishment (*138*) and multiple human cancers exhibit overexpressed or mutant EGFR (*136*). The majority of EGFR is present on the basolateral membrane of polarized epithelial cells and its basolateral targeting motif is mapped to a juxtamembrane region that is sufficient to direct EGFR to the basolateral surface (*139, 140*).

Leucine-rich and immunoglobulin-like domains-1 (LRIG1), a negative regulator of EGFR levels, is preferentially trafficked to the basolateral surface of Caco-2 cells (a

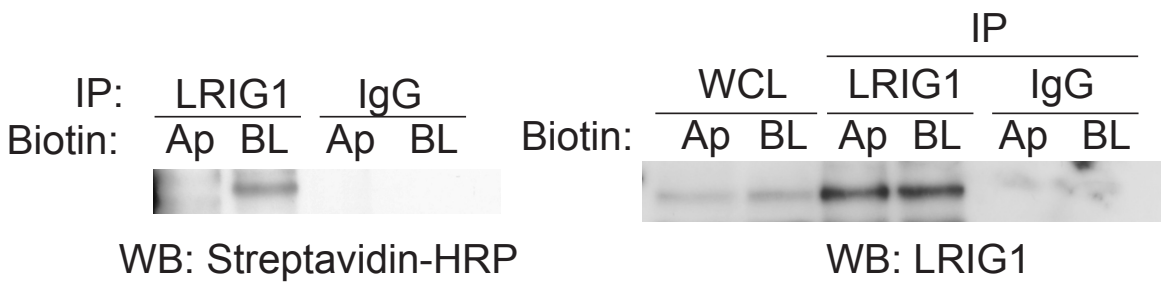

Figure A.1. Endogenous LRIG1 is expressed on the basolateral surface of Caco-2 cells. Polarized Caco-2 cells were selectively cell surface biotinylated. Total LRIG1 was immunoprecipitated from both apical and basolateral biotinylated cell lysates, but biotinylated LRIG1 was only detected on the basolateral surface by streptavidin western blotting.

polarizing colorectal cancer cell line) (Figure A.1.), suggesting that, as with EGFR, there are specific mechanisms regulating its cell surface localization. Together, preferential trafficking of EGFR and LRIG1 to the basolateral cell surface, the role of EGFR in cancer, and the tumor suppressor function of LRIG1 suggest LRIG1 trafficking fidelity is important for EGFR signaling regulation. In this chapter, I will describe my attempts to characterize the LRIG1 basolateral targeting motif as a first step in determining whether LRIG1 mistrafficking affects EGFR signaling.

To identify the basolateral targeting motif, I generated LRIG1-EGFP-expressing Madin-Darby canine kidney (MDCK) cells and six sequential mutations of the cytoplasmic domain (Figure A.2). However, I found that the EGFP tag affects trafficking of wild type LRIG1; apical only, or mostly apical expression of LRIG1-EGFP was observed (Figure A.3). In addition, an inducible LRIG1-HA construct (C-terminal HA tag) was exclusively localized to the apical surface of human Caco-2 cells (data not shown). Preliminary experiments demonstrated that wild type, untagged LRIG1 was expressed on the apical surface as well, although some basolateral expression was seen (data not shown). Therefore, these results suggest that: 1) the C-terminal tag might interfere with trafficking; or 2) high levels of overexpression affect trafficking.

Although the LRIG1-EGFP MDCK cell lines are not useful to study the basolateral trafficking of LRIG1, they are fortuitous in other ways. First, they provide an excellent mechanism to study the biological significance of its mistrafficking. Second, in a non-polarized setting, the truncation mutants are useful for the lab to study potential LRIG1-interacting proteins. If this project were to be revisited, we should demonstrate that overexpressed LRIG1 was not being directed to the surface because of N-

glycosylation marks, which are postulated to be an apical sorting signal (*141*). Treatment of polarized cells with tunicamycin before biotinylation will prevent N-glycosylation of proteins; if N-glycosylation marks are directing LRIG1 to the apical surface, tunicamycin treatment should prevent that trafficking event.

Materials and Methods

Generation of LRIG1-EGFP

Full-length human *LRIG1* cDNA (accession number: BC071561) was cloned into the pEGFP-N1 plasmid (#6085-1, Clonetech), resulting in the LRIG1-EGFP C-terminal fusion protein.

Transfection, selection, and biotinylation

Lrig1-pEGFP-N1 (Lrig1-EGFP) and pEGFP-N1 (EGFP) were transiently transfected into human HEK293T cells using Metafectene (Biontex, Germany) according to the manufacturer's instructions. Cells were selected for ten days in 1 mg/mL G418. Cells were thereafter maintained in 300 µg/mL G418. G418 was removed for experiments. Selective cell surface biotinylation was performed as previously described (*142*).

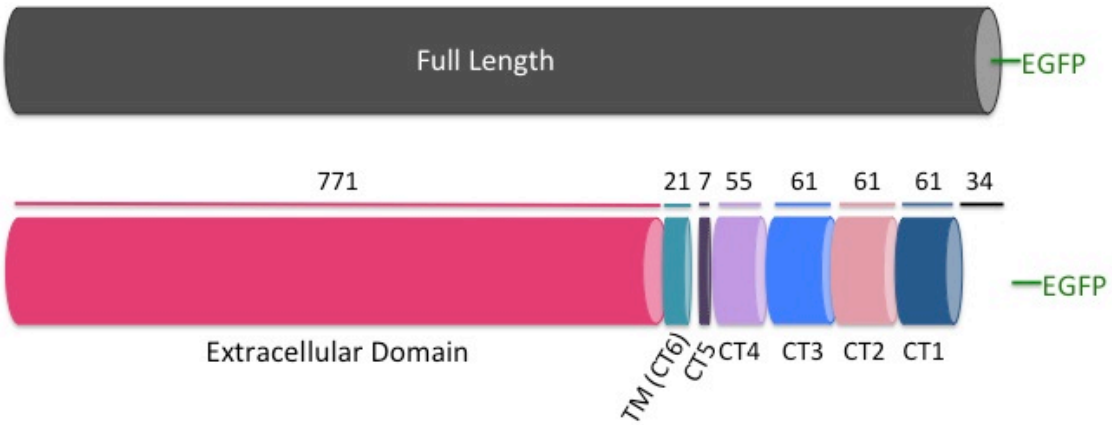

Figure A.2. Schematic of LRIG1-EGFP sequential cytoplasmic domain mutations. CT, cytoplasmic tail.

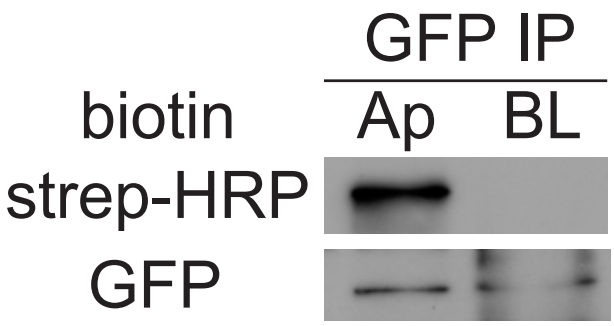

Figure A.3. Cells expressing a C-terminal-tagged LRIG1 construct express LRIG1 on the apical surface. MDCK cells stably expressing LRIG1-EGFP displayed apical LRIG1. strep-HRP, streptavidin-HRP-conjugated secondary antibody.

REFERENCES

1. S. J. Buczacki *et al.*, Intestinal label-retaining cells are secretory precursors expressing Lgr5. *Nature* **495**, 65 (Mar 7, 2013).
2. I. A. Brownlee, M. E. Havler, P. W. Dettmar, A. Allen, J. P. Pearson, Colonic mucus: secretion and turnover in relation to dietary fibre intake. *The Proceedings of the Nutrition Society* **62**, 245 (Feb, 2003).
3. J. A. Maykel, F. G. Opelka, Colonic diverticulosis and diverticular hemorrhage. *Clinics in colon and rectal surgery* **17**, 195 (Aug, 2004).
4. R. C. Mifflin, I. V. Pinchuk, J. I. Saada, D. W. Powell, Intestinal myofibroblasts: targets for stem cell therapy. *American journal of physiology. Gastrointestinal and liver physiology* **300**, G684 (May, 2011).
5. D. W. Powell, I. V. Pinchuk, J. I. Saada, X. Chen, R. C. Mifflin, Mesenchymal cells of the intestinal lamina propria. *Annual review of physiology* **73**, 213 (2011).
6. I. V. Pinchuk, R. C. Mifflin, J. I. Saada, D. W. Powell, Intestinal mesenchymal cells. *Current gastroenterology reports* **12**, 310 (Oct, 2010).
7. E. Marshman, C. Booth, C. S. Potten, The intestinal epithelial stem cell. *BioEssays : news and reviews in molecular, cellular and developmental biology* **24**, 91 (Jan, 2002).
8. B. Z. Stanger, R. Datar, L. C. Murtaugh, D. A. Melton, Direct regulation of intestinal fate by Notch. *Proceedings of the National Academy of Sciences of the United States of America* **102**, 12443 (Aug 30, 2005).
9. W. de Lau *et al.*, Peyer's patch M cells derived from Lgr5(+) stem cells require SpiB and are induced by RankL in cultured "miniguts". *Molecular and cellular biology* **32**, 3639 (Sep, 2012).
10. N. Barker, Adult intestinal stem cells: critical drivers of epithelial homeostasis and regeneration. *Nature reviews. Molecular cell biology* **15**, 19 (Jan, 2014).
11. A. J. Carulli, L. C. Samuelson, S. Schnell, Unraveling intestinal stem cell behavior with models of crypt dynamics. *Integrative biology : quantitative biosciences from nano to macro* **6**, 243 (Mar, 2014).
12. B. M. Boman, J. Z. Fields, An APC:WNT Counter-Current-Like Mechanism Regulates Cell Division Along the Human Colonic Crypt Axis: A Mechanism That Explains How APC Mutations Induce Proliferative Abnormalities That Drive Colon Cancer Development. *Frontiers in oncology* **3**, 244 (2013).
13. A. D. Gracz, S. T. Magness, Defining hierarchies of stemness in the intestine: evidence from biomarkers and regulatory pathways. *American journal of physiology. Gastrointestinal and liver physiology* **307**, G260 (Aug 1, 2014).
14. L. G. van der Flier, H. Clevers, Stem cells, self-renewal, and differentiation in the intestinal epithelium. *Annual review of physiology* **71**, 241 (2009).
15. F. Gerbe *et al.*, Distinct ATOH1 and Neurog3 requirements define tuft cells as a new secretory cell type in the intestinal epithelium. *The Journal of cell biology* **192**, 767 (Mar 7, 2011).
16. M. R. Neutra, Current concepts in mucosal immunity. V Role of M cells in transepithelial transport of antigens and pathogens to the mucosal immune system. *The American journal of physiology* **274**, G785 (May, 1998).

17. J. L. Madara, Cup cells: structure and distribution of a unique class of epithelial cells in guinea pig, rabbit, and monkey small intestine. *Gastroenterology* **83**, 981 (Nov, 1982).
18. F. Gerbe, C. Legraverend, P. Jay, The intestinal epithelium tuft cells: specification and function. *Cellular and molecular life sciences : CMLS* **69**, 2907 (Sep, 2012).
19. C. S. Potten, M. Loeffler, Stem cells: attributes, cycles, spirals, pitfalls and uncertainties. Lessons for and from the crypt. *Development* **110**, 1001 (Dec, 1990).
20. H. Cheng, C. P. Leblond, Origin, differentiation and renewal of the four main epithelial cell types in the mouse small intestine. V. Unitarian Theory of the origin of the four epithelial cell types. *The American journal of anatomy* **141**, 537 (Dec, 1974).
21. N. Barker, M. van de Wetering, H. Clevers, The intestinal stem cell. *Genes & development* **22**, 1856 (Jul 15, 2008).
22. C. S. Potten, G. Owen, D. Booth, Intestinal stem cells protect their genome by selective segregation of template DNA strands. *Journal of cell science* **115**, 2381 (Jun 1, 2002).
23. J. Cairns, Mutation selection and the natural history of cancer. *Nature* **255**, 197 (May 15, 1975).
24. C. S. Potten, W. J. Hume, P. Reid, J. Cairns, The segregation of DNA in epithelial stem cells. *Cell* **15**, 899 (Nov, 1978).
25. N. Barker *et al.*, Identification of stem cells in small intestine and colon by marker gene Lgr5. *Nature* **449**, 1003 (Oct 25, 2007).
26. W. de Lau *et al.*, Lgr5 homologues associate with Wnt receptors and mediate R-spondin signalling. *Nature* **476**, 293 (Aug 18, 2011).
27. K. S. Carmon, X. Gong, Q. Lin, A. Thomas, Q. Liu, R-spondins function as ligands of the orphan receptors LGR4 and LGR5 to regulate Wnt/beta-catenin signaling. *Proceedings of the National Academy of Sciences of the United States of America* **108**, 11452 (Jul 12, 2011).
28. A. Glinka *et al.*, LGR4 and LGR5 are R-spondin receptors mediating Wnt/beta-catenin and Wnt/PCP signalling. *EMBO reports* **12**, 1055 (Oct, 2011).
29. E. Sangiorgi, M. R. Capecchi, Bmi1 is expressed in vivo in intestinal stem cells. *Nature genetics* **40**, 915 (Jul, 2008).
30. K. S. Yan *et al.*, The intestinal stem cell markers Bmi1 and Lgr5 identify two functionally distinct populations. *Proceedings of the National Academy of Sciences of the United States of America* **109**, 466 (Jan 10, 2012).
31. H. J. Snippert *et al.*, Prominin-1/CD133 marks stem cells and early progenitors in mouse small intestine. *Gastroenterology* **136**, 2187 (Jun, 2009).
32. A. E. Powell *et al.*, The pan-ErbB negative regulator Lrig1 is an intestinal stem cell marker that functions as a tumor suppressor. *Cell* **149**, 146 (Mar 30, 2012).
33. R. K. Montgomery *et al.*, Mouse telomerase reverse transcriptase (mTert) expression marks slowly cycling intestinal stem cells. *Proceedings of the National Academy of Sciences of the United States of America* **108**, 179 (Jan 4, 2011).
34. J. Munoz *et al.*, The Lgr5 intestinal stem cell signature: robust expression of proposed quiescent '+4' cell markers. *The EMBO journal* **31**, 3079 (Jul 18, 2012).

35. D. T. Breault *et al.*, Generation of mTert-GFP mice as a model to identify and study tissue progenitor cells. *Proceedings of the National Academy of Sciences of the United States of America* **105**, 10420 (Jul 29, 2008).
36. N. Takeda *et al.*, Interconversion between intestinal stem cell populations in distinct niches. *Science* **334**, 1420 (Dec 9, 2011).
37. V. W. Wong *et al.*, Lrig1 controls intestinal stem-cell homeostasis by negative regulation of ErbB signalling. *Nature cell biology* **14**, 401 (Apr, 2012).
38. G. Gur *et al.*, LRIG1 restricts growth factor signaling by enhancing receptor ubiquitylation and degradation. *The EMBO journal* **23**, 3270 (Aug 18, 2004).
39. M. B. Laederich *et al.*, The leucine-rich repeat protein LRIG1 is a negative regulator of ErbB family receptor tyrosine kinases. *The Journal of biological chemistry* **279**, 47050 (Nov 5, 2004).
40. D. L. Shattuck *et al.*, LRIG1 is a novel negative regulator of the Met receptor and opposes Met and Her2 synergy. *Molecular and cellular biology* **27**, 1934 (Mar, 2007).
41. F. Ledda, O. Bieraugel, S. S. Fard, M. Vilar, G. Paratcha, Lrig1 is an endogenous inhibitor of Ret receptor tyrosine kinase activation, downstream signaling, and biological responses to GDNF. *The Journal of neuroscience : the official journal of the Society for Neuroscience* **28**, 39 (Jan 2, 2008).
42. V. Rondahl *et al.*, Lrig2-deficient mice are protected against PDGFB-induced glioma. *PloS one* **8**, e73635 (2013).
43. H. Tian *et al.*, A reserve stem cell population in small intestine renders Lgr5-positive cells dispensable. *Nature* **478**, 255 (Oct 13, 2011).
44. H. Clevers, Stem Cells: A unifying theory for the crypt. *Nature* **495**, 53 (Mar 7, 2013).
45. J. H. van Es *et al.*, Dll1+ secretory progenitor cells revert to stem cells upon crypt damage. *Nature cell biology* **14**, 1099 (Oct, 2012).
46. L. Vermeulen, H. J. Snippert, Stem cell dynamics in homeostasis and cancer of the intestine. *Nature reviews. Cancer* **14**, 468 (Jul, 2014).
47. T. H. Kim *et al.*, Broadly permissive intestinal chromatin underlies lateral inhibition and cell plasticity. *Nature* **506**, 511 (Feb 27, 2014).
48. R. Siegel, J. Ma, Z. Zou, A. Jemal, Cancer statistics, 2014. *CA: a cancer journal for clinicians* **64**, 9 (Jan-Feb, 2014).
49. E. R. Fearon, B. Vogelstein, A genetic model for colorectal tumorigenesis. *Cell* **61**, 759 (Jun 1, 1990).
50. Comprehensive molecular characterization of human colon and rectal cancer. *Nature* **487**, 330 (Jul 19, 2012).
51. E. R. Fearon, Molecular genetics of colorectal cancer. *Annual review of pathology* **6**, 479 (2011).
52. A. K. Rustgi, The genetics of hereditary colon cancer. *Genes & development* **21**, 2525 (Oct 15, 2007).
53. V. Korinek *et al.*, Depletion of epithelial stem-cell compartments in the small intestine of mice lacking Tcf-4. *Nature genetics* **19**, 379 (Aug, 1998).
54. J. H. van Es *et al.*, A critical role for the Wnt effector Tcf4 in adult intestinal homeostatic self-renewal. *Molecular and cellular biology* **32**, 1918 (May, 2012).

55. T. Fevr, S. Robine, D. Louvard, J. Huelsken, Wnt/beta-catenin is essential for intestinal homeostasis and maintenance of intestinal stem cells. *Molecular and cellular biology* **27**, 7551 (Nov, 2007).
56. J. Schuijers, H. Clevers, Adult mammalian stem cells: the role of Wnt, Lgr5 and R-spondins. *The EMBO journal* **31**, 2685 (Jun 13, 2012).
57. W. H. Lien, E. Fuchs, Wnt some lose some: transcriptional governance of stem cells by Wnt/beta-catenin signaling. *Genes & development* **28**, 1517 (Jul 15, 2014).
58. H. Clevers, R. Nusse, Wnt/beta-catenin signaling and disease. *Cell* **149**, 1192 (Jun 8, 2012).
59. B. Rubinfeld *et al.*, Association of the APC gene product with beta-catenin. *Science* **262**, 1731 (Dec 10, 1993).
60. L. K. Su, B. Vogelstein, K. W. Kinzler, Association of the APC tumor suppressor protein with catenins. *Science* **262**, 1734 (Dec 10, 1993).
61. L. K. Su *et al.*, Multiple intestinal neoplasia caused by a mutation in the murine homolog of the APC gene. *Science* **256**, 668 (May 1, 1992).
62. R. Fodde *et al.*, A targeted chain-termination mutation in the mouse Apc gene results in multiple intestinal tumors. *Proceedings of the National Academy of Sciences of the United States of America* **91**, 8969 (Sep 13, 1994).
63. S. Munemitsu, I. Albert, B. Souza, B. Rubinfeld, P. Polakis, Regulation of intracellular beta-catenin levels by the adenomatous polyposis coli (APC) tumor-suppressor protein. *Proceedings of the National Academy of Sciences of the United States of America* **92**, 3046 (Mar 28, 1995).
64. K. J. Smith *et al.*, The APC gene product in normal and tumor cells. *Proceedings of the National Academy of Sciences of the United States of America* **90**, 2846 (Apr 1, 1993).
65. S. M. Powell *et al.*, APC mutations occur early during colorectal tumorigenesis. *Nature* **359**, 235 (Sep 17, 1992).
66. Y. Miyoshi *et al.*, Germ-line mutations of the APC gene in 53 familial adenomatous polyposis patients. *Proceedings of the National Academy of Sciences of the United States of America* **89**, 4452 (May 15, 1992).
67. A. Humphries, N. A. Wright, Colonic crypt organization and tumorigenesis. *Nature reviews. Cancer* **8**, 415 (Jun, 2008).
68. B. M. Boman *et al.*, Colonic crypt changes during adenoma development in familial adenomatous polyposis: immunohistochemical evidence for expansion of the crypt base cell population. *The American journal of pathology* **165**, 1489 (Nov, 2004).
69. K. M. Haigis, W. F. Dove, A Robertsonian translocation suppresses a somatic recombination pathway to loss of heterozygosity. *Nature genetics* **33**, 33 (Jan, 2003).
70. C. Luongo, A. R. Moser, S. Gledhill, W. F. Dove, Loss of Apc+ in intestinal adenomas from Min mice. *Cancer research* **54**, 5947 (Nov 15, 1994).
71. D. B. Levy *et al.*, Inactivation of both APC alleles in human and mouse tumors. *Cancer research* **54**, 5953 (Nov 15, 1994).
72. H. J. Snippert *et al.*, Intestinal crypt homeostasis results from neutral competition between symmetrically dividing Lgr5 stem cells. *Cell* **143**, 134 (Oct 1, 2010).

73. C. Lopez-Garcia, A. M. Klein, B. D. Simons, D. J. Winton, Intestinal stem cell replacement follows a pattern of neutral drift. *Science* **330**, 822 (Nov 5, 2010).
74. L. Vermeulen *et al.*, Defining stem cell dynamics in models of intestinal tumor initiation. *Science* **342**, 995 (Nov 22, 2013).
75. H. S. Park, R. A. Goodlad, N. A. Wright, Crypt fission in the small intestine and colon. A mechanism for the emergence of G6PD locus-mutated crypts after treatment with mutagens. *The American journal of pathology* **147**, 1416 (Nov, 1995).
76. N. Barker *et al.*, Crypt stem cells as the cells-of-origin of intestinal cancer. *Nature* **457**, 608 (Jan 29, 2009).
77. S. Schwitalla *et al.*, Intestinal tumorigenesis initiated by dedifferentiation and acquisition of stem-cell-like properties. *Cell* **152**, 25 (Jan 17, 2013).
78. A. G. Schepers *et al.*, Lineage tracing reveals Lgr5+ stem cell activity in mouse intestinal adenomas. *Science* **337**, 730 (Aug 10, 2012).
79. K. M. Haigis *et al.*, Differential effects of oncogenic K-Ras and N-Ras on proliferation, differentiation and tumor progression in the colon. *Nature genetics* **40**, 600 (May, 2008).
80. K. E. Hung *et al.*, Development of a mouse model for sporadic and metastatic colon tumors and its use in assessing drug treatment. *Proceedings of the National Academy of Sciences of the United States of America* **107**, 1565 (Jan 26, 2010).
81. A. J. Byun *et al.*, Colon-specific tumorigenesis in mice driven by Cre-mediated inactivation of Apc and activation of mutant Kras. *Cancer letters* **347**, 191 (Jun 1, 2014).
82. A. E. Powell *et al.*, Inducible loss of one Apc allele in Lrig1-expressing progenitor cells results in multiple distal colonic tumors with features of familial adenomatous polyposis. *American journal of physiology. Gastrointestinal and liver physiology* **307**, G16 (Jul 1, 2014).
83. E. J. Poulin *et al.*, Using a new Lrig1 reporter mouse to assess differences between two Lrig1 antibodies in the intestine. *Stem cell research* **13**, 422 (Sep 20, 2014).
84. J. Nilsson *et al.*, Cloning, characterization, and expression of human LIG1. *Biochemical and biophysical research communications* **284**, 1155 (Jun 29, 2001).
85. H. Kaji *et al.*, Large-scale identification of N-glycosylated proteins of mouse tissues and construction of a glycoprotein database, GlycoProtDB. *Journal of proteome research* **11**, 4553 (Sep 7, 2012).
86. F. el Marjou *et al.*, Tissue-specific and inducible Cre-mediated recombination in the gut epithelium. *Genesis* **39**, 186 (Jul, 2004).
87. Y. Xue, R. Johnson, M. Desmet, P. W. Snyder, J. C. Fleet, Generation of a transgenic mouse for colorectal cancer research with intestinal cre expression limited to the large intestine. *Molecular cancer research : MCR* **8**, 1095 (Aug, 2010).
88. S. K. Chang *et al.*, Localization of mucin (MUC2 and MUC3) messenger RNA and peptide expression in human normal intestine and colon cancer. *Gastroenterology* **107**, 28 (Jul, 1994).

89. M. E. Rothenberg *et al.*, Identification of a cKit(+) colonic crypt base secretory cell that supports Lgr5(+) stem cells in mice. *Gastroenterology* **142**, 1195 (May, 2012).
90. G. Gur *et al.*, LRIG1 restricts growth factor signaling by enhancing receptor ubiquitylation and degradation. *The EMBO journal* **23**, 3270 (Aug, 2004).
91. K. Ohtsubo, J. D. Marth, Glycosylation in cellular mechanisms of health and disease. *Cell* **126**, 855 (Sep 8, 2006).
92. M. A. Daniels, K. A. Hogquist, S. C. Jameson, Sweet 'n' sour: the impact of differential glycosylation on T cell responses. *Nature immunology* **3**, 903 (Oct, 2002).
93. S. Hakomori, Glycosylation defining cancer malignancy: new wine in an old bottle. *Proceedings of the National Academy of Sciences of the United States of America* **99**, 10231 (Aug 6, 2002).
94. J. Nilsson, A. Starefeldt, R. Henriksson, H. Hedman, LRIG1 protein in human cells and tissues. *Cell and tissue research* **312**, 65 (Apr, 2003).
95. R. H. Whitehead, A. Brown, P. S. Bhathal, A method for the isolation and culture of human colonic crypts in collagen gels. *In vitro cellular & developmental biology : journal of the Tissue Culture Association* **23**, 436 (Jun, 1987).
96. Y. Li, H. Zhang, S. C. Choi, Y. Litingtung, C. Chiang, Sonic hedgehog signaling regulates Gli3 processing, mesenchymal proliferation, and differentiation during mouse lung organogenesis. *Developmental biology* **270**, 214 (Jun 1, 2004).
97. C. W. Tan, Y. Hirokawa, B. S. Gardiner, D. W. Smith, A. W. Burgess, Colon cryptogenesis: asymmetric budding. *PloS one* **8**, e78519 (2013).
98. A. E. Powell *et al.*, Fusion between Intestinal epithelial cells and macrophages in a cancer context results in nuclear reprogramming. *Cancer research* **71**, 1497 (Feb 15, 2011).
99. P. S. Davies, A. E. Powell, J. R. Swain, M. H. Wong, Inflammation and proliferation act together to mediate intestinal cell fusion. *PloS one* **4**, e6530 (2009).
100. H. Kaji *et al.*, Lectin affinity capture, isotope-coded tagging and mass spectrometry to identify N-linked glycoproteins. *Nature biotechnology* **21**, 667 (Jun, 2003).
101. H. Kaji, Y. Yamauchi, N. Takahashi, T. Isobe, Mass spectrometric identification of N-linked glycopeptides using lectin-mediated affinity capture and glycosylation site-specific stable isotope tagging. *Nature protocols* **1**, 3019 (2006).
102. B. Vogelstein *et al.*, Cancer genome landscapes. *Science* **339**, 1546 (Mar 29, 2013).
103. Y. Pylayeva-Gupta, E. Grabocka, D. Bar-Sagi, RAS oncogenes: weaving a tumorigenic web. *Nature reviews. Cancer* **11**, 761 (Nov, 2011).
104. S. Velho, K. M. Haigis, Regulation of homeostasis and oncogenesis in the intestinal epithelium by Ras. *Experimental cell research* **317**, 2732 (Nov 15, 2011).
105. E. L. Jackson *et al.*, Analysis of lung tumor initiation and progression using conditional expression of oncogenic K-ras. *Genes & development* **15**, 3243 (Dec 15, 2001).

106. C. Caulin *et al.*, Inducible activation of oncogenic K-ras results in tumor formation in the oral cavity. *Cancer research* **64**, 5054 (Aug 1, 2004).
107. S. P. Robinson, S. M. Langan-Fahey, D. A. Johnson, V. C. Jordan, Metabolites, pharmacodynamics, and pharmacokinetics of tamoxifen in rats and mice compared to the breast cancer patient. *Drug metabolism and disposition: the biological fate of chemicals* **19**, 36 (Jan-Feb, 1991).
108. M. Bennecke *et al.*, Ink4a/Arf and oncogene-induced senescence prevent tumor progression during alternative colorectal tumorigenesis. *Cancer cell* **18**, 135 (Aug 9, 2010).
109. Y. Feng *et al.*, Mutant KRAS promotes hyperplasia and alters differentiation in the colon epithelium but does not expand the presumptive stem cell pool. *Gastroenterology* **141**, 1003 (Sep, 2011).
110. R. L. Johnson, J. C. Fleet, Animal models of colorectal cancer. *Cancer metastasis reviews* **32**, 39 (Jun, 2013).
111. D. Hanahan, R. A. Weinberg, Hallmarks of cancer: the next generation. *Cell* **144**, 646 (Mar 4, 2011).
112. K. N. Rajagopalan, R. J. DeBerardinis, Role of glutamine in cancer: therapeutic and imaging implications. *Journal of nuclear medicine : official publication, Society of Nuclear Medicine* **52**, 1005 (Jul, 2011).
113. H. Ying *et al.*, Oncogenic Kras maintains pancreatic tumors through regulation of anabolic glucose metabolism. *Cell* **149**, 656 (Apr 27, 2012).
114. J. Son *et al.*, Glutamine supports pancreatic cancer growth through a KRAS-regulated metabolic pathway. *Nature* **496**, 101 (Apr 4, 2013).
115. T. Kuilman, C. Michaloglou, W. J. Mooi, D. S. Peeper, The essence of senescence. *Genes & development* **24**, 2463 (Nov 15, 2010).
116. G. Levidou *et al.*, ERK/pERK expression and B-raf mutations in colon adenocarcinomas: correlation with clinicopathological characteristics. *World journal of surgical oncology* **10**, 47 (2012).
117. S. Colnot *et al.*, Liver-targeted disruption of Apc in mice activates beta-catenin signaling and leads to hepatocellular carcinomas. *Proceedings of the National Academy of Sciences of the United States of America* **101**, 17216 (Dec 7, 2004).
118. W. Qu *et al.*, Synthesis of optically pure 4-fluoro-glutamines as potential metabolic imaging agents for tumors. *Journal of the American Chemical Society* **133**, 1122 (Feb 2, 2011).
119. M. Dandekar, J. R. Tseng, S. S. Gambhir, Reproducibility of 18F-FDG microPET studies in mouse tumor xenografts. *Journal of nuclear medicine : official publication, Society of Nuclear Medicine* **48**, 602 (Apr, 2007).
120. B. J. Fueger *et al.*, Impact of animal handling on the results of 18F-FDG PET studies in mice. *Journal of nuclear medicine : official publication, Society of Nuclear Medicine* **47**, 999 (Jun, 2006).
121. E. T. McKinley *et al.*, 18FDG-PET predicts pharmacodynamic response to OSI-906, a dual IGF-1R/IR inhibitor, in preclinical mouse models of lung cancer. *Clinical cancer research : an official journal of the American Association for Cancer Research* **17**, 3332 (May 15, 2011).
122. T. Sato *et al.*, Single Lgr5 stem cells build crypt-villus structures in vitro without a mesenchymal niche. *Nature* **459**, 262 (May 14, 2009).

123. S. B. Bradfute, T. A. Graubert, M. A. Goodell, Roles of Sca-1 in hematopoietic stem/progenitor cell function. *Experimental hematology* **33**, 836 (Jul, 2005).
124. T. Mitamura, S. Higashiyama, N. Taniguchi, M. Klagsbrun, E. Mekada, Diphtheria toxin binds to the epidermal growth factor (EGF)-like domain of human heparin-binding EGF-like growth factor/diphtheria toxin receptor and inhibits specifically its mitogenic activity. *The Journal of biological chemistry* **270**, 1015 (Jan 20, 1995).
125. E. Reynders, F. Foulquier, W. Annaert, G. Matthijs, How Golgi glycosylation meets and needs trafficking: the case of the COG complex. *Glycobiology* **21**, 853 (Jul, 2011).
126. M. B. Laederich *et al.*, The leucine-rich repeat protein LRIG1 is a negative regulator of ErbB family receptor tyrosine kinases. *The Journal of biological chemistry* **279**, 47050 (Nov, 2004).
127. M. A. Stutz, D. L. Shattuck, M. B. Laederich, K. L. Carraway, 3rd, C. Sweeney, LRIG1 negatively regulates the oncogenic EGF receptor mutant EGFRvIII. *Oncogene* **27**, 5741 (Sep 25, 2008).
128. R. F. Hagemann, J. J. Stragand, Fasting and refeeding: cell kinetic response of jejunum, ileum and colon. *Cell and tissue kinetics* **10**, 3 (Jan, 1977).
129. I. Okayasu *et al.*, A novel method in the induction of reliable experimental acute and chronic ulcerative colitis in mice. *Gastroenterology* **98**, 694 (Mar, 1990).
130. M. L. Clapper, H. S. Cooper, W. C. Chang, Dextran sulfate sodium-induced colitis-associated neoplasia: a promising model for the development of chemopreventive interventions. *Acta pharmacologica Sinica* **28**, 1450 (Sep, 2007).
131. J. Chen, X. F. Huang, The signal pathways in azoxymethane-induced colon cancer and preventive implications. *Cancer biology & therapy* **8**, 1313 (Jul, 2009).
132. J. Liu *et al.*, Non-parallel recombination limits Cre-LoxP-based reporters as precise indicators of conditional genetic manipulation. *Genesis* **51**, 436 (Jun, 2013).
133. A. R. Moser, H. C. Pitot, W. F. Dove, A dominant mutation that predisposes to multiple intestinal neoplasia in the mouse. *Science* **247**, 322 (Jan 19, 1990).
134. X. Lu *et al.*, Optochemogenetics (OCG) allows more precise control of genetic engineering in mice with CreER regulators. *Bioconjugate chemistry* **23**, 1945 (Sep 19, 2012).
135. C. Royer, X. Lu, Epithelial cell polarity: a major gatekeeper against cancer? *Cell death and differentiation* **18**, 1470 (Sep, 2011).
136. R. Avraham, Y. Yarden, Feedback regulation of EGFR signalling: decision making by early and delayed loops. *Nature reviews. Molecular cell biology* **12**, 104 (Feb, 2011).
137. Y. Wang, E. J. Poulin, R. J. Coffey, LRIG1 is a triple threat: ERBB negative regulator, intestinal stem cell marker and tumour suppressor. *British journal of cancer*, (Apr 4, 2013).
138. R. B. Roberts *et al.*, Importance of epidermal growth factor receptor signaling in establishment of adenomas and maintenance of carcinomas during intestinal

tumorigenesis. *Proceedings of the National Academy of Sciences of the United States of America* **99**, 1521 (Feb 5, 2002).
139. M. E. Hobert, S. J. Kil, M. E. Medof, C. R. Carlin, The cytoplasmic juxtamembrane domain of the epidermal growth factor receptor contains a novel autonomous basolateral sorting determinant. *The Journal of biological chemistry* **272**, 32901 (Dec 26, 1997).
140. M. Hobert, C. Carlin, Cytoplasmic juxtamembrane domain of the human EGF receptor is required for basolateral localization in MDCK cells. *Journal of cellular physiology* **162**, 434 (Mar, 1995).
141. B. Singh, R. J. Coffey, Trafficking of epidermal growth factor receptor ligands in polarized epithelial cells. *Annual review of physiology* **76**, 275 (2014).
142. B. Singh, G. Bogatcheva, M. K. Washington, R. J. Coffey, Transformation of polarized epithelial cells by apical mistrafficking of epiregulin. *Proceedings of the National Academy of Sciences of the United States of America* **110**, 8960 (May 28, 2013).